

SEE THINGS DIFFERENTLY



Semurup – 3D MT + Gravity Modeling Pertamina Geothermal Energy

18 March 2025

Introduction

Pertamina Geothermal Energy (PGE) has contracted Viridien to perform a 3D modeling project of MT and Gravity data over the Semurup area.

PGE provided a total of 90 MT stations, 70 acquired in 2022 and 20 in 2024, and Gravity measurements at 364 locations.

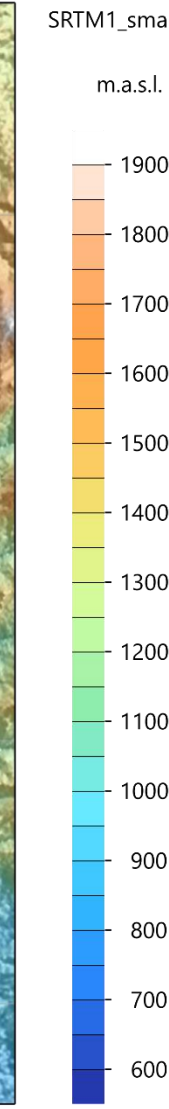
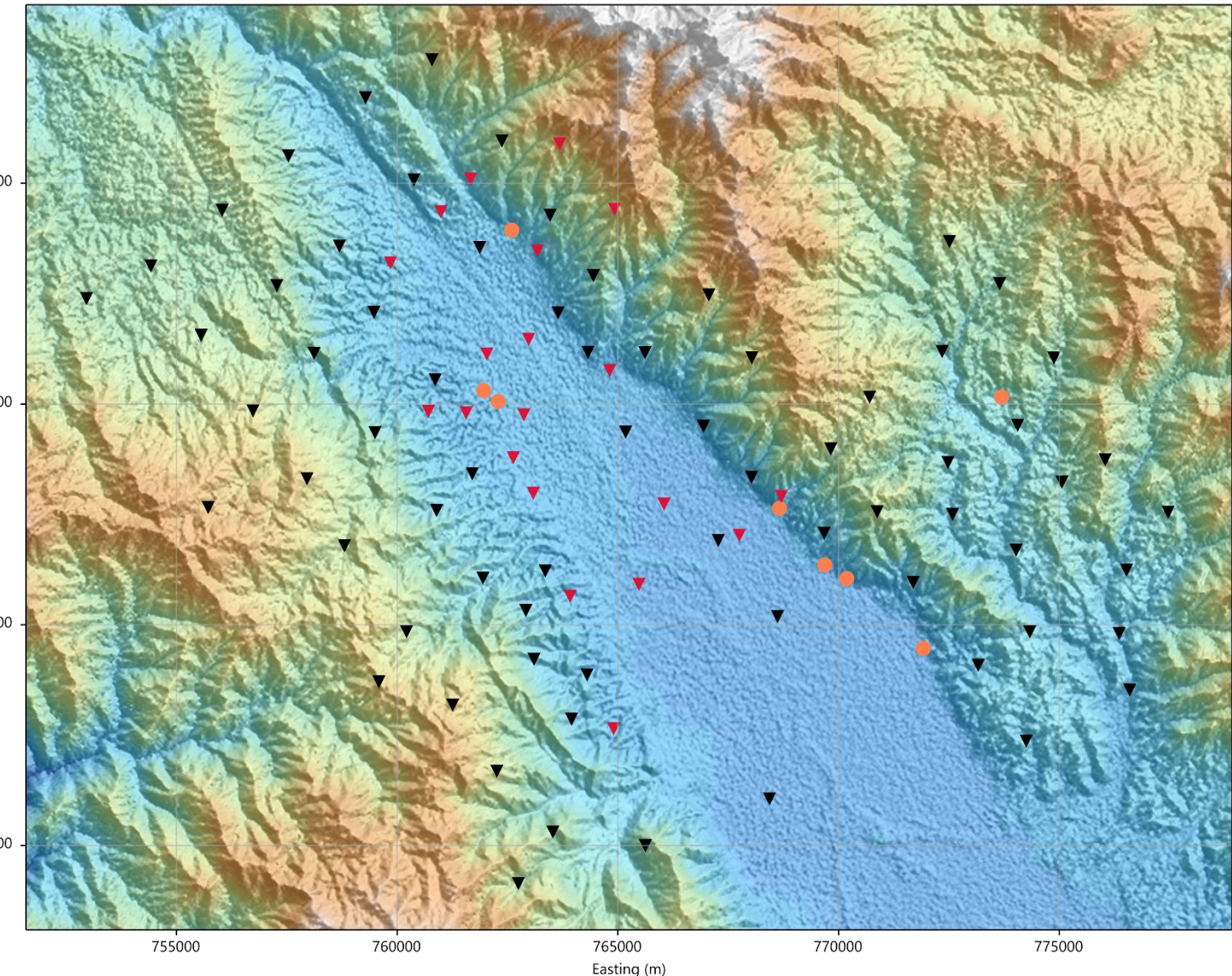
All data have been carefully reviewed and prepared for the 3D modeling project, that consisted in:

- 3D MT and gravity single domain inversions
- 3D MT + gravity joint inversions

The 3D inversions were carried out with Viridien's Geotools platform using the RLM-3D inversion and modeling algorithm.

Results from modeling are presented in this report.

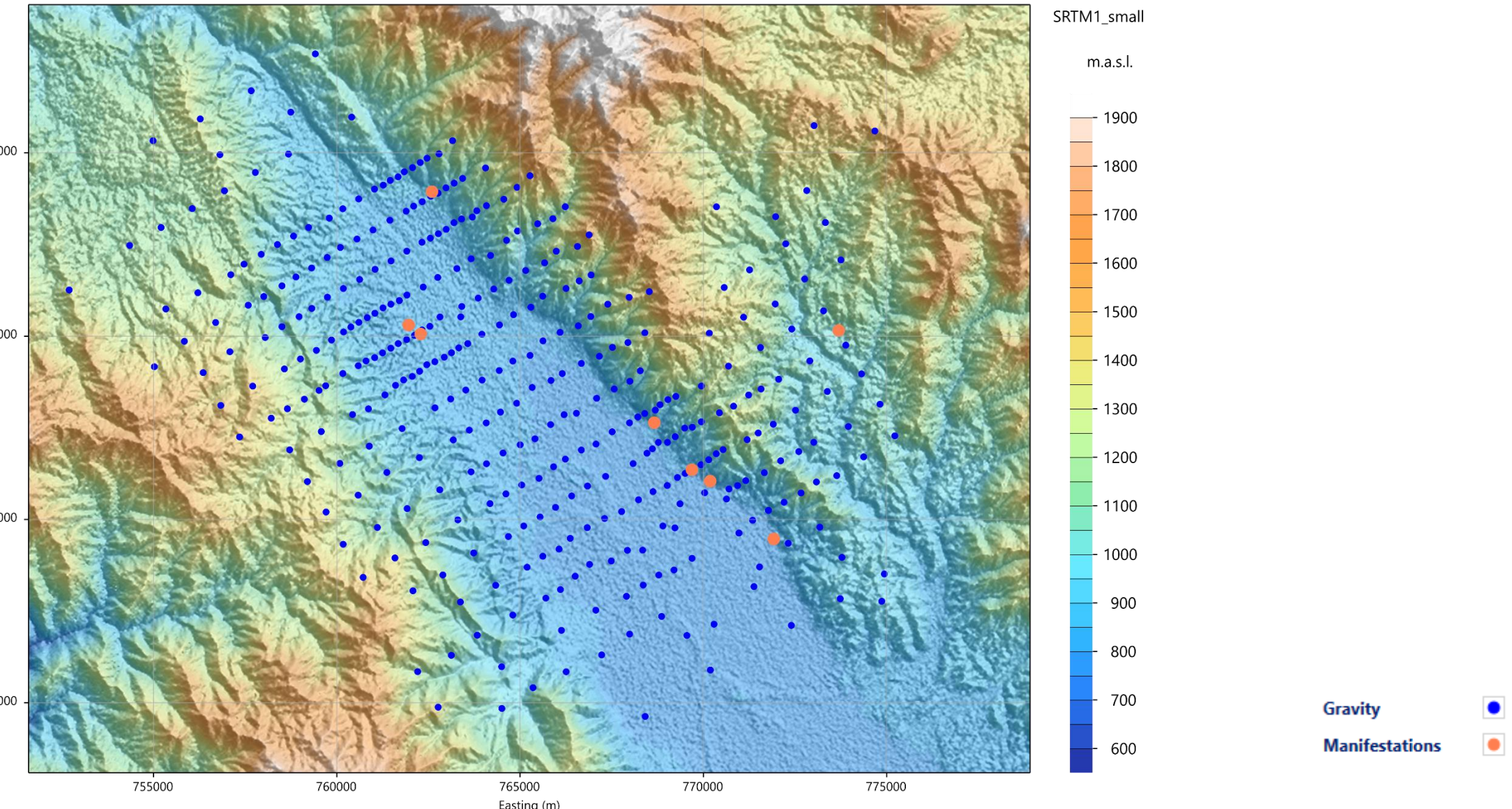
Location Map – MT stations



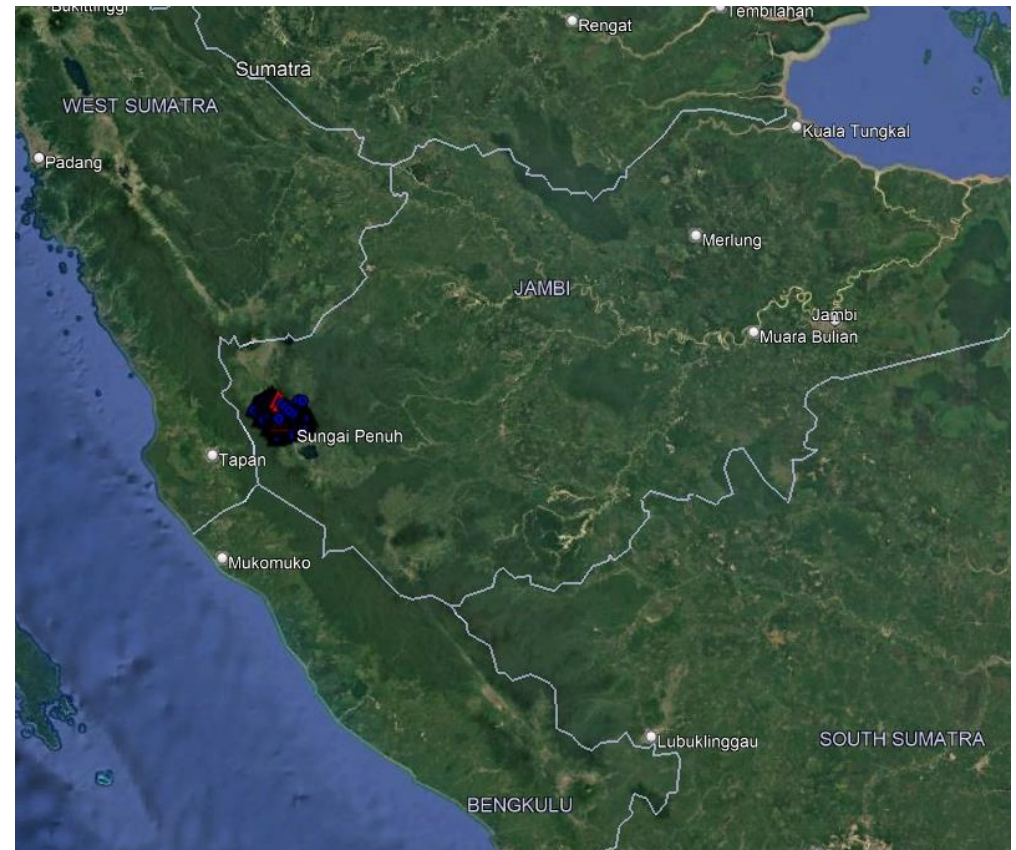
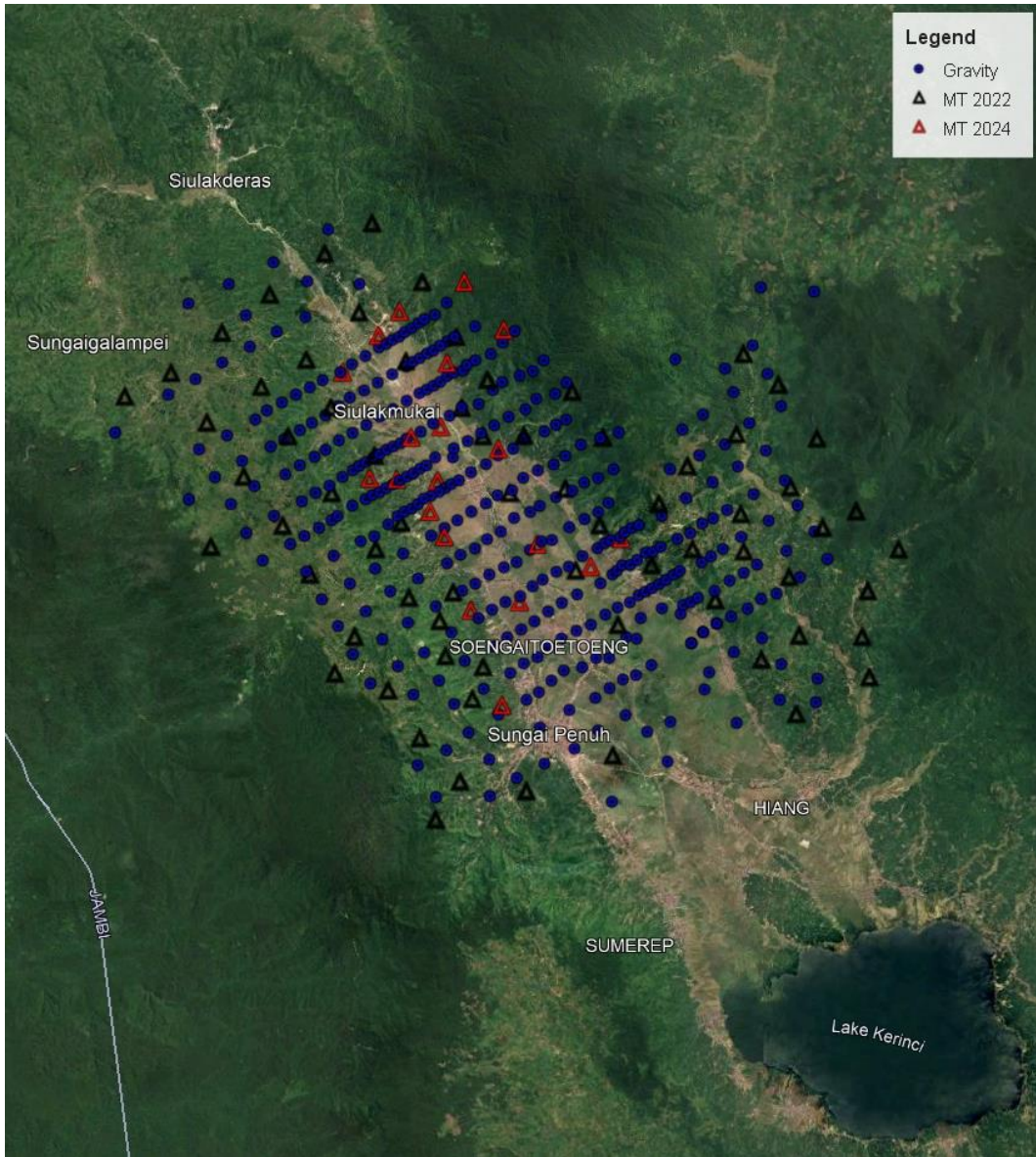
2024 MT: 20 soundings
2022 MT: 70 soundings

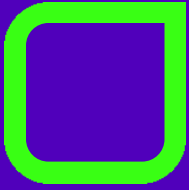
- MT 2024 ▼
- MT 2022 ▼
- Manifestations ○

Location Map – Gravity measurements, survey area



Satellite Imagery – MT and Gravity locations



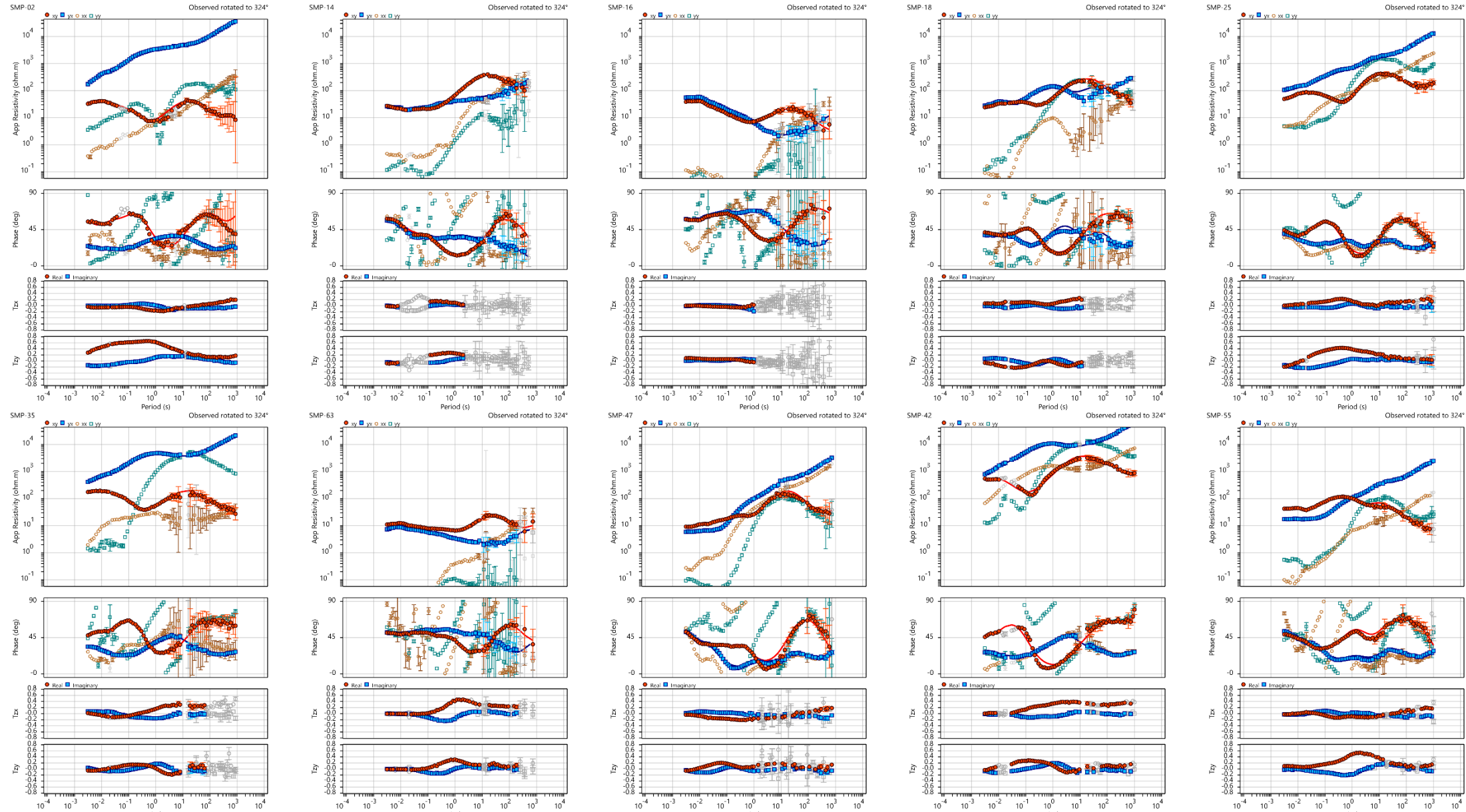


MAGNETOTELLURIC DATA

2022-2024 datasets overview
MT Data maps



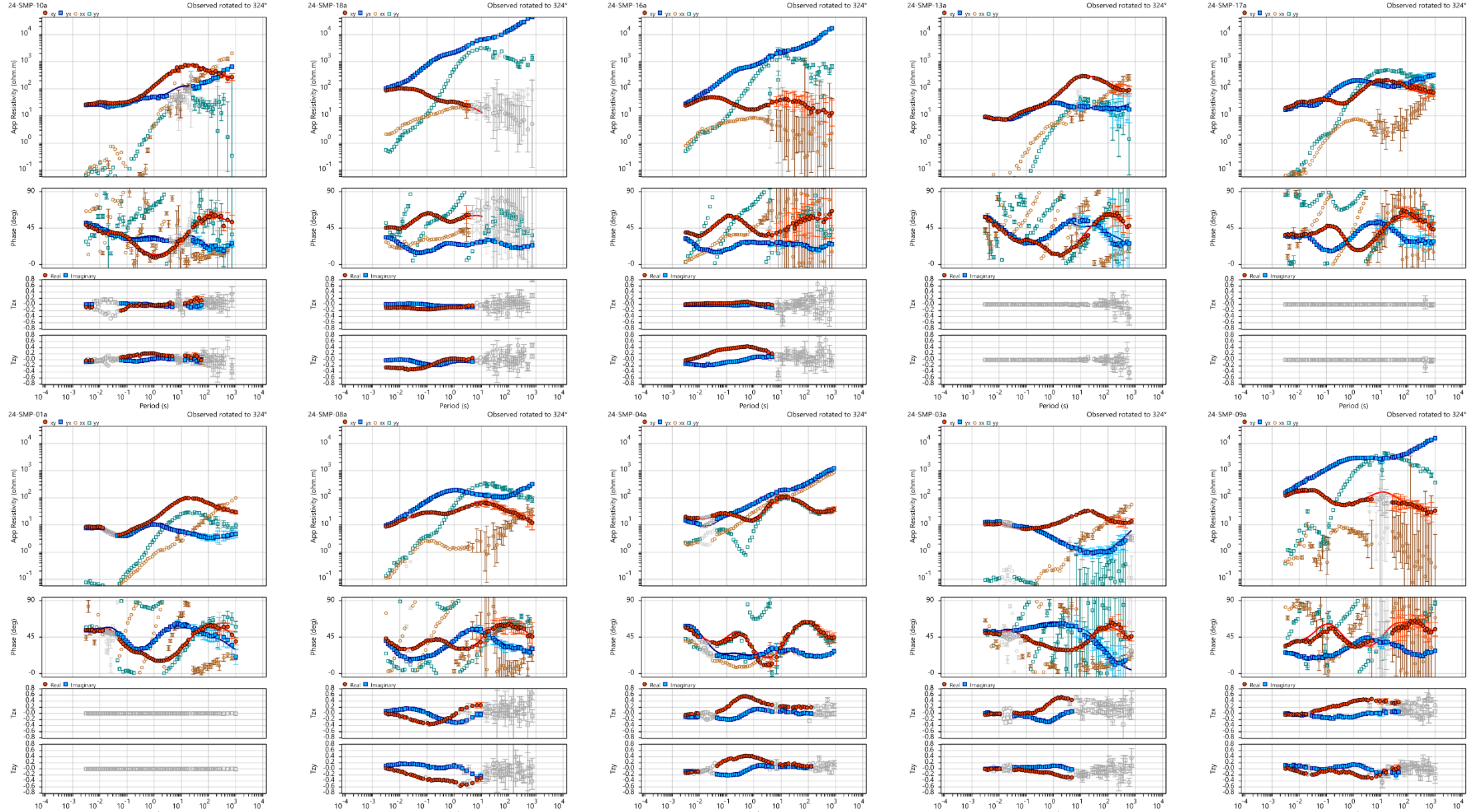
MT Data, 2022 dataset





Data Rotation: 324°

MT Data, 2024 dataset



MT Data Review

MT data show a strong variation over the surveyed area.

Some sites show strong 3D effects already at short periods, in particular the ones located in the NW and SE of the area. Sites located in the central flat area show 3D effects as well, but at longer periods.

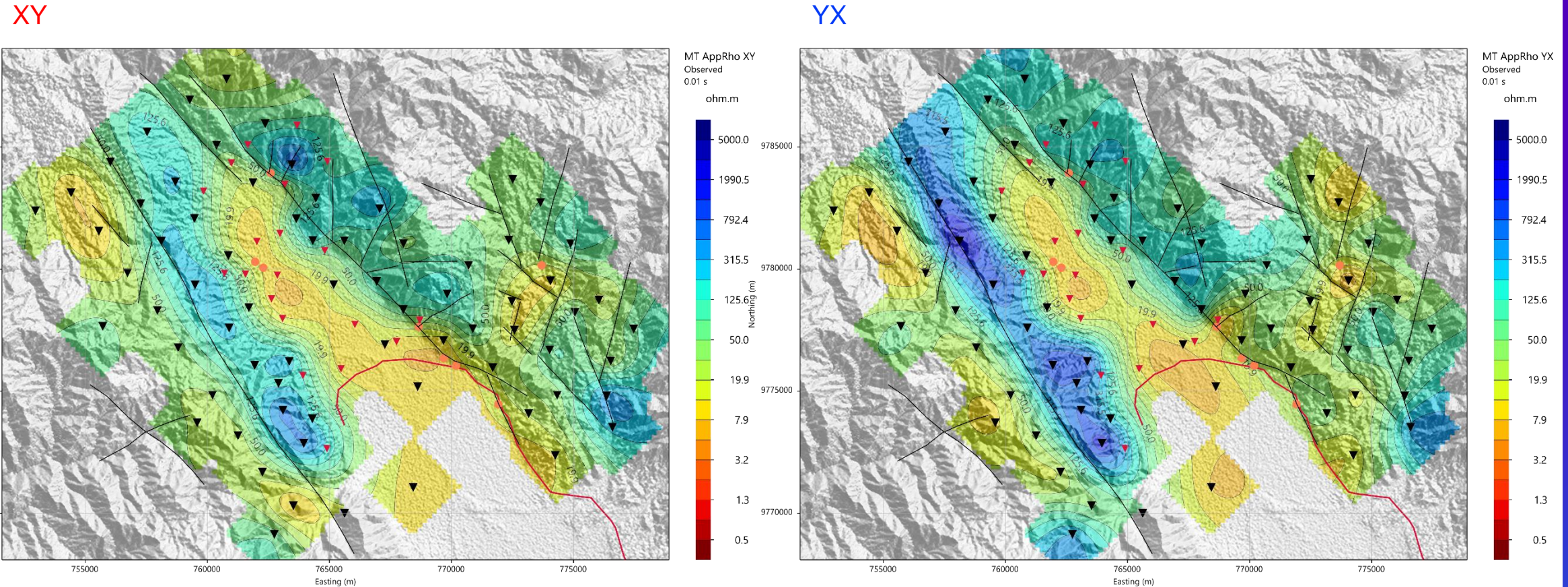
These effects are mainly correlated with topography and geology of the area.

All sites have been carefully edited, masking outliers and poor quality samples. Masked data points are grayed out in the presented sounding plots (previous slides).

Tipper data for the 2024 dataset are available only for some sites, as shown in the previous slide.

All the maps and data presented in this report have masking applied and data are rotated at 324 deg.

Apparent resistivity 100 Hz



MT 2024



MT 2022



Powerline

Manifestations

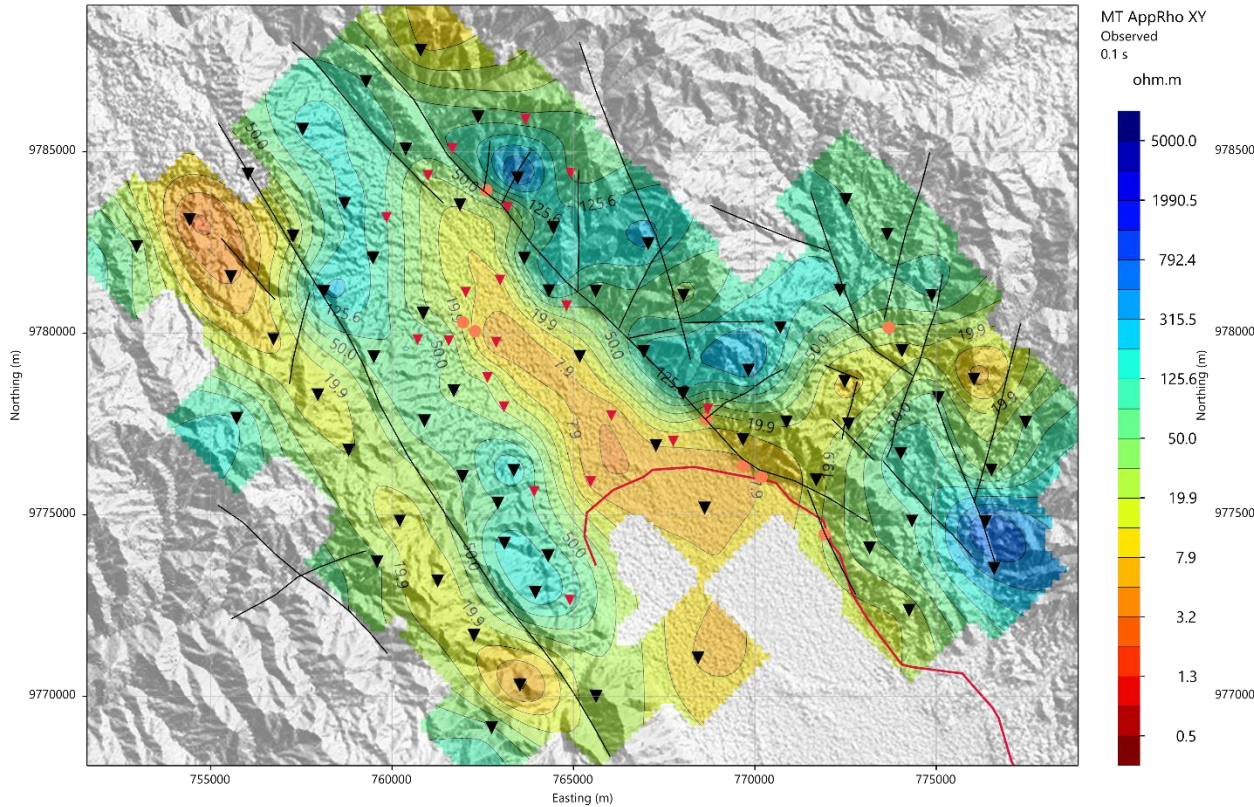


smp_struktur_b_w84_i

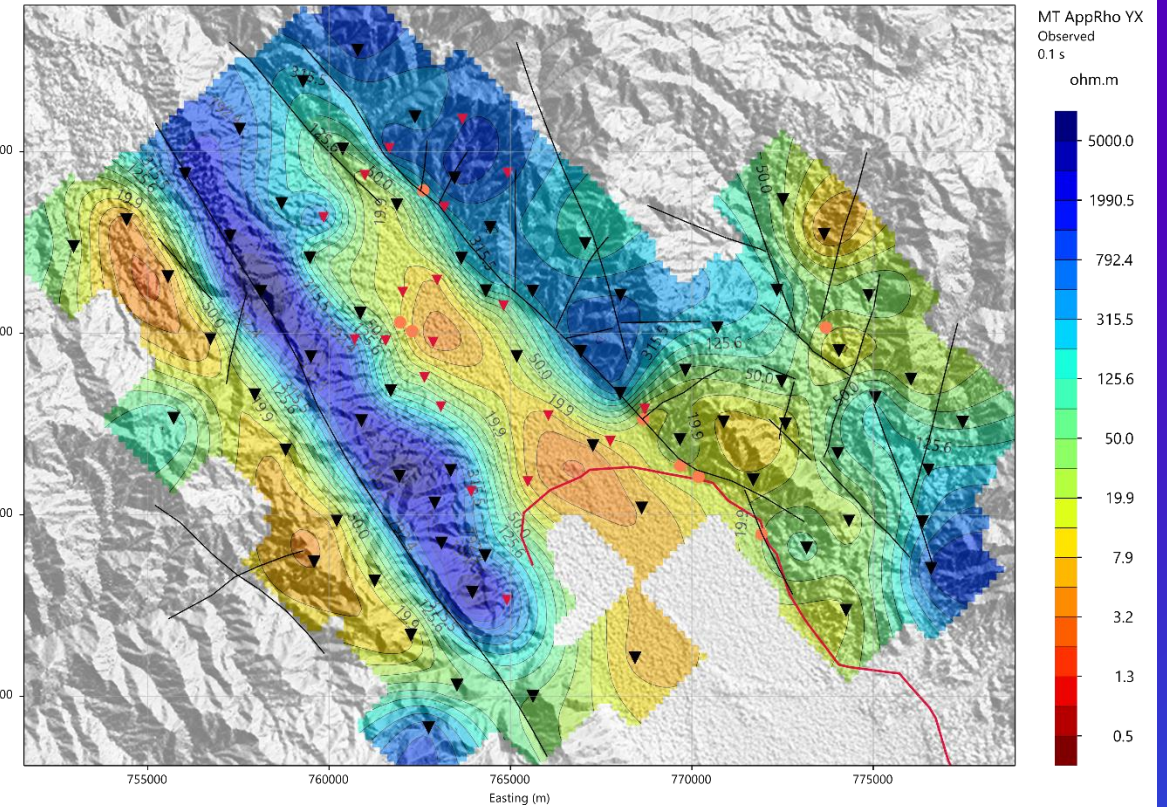


Apparent resistivity 10 Hz

XY



YX



MT 2024



MT 2022



Manifestations



Powerline



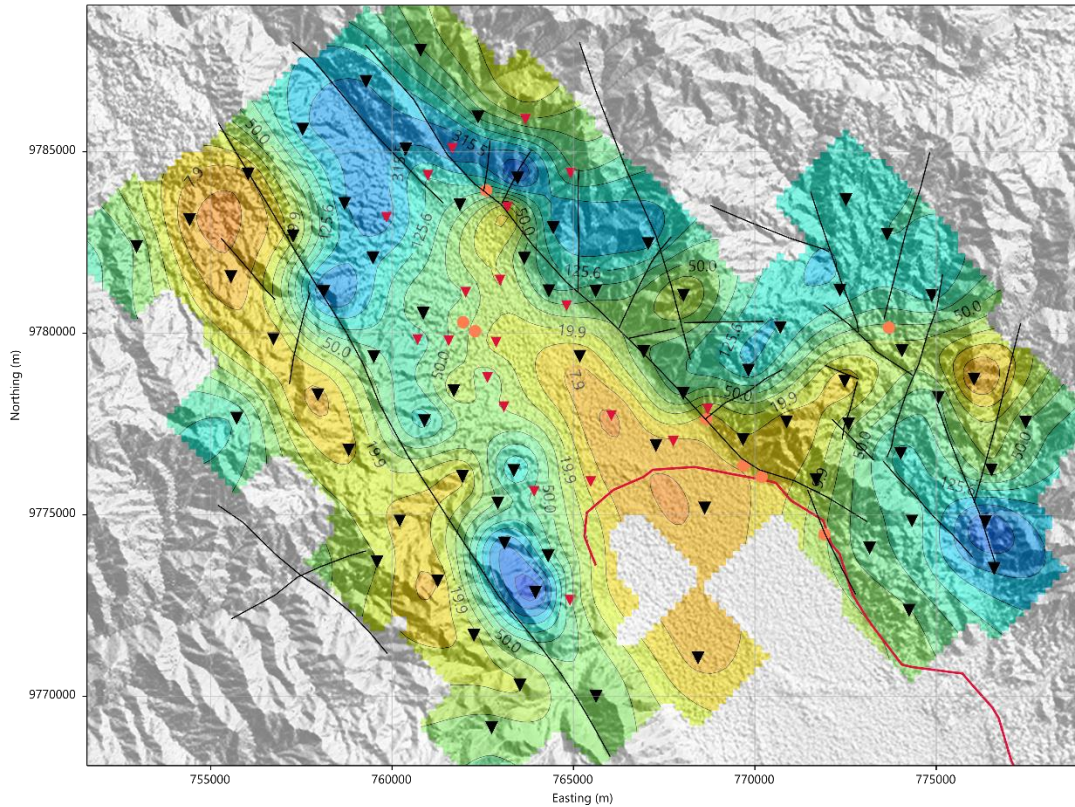
smp_struktur_b_w84_i



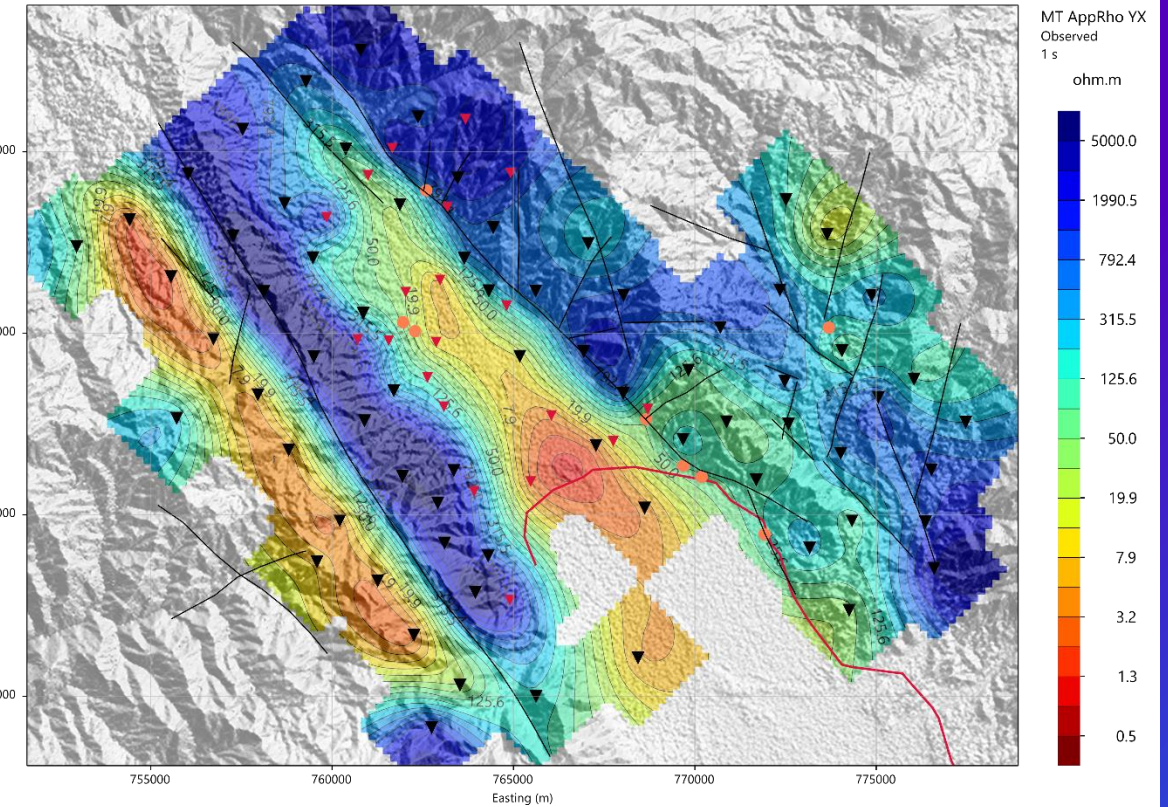


Apparent resistivity 1 Hz

XY



YX



MT 2024



MT 2022



Powerline



Manifestations



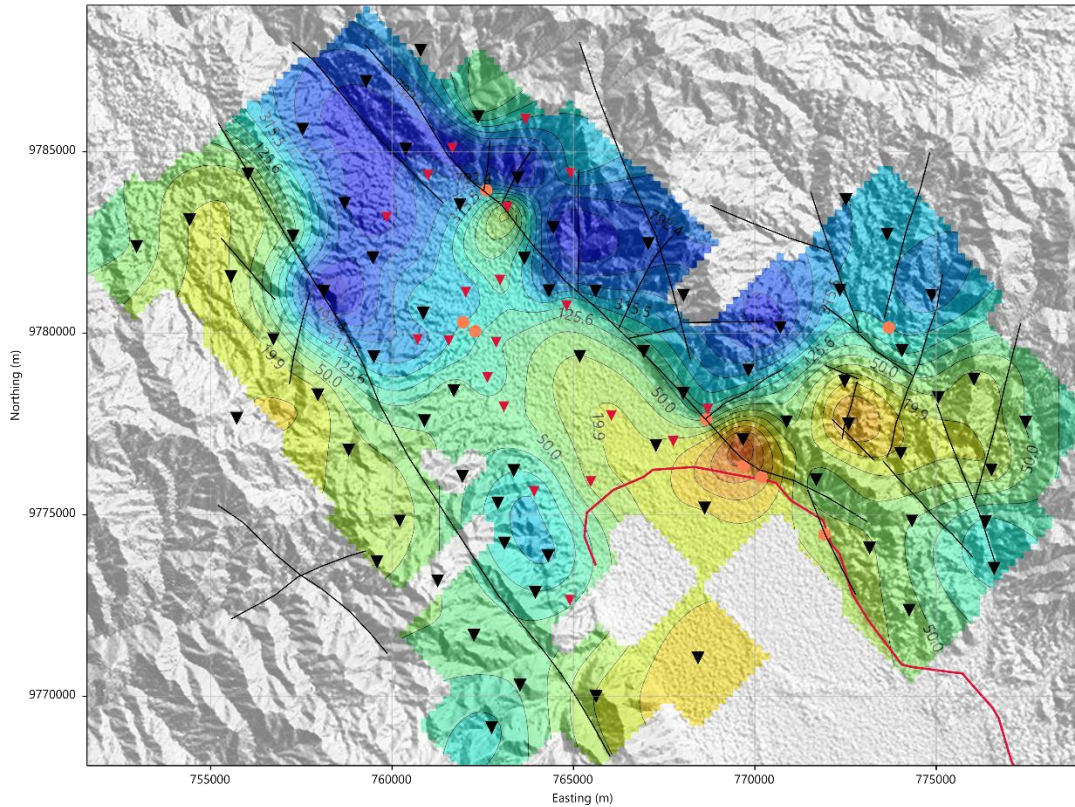
smp_struktur_b_w84_i



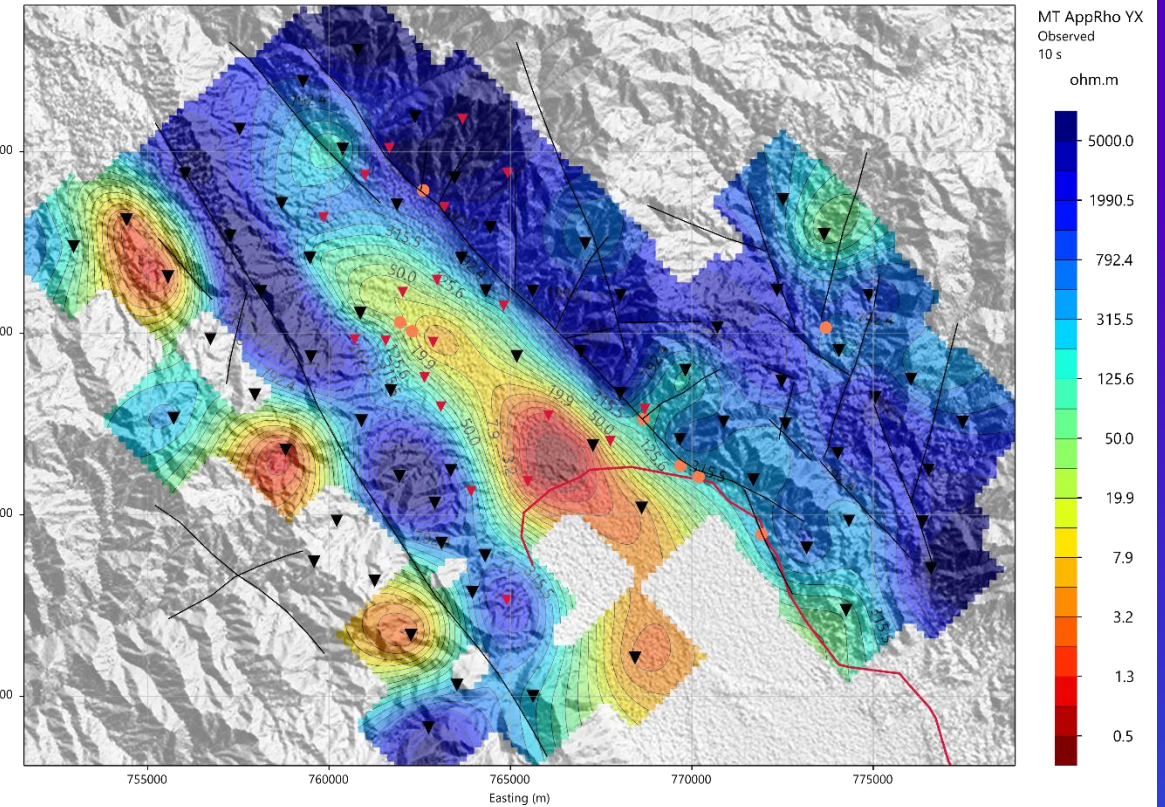


Apparent resistivity 0.1 Hz

XY



YX



MT 2024



MT 2022



Powerline



Manifestations

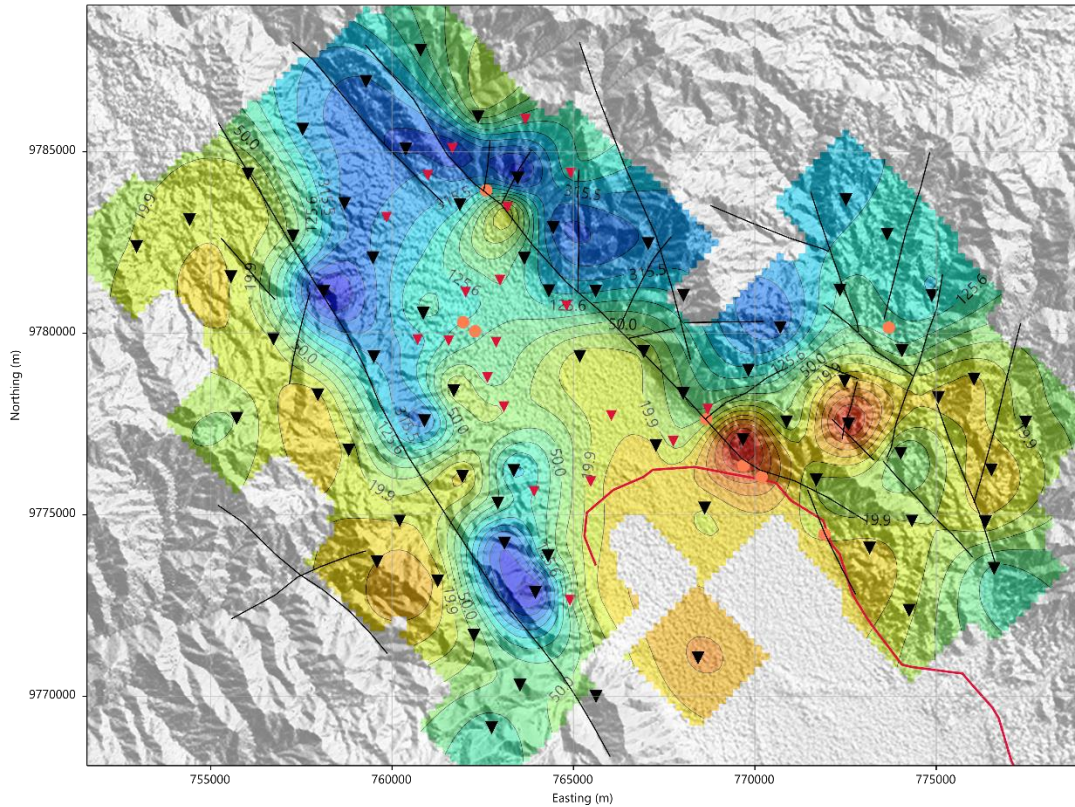


smp_struktur_b_w84_i

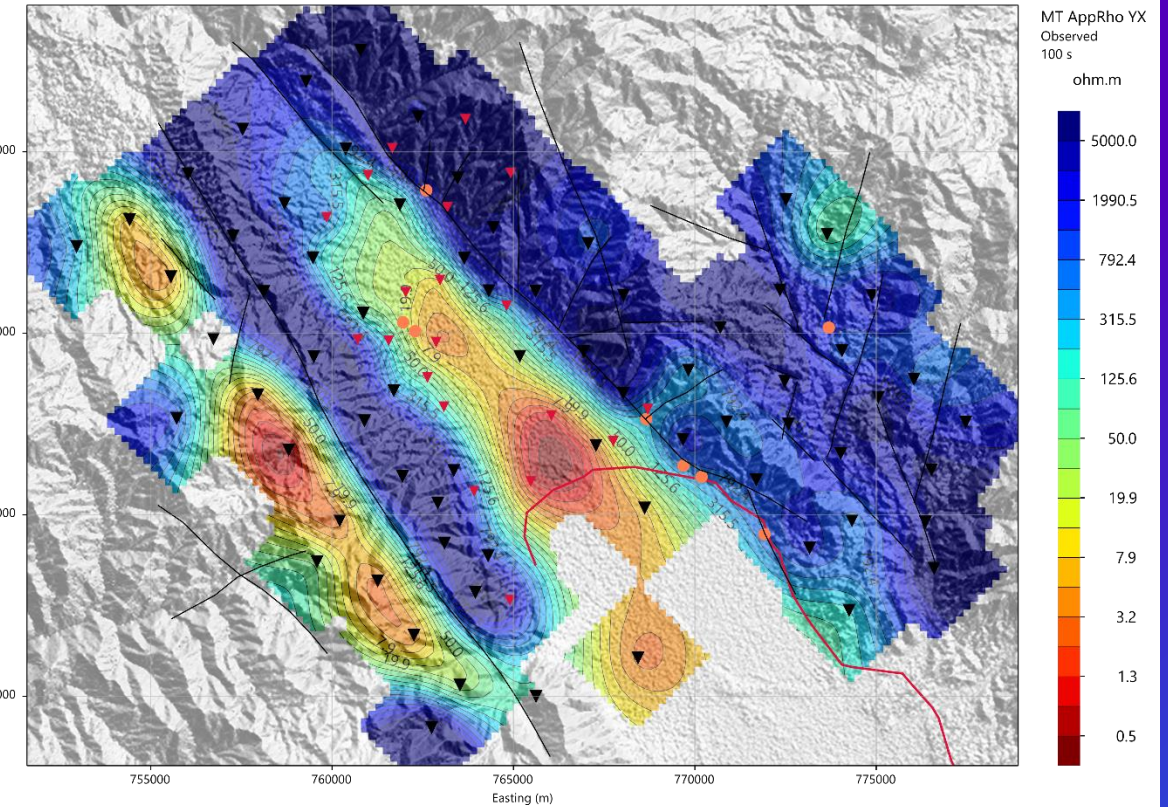


Apparent resistivity 0.01 Hz

XY



YX



MT 2024



MT 2022



Manifestations



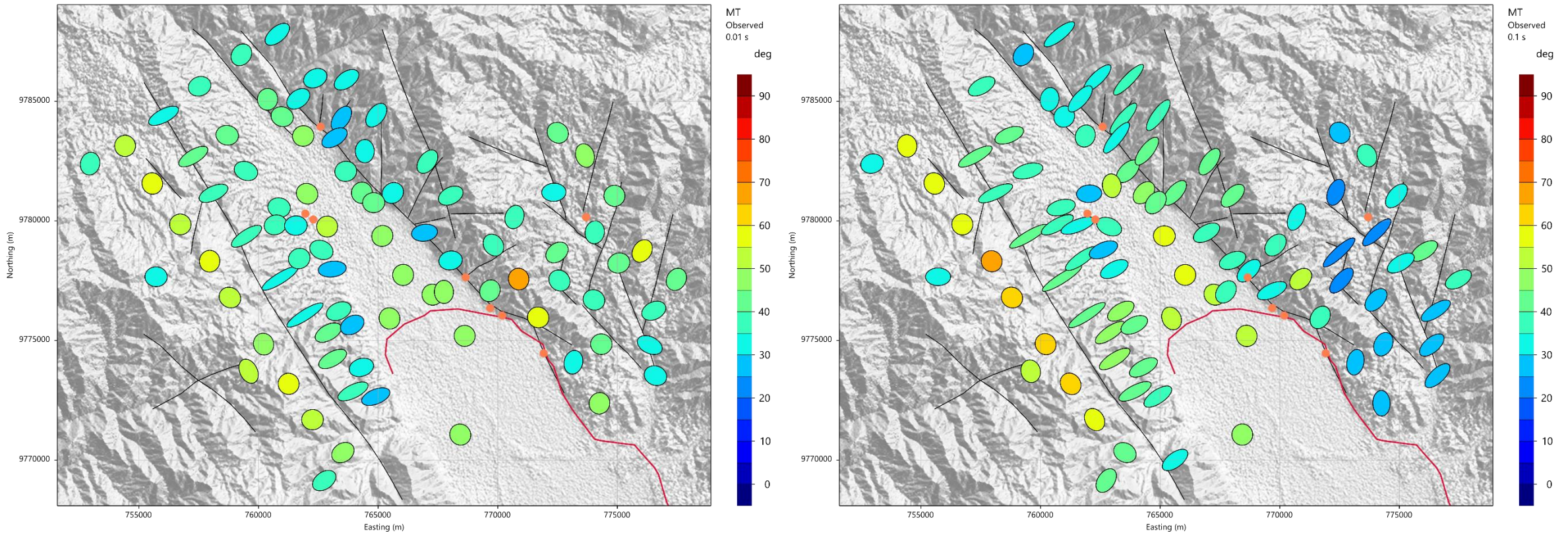
Powerline



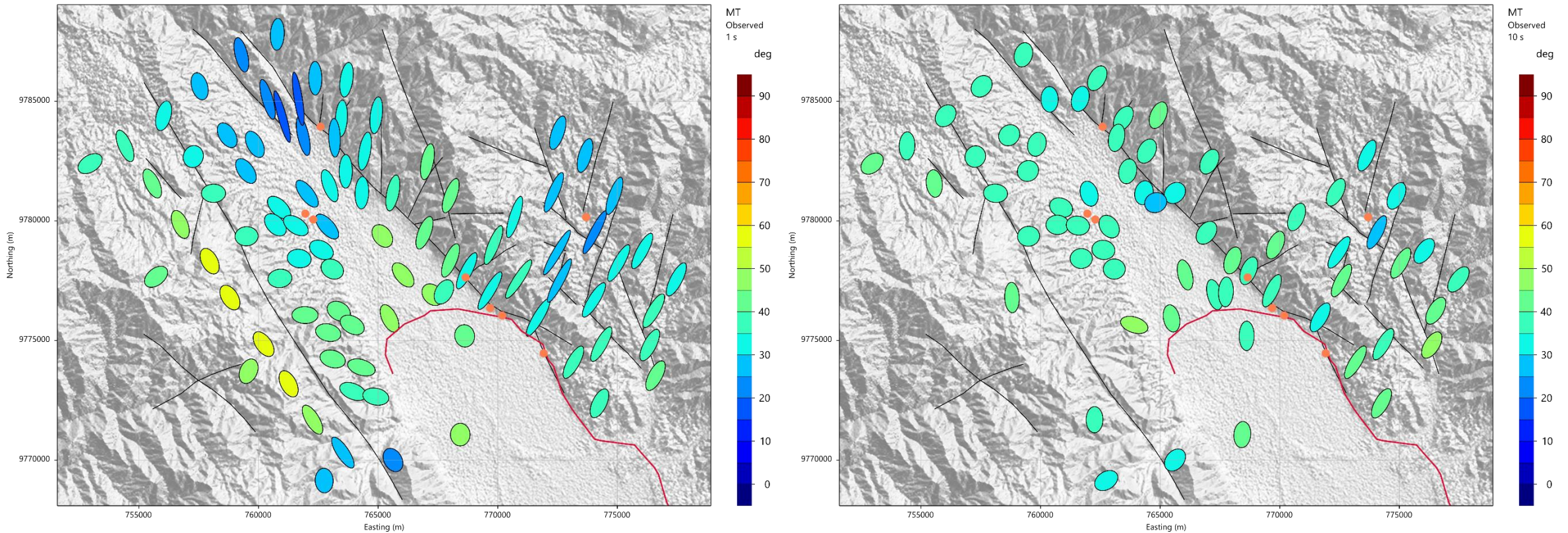
smp_struktur_b_w84_i



Phase Tensors 100 / 10 Hz



Phase Tensors 1 / 0.1 Hz



MT 2024



MT 2022



Manifestations



Powerline

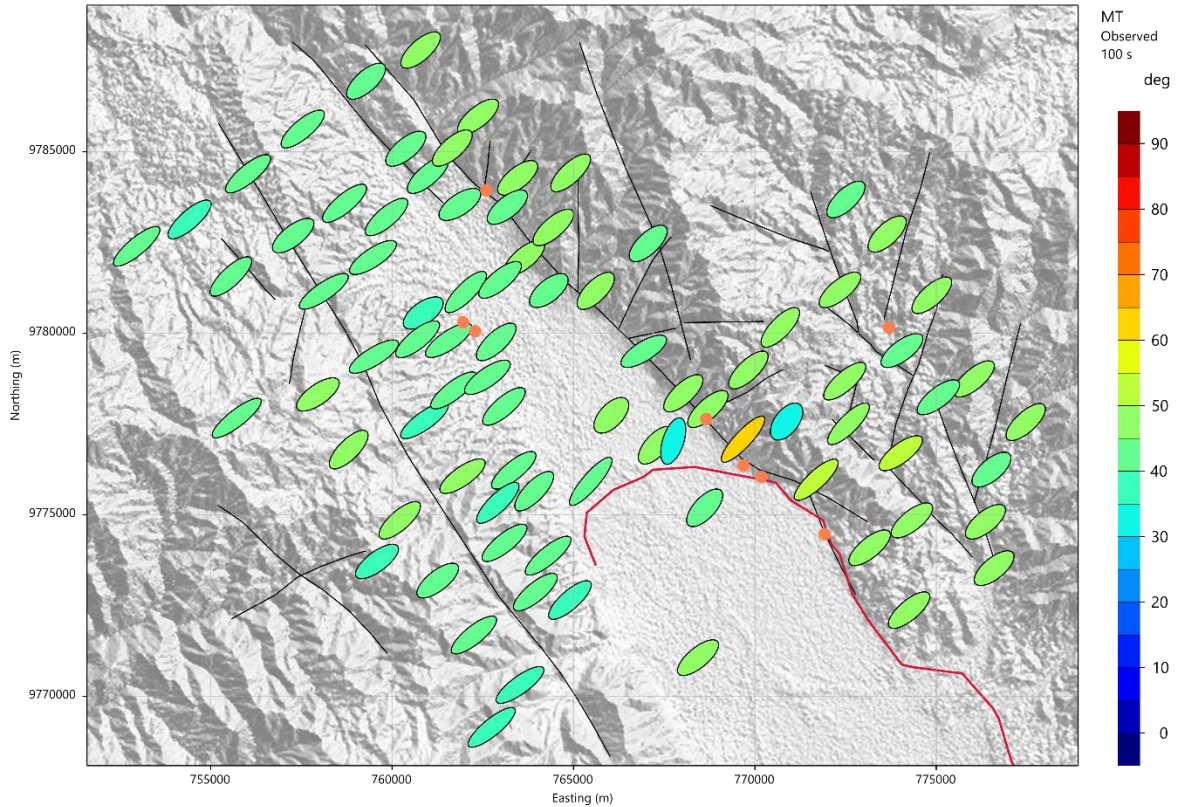


smp_struktur_b_w84_i





Phase Tensors 0.01 Hz



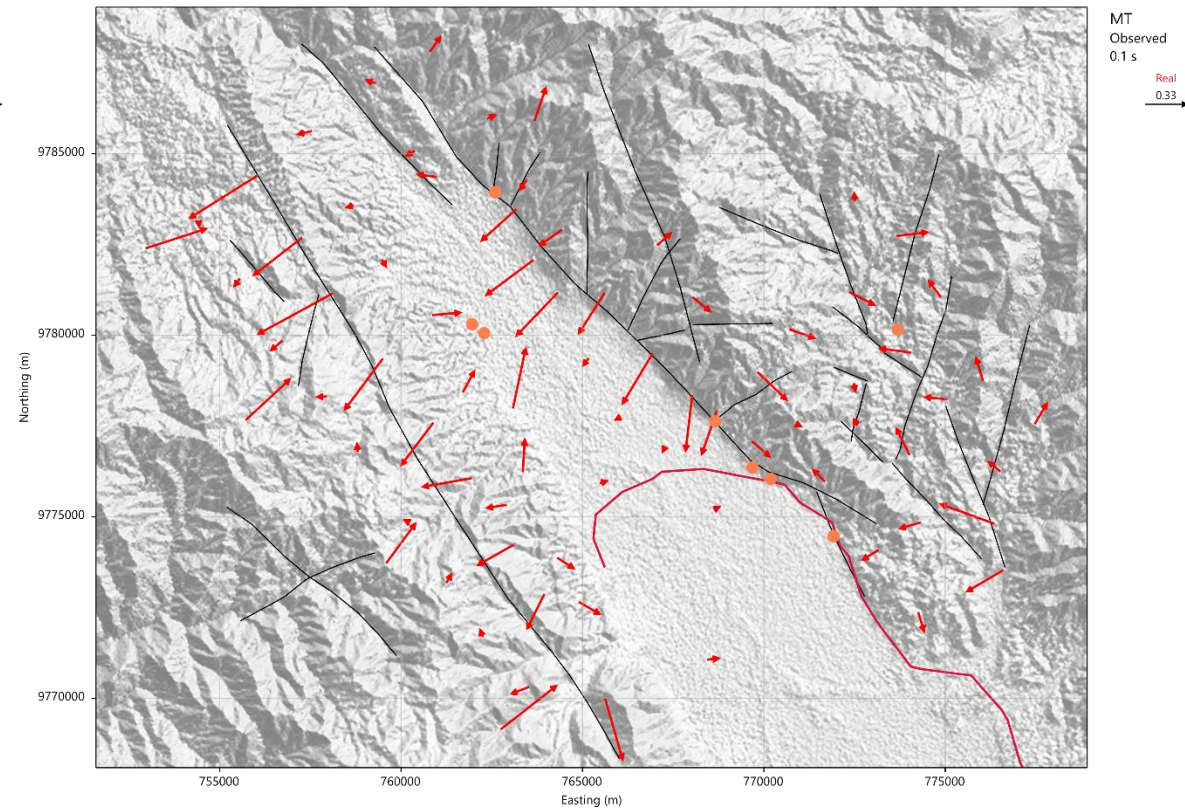
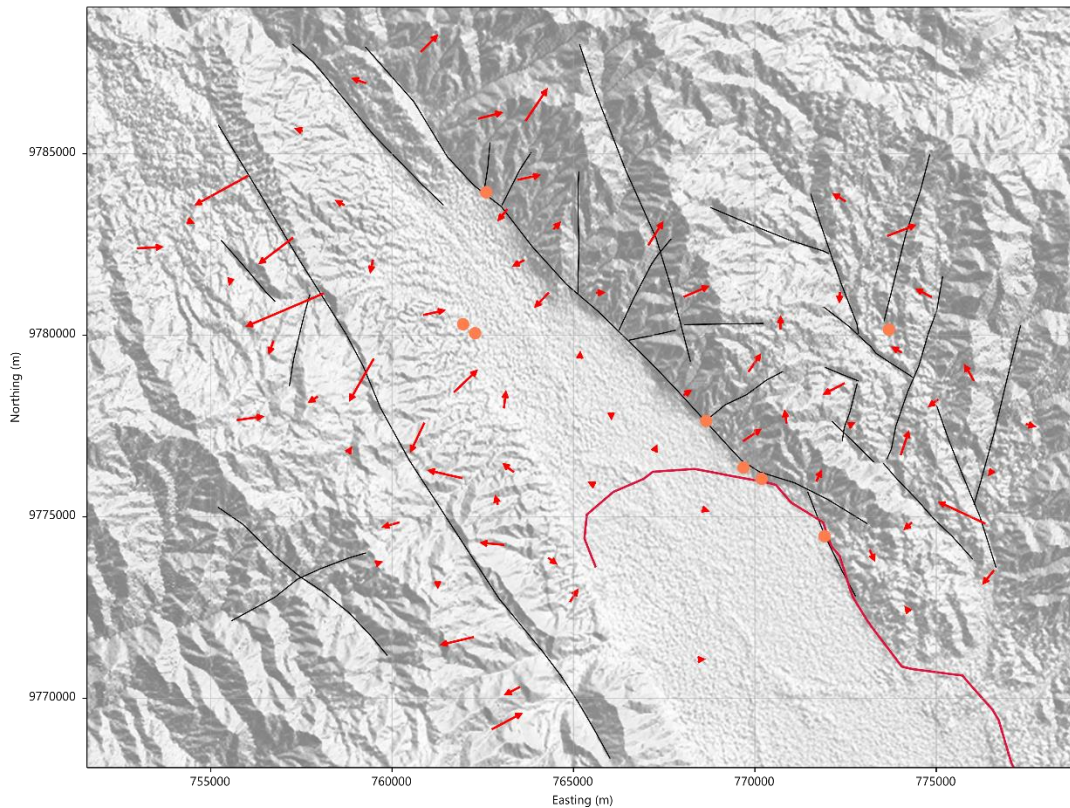
MT 2024





Induction arrows 100 / 10 Hz

Display convention: arrows pointing *towards* conductors.



MT 2024



MT 2022



Powerline



Manifestations

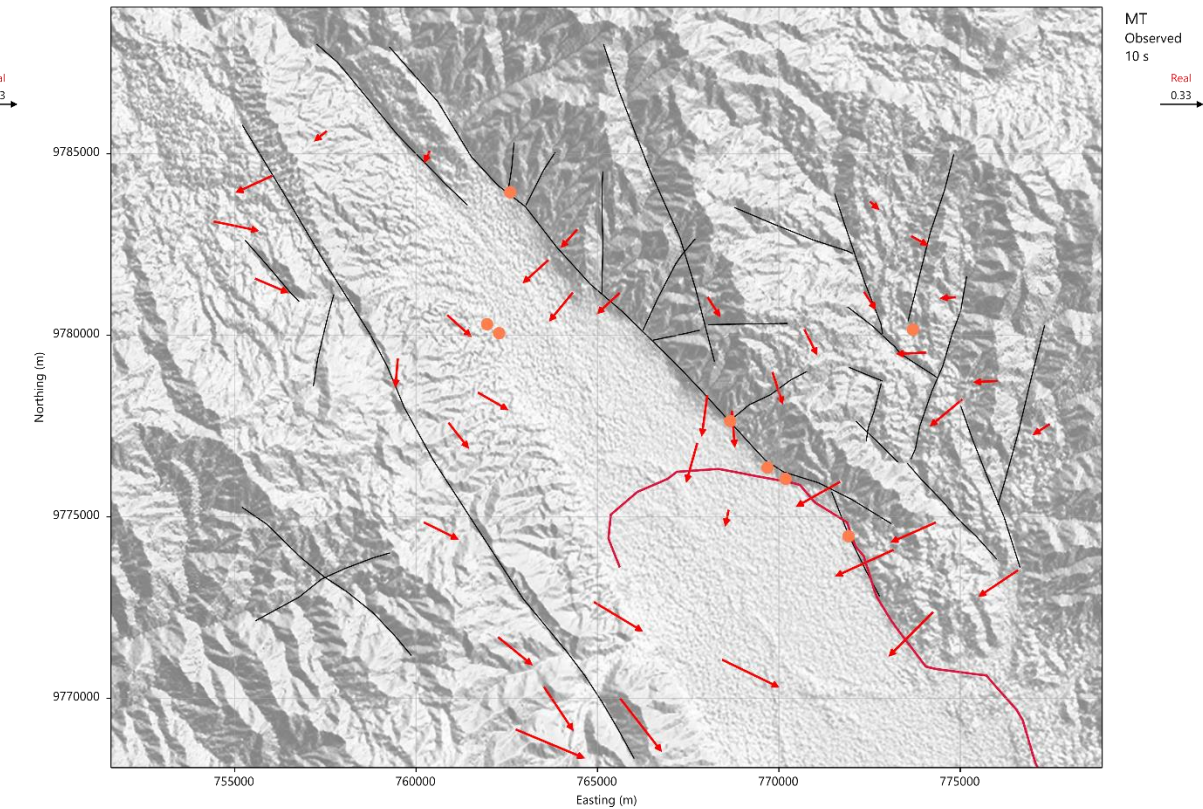
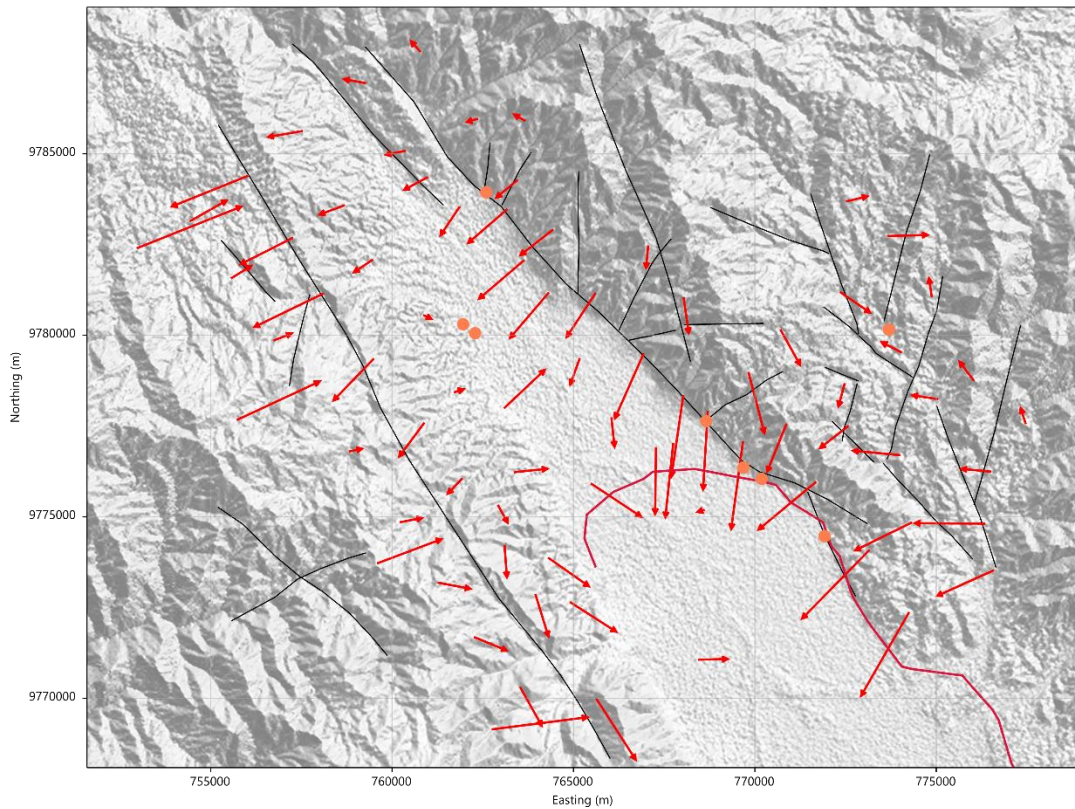


smp_struktur_b_w84_i



Induction arrows 1 / 0.1 Hz

Display convention: arrows pointing *towards* conductors.



MT 2024



MT 2022



Powerline



Manifestations



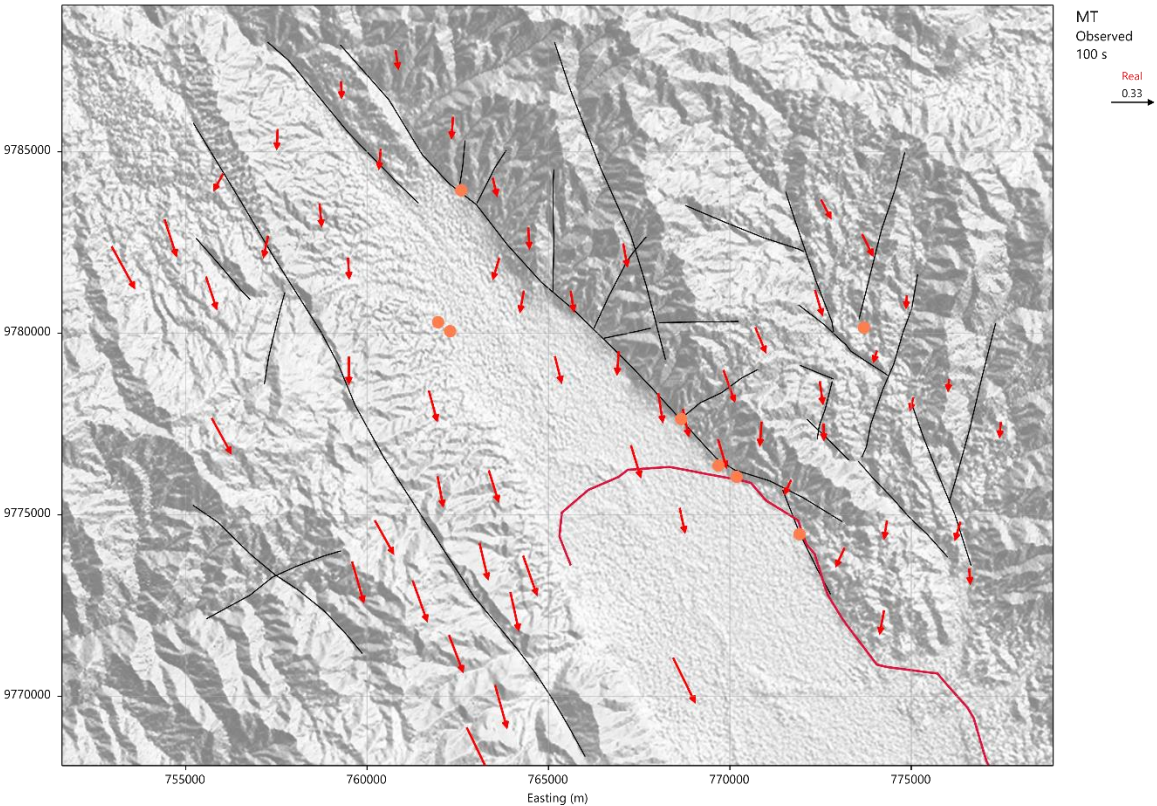
smp_struktur_b_w84_i





Induction arrows 0.01 Hz

Display convention: arrows pointing *towards* conductors.



MT 2024



MT 2022



Powerline

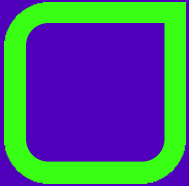


Manifestations



smp_struktur_b_w84_i





GRAVITY DATA

Gravity dataset

Nettleton profiles

Complete Bouguer Anomaly map

Comparison with geological map



Gravity dataset

The gravity dataset provided by PGE consisted of 364 measurements. Almost all readings are located along profiles.

PGE provided gravity sites ID, coordinates, Observed Gravity, Latitude and Terrain correction (inner and outer) and Complete Bouguer anomaly data.

Complete Bouguer Anomaly has been calculated applying a Terrain correction based on SRTM1 (30m) grid and considering a radius of 50km around each station.

Input to 3D modeling is complete Bouguer gravity, and 3D density models are accordingly of relative density, i.e. density is inverted around the reduction density.

One challenge in gravity inversions is to use a reasonable starting density – true shallow density is likely lower, and true deep density higher.

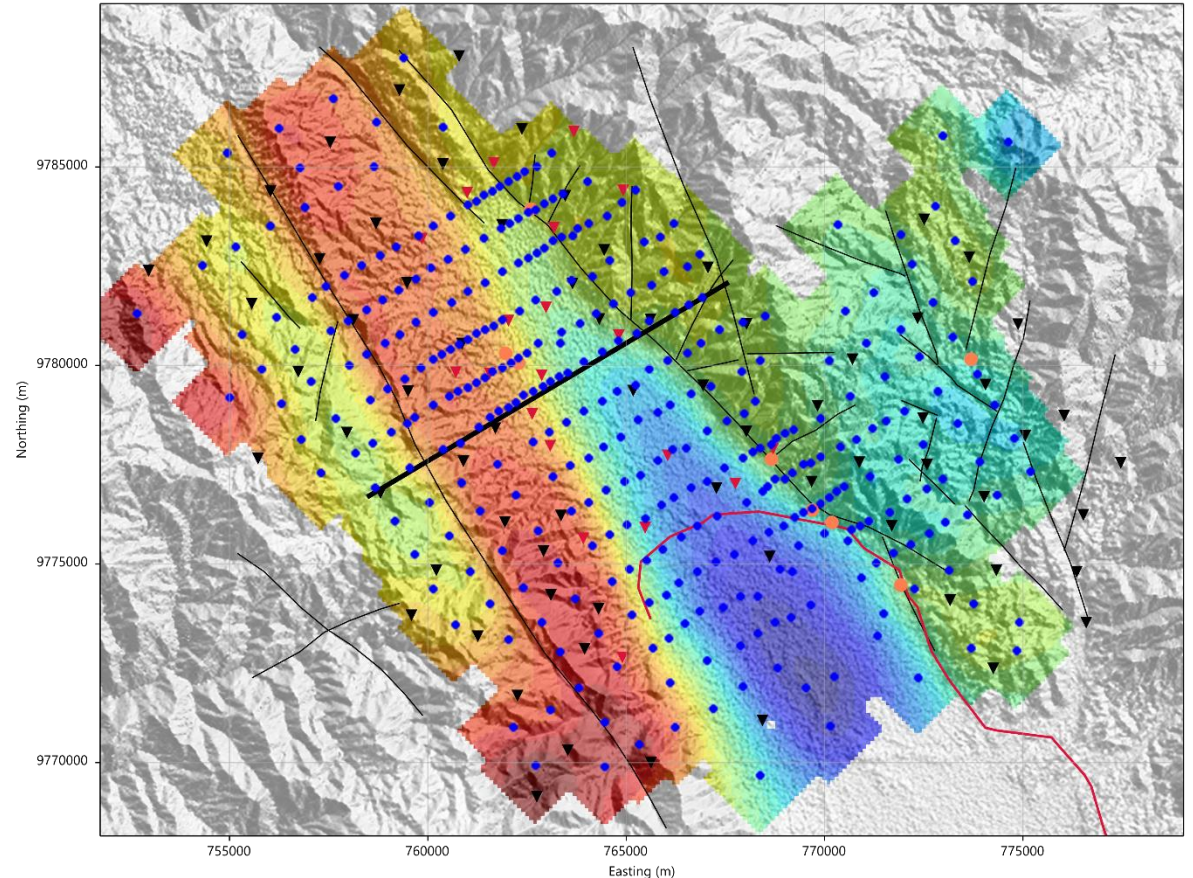
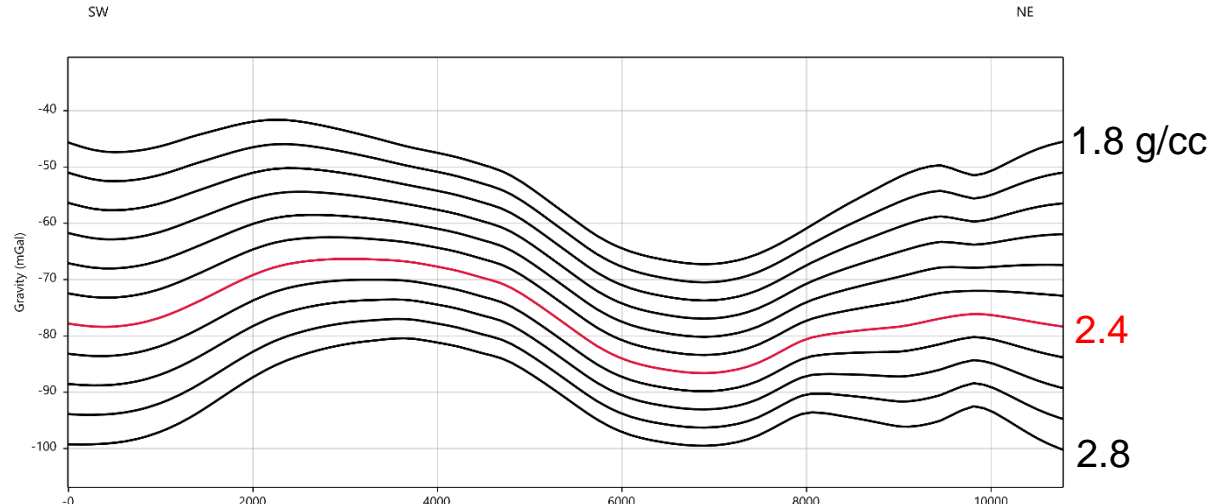
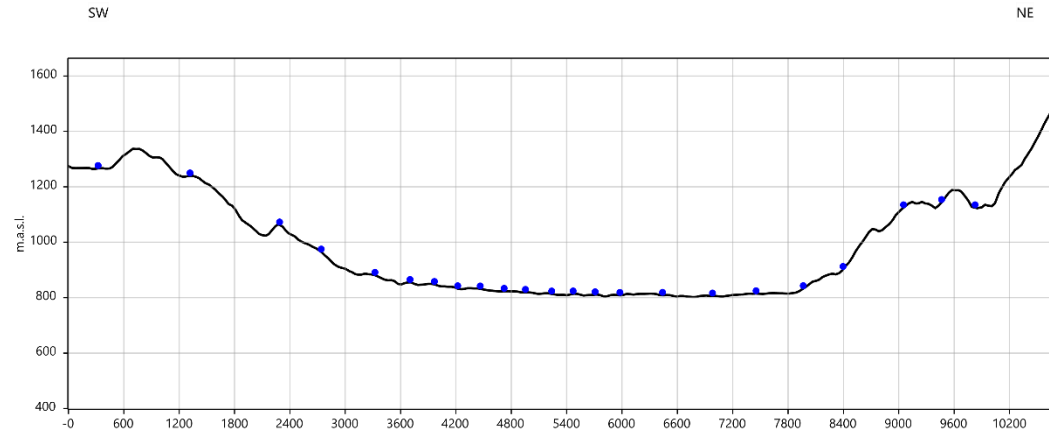
To assess subsurface density, gridded complete Bouguer anomaly at different reduction densities was plotted along a profile and compared with topography (Nettleton technique). In this approach, *low correlation* indicates the reduction density is close to true shallow (i.e. topography dominating) density. 2.4g/cc has been considered a proper value for the reduction density over this area.

Seven gravity measurements have been excluded from the input dataset because close/co-located with other readings or generating single point anomalies.

The total number of gravity sites included in the 3D inversion process is 357.



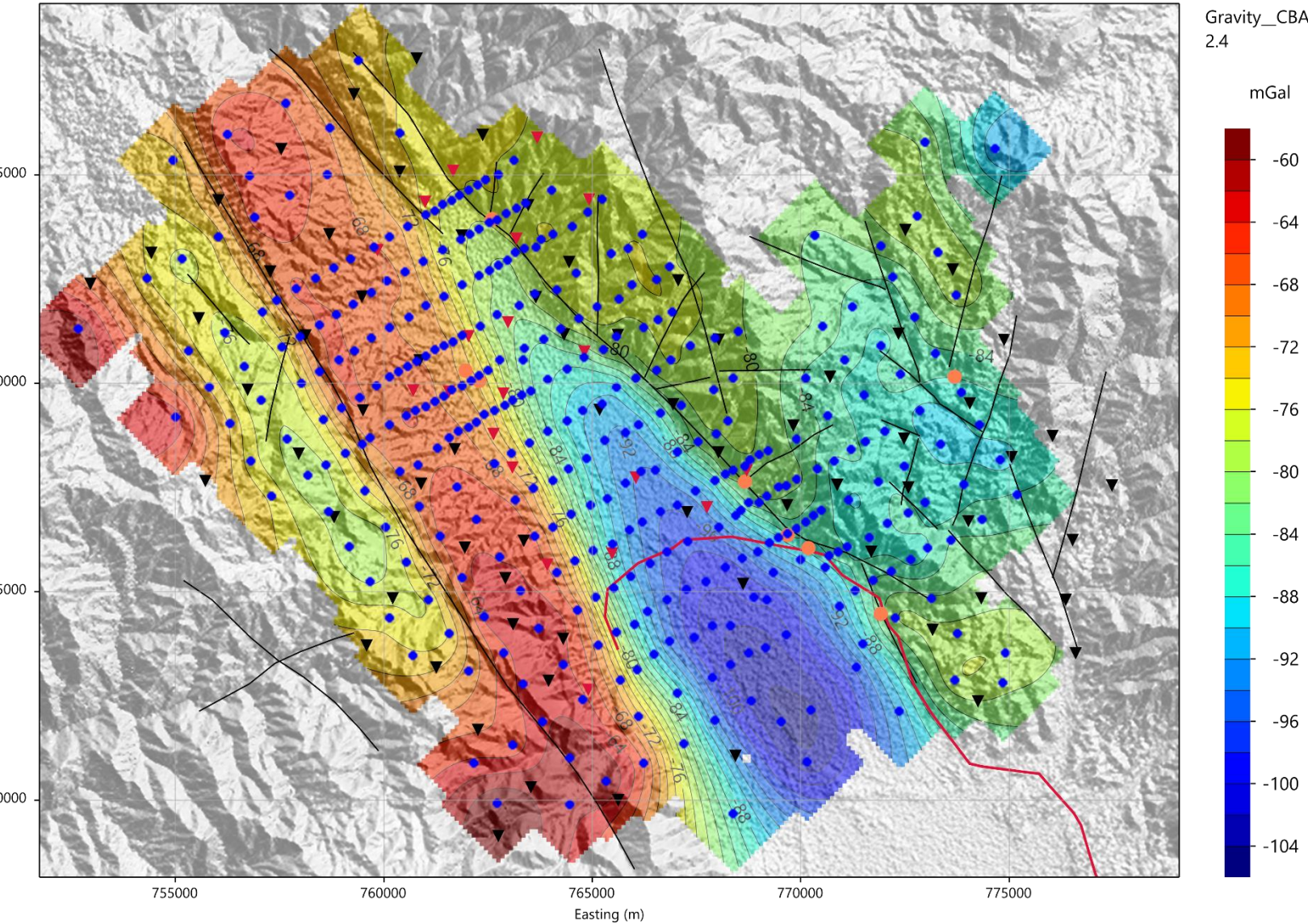
Nettleton technique – CBA and topography



Gridded complete Bouguer anomaly at different reduction densities plotted along a profile and compared with topography (Nettleton technique).

357 measurements are included in the Complete Bouguer anomaly shown in map.

Complete Bouguer Anomaly at 2.40 g/cc data map



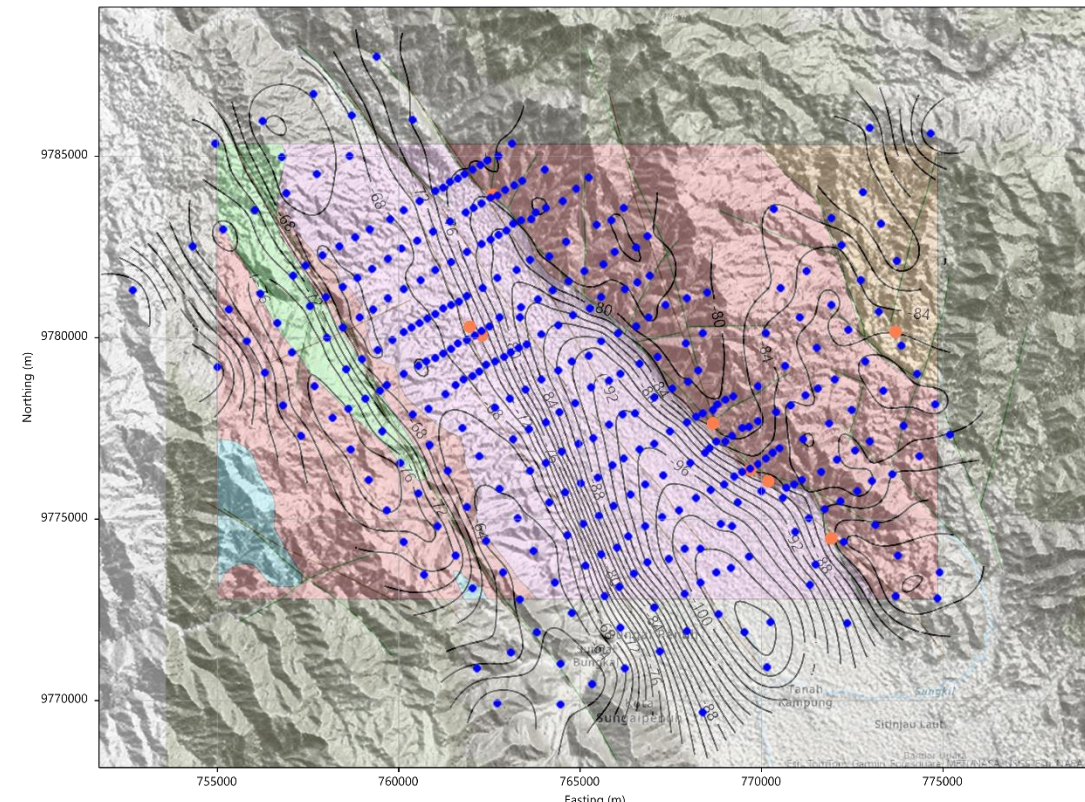
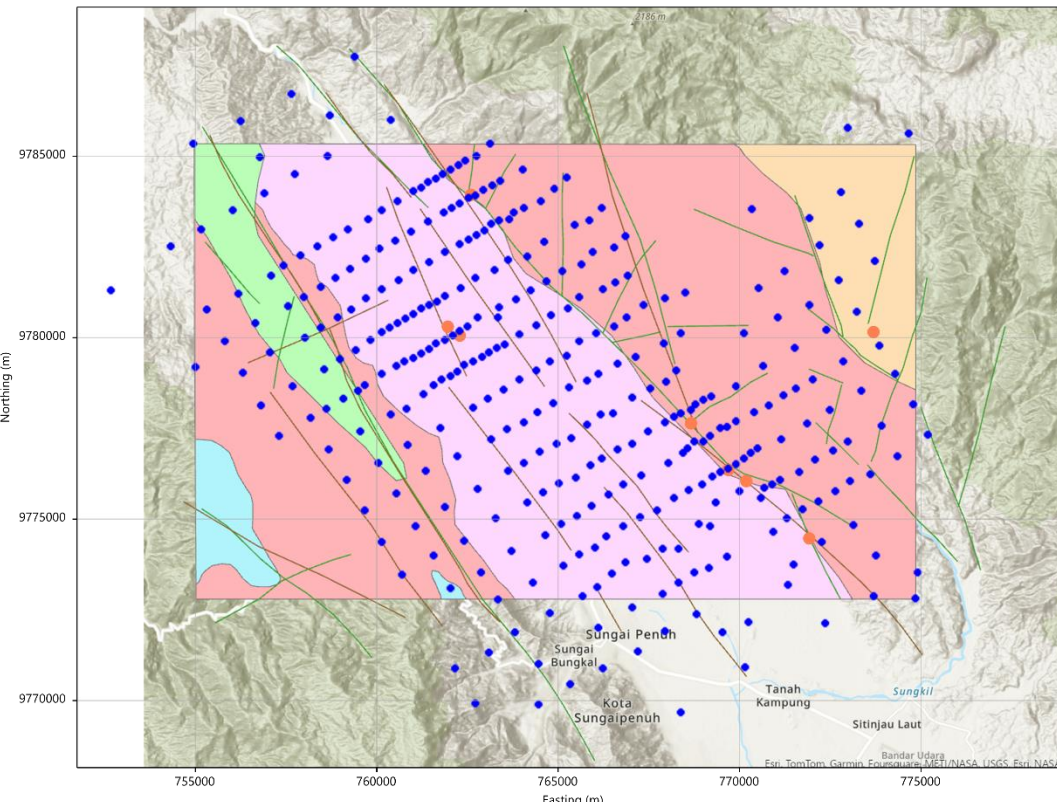
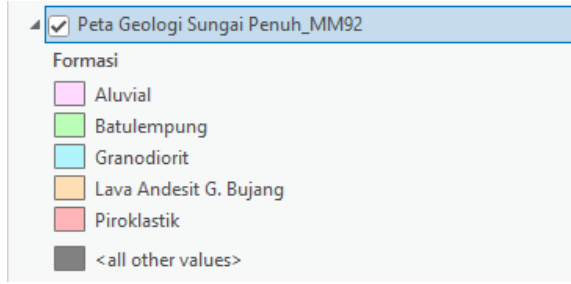
Gravity_CBA
2.4

mGal

-60
-64
-68
-72
-76
-80
-84
-88
-92
-96
-100
-104

Complete Bouguer anomaly
at 2.40g/cc reduction density.
Data from 357 gravity sites,
used as input for the 3D
inversions.

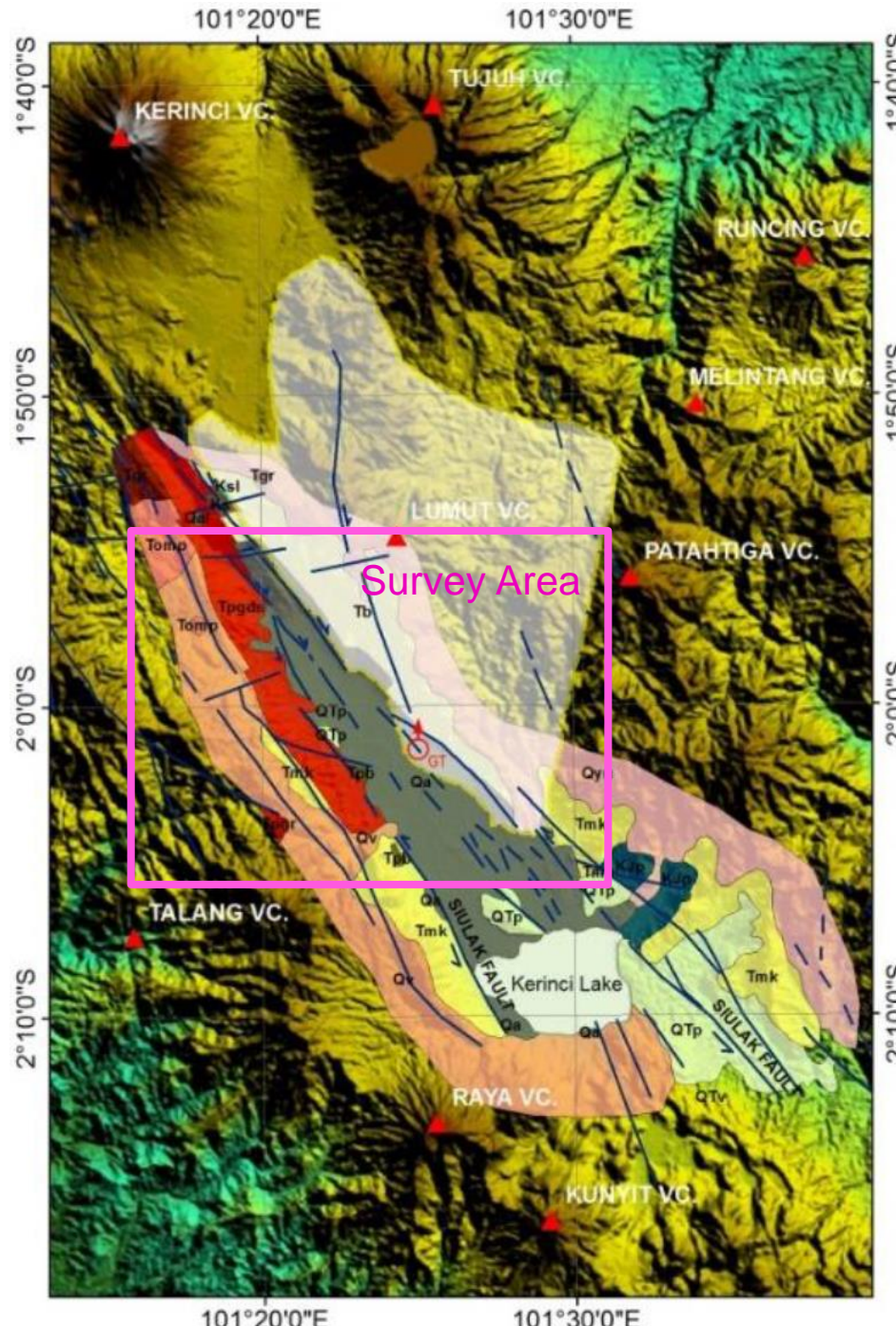
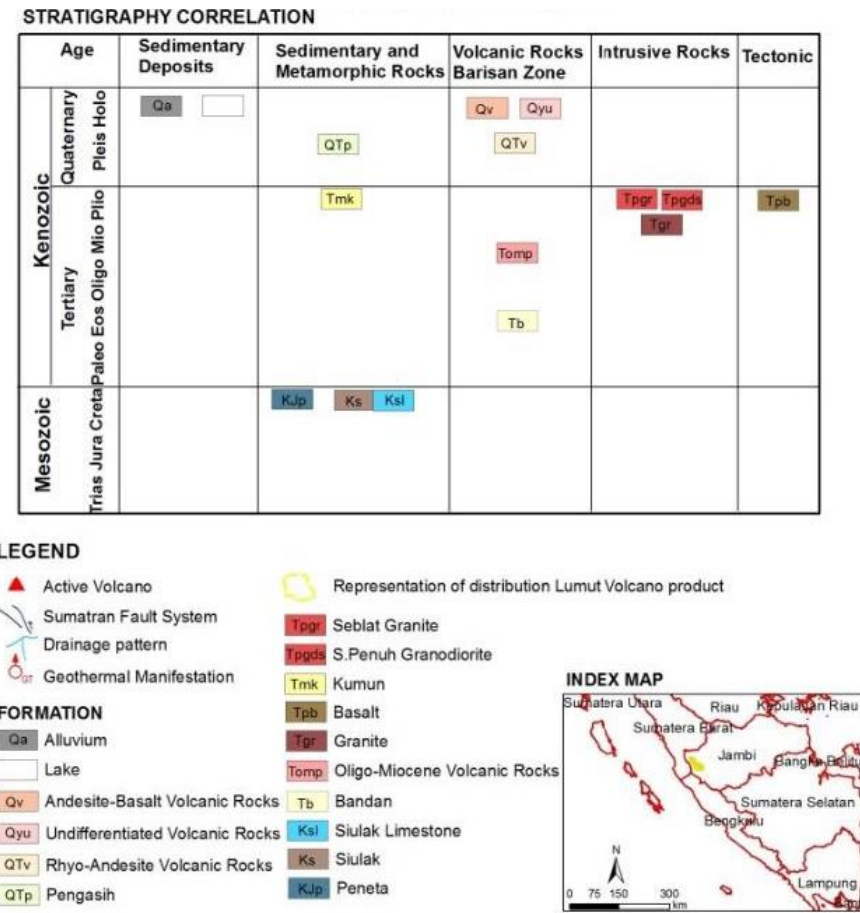
Comparison of Bouguer Anomaly and Geology - I



Geological map – II

Geological map from:

W Jarot et al 2019 IOP Conf. Ser.: Earth Environ. Sci. 391 012051



Comparison of Bouguer Anomaly and Geology - II

LEGEND

- ▲ Active Volcano
- ↙ Sumatran Fault System
- ↔ Drainage pattern
- ♨ Geothermal Manifestation

Representation of distribution Lumut Volcano product

Tpgi Seblat Granite

Tppds S.Penuh Granodiorite

Tmk Kumun

Tpb Basalt

Tgr Granite

Tomp Oligo-Miocene Volcanic Rocks

FORMATION

Qa Alluvium

Lake

Qv Andesite-Basalt Volcanic Rocks

Qyu Undifferentiated Volcanic Rocks

QTv Rhyo-Andesite Volcanic Rocks

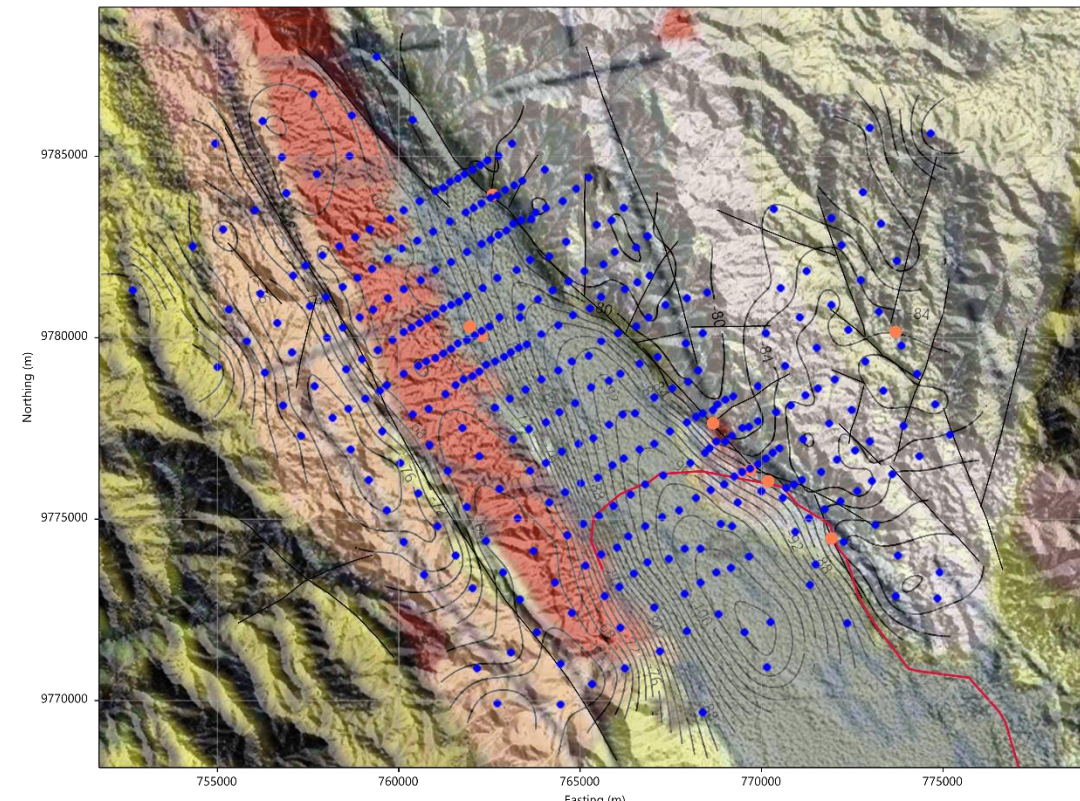
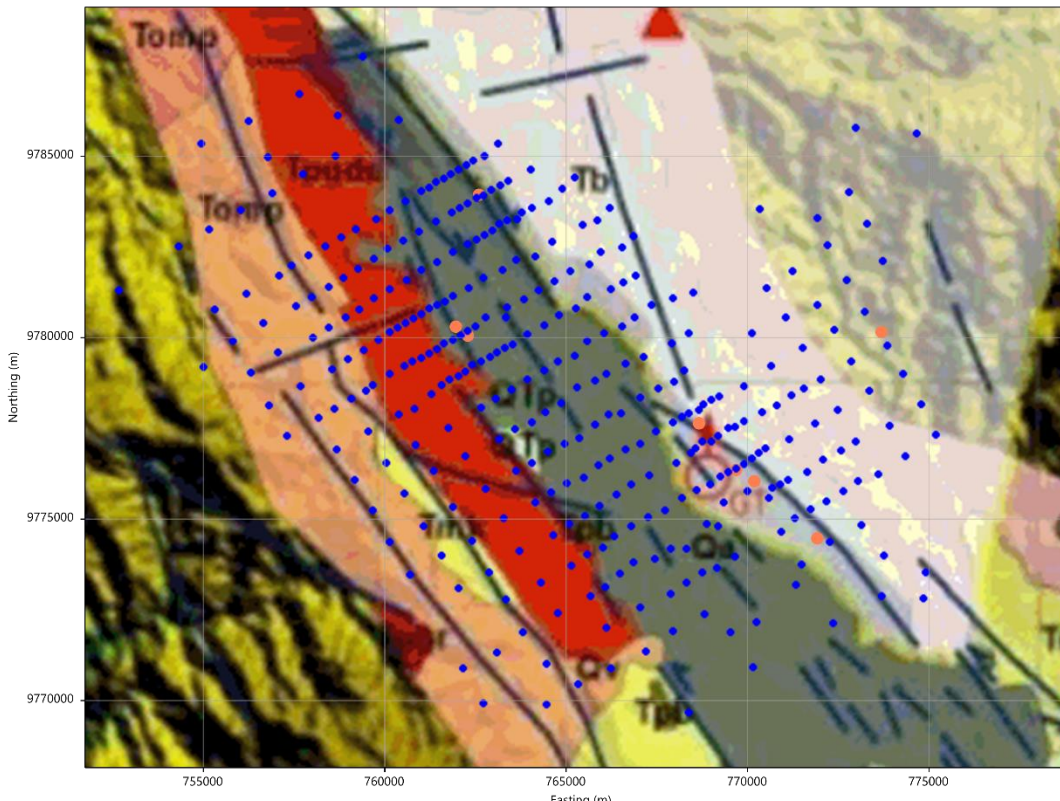
QTP Pengasih

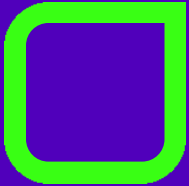
Tb Bandan

Ksl Siulak Limestone

Ks Siulak

KJp Peneta





3D MODELING

Mesh Geometry and Inversion Parameters

Single domain MT and Gravity

JI MT+Gravity

Resistivity and Gravity Sections along Profiles

Resistivity and Gravity Maps at fixed Elevation (JI MT+Gravity)

3D Modeling – Mesh Geometry and MT Inversion Parameters

Model:

Core cell size: 250m x 250m x 25m

Rotation: 36° counterclockwise from East
Cells: 1,917,201

Initial resistivity: 100 Ωm

Topography from DEM SRTM1, 30m
Bathymetry from DEM SRTM15

MT 3D Inversion parameters (MT02/07):

Data inverted: # 90 sites

Full tensor complex Impedances
and Magnetic transfer functions

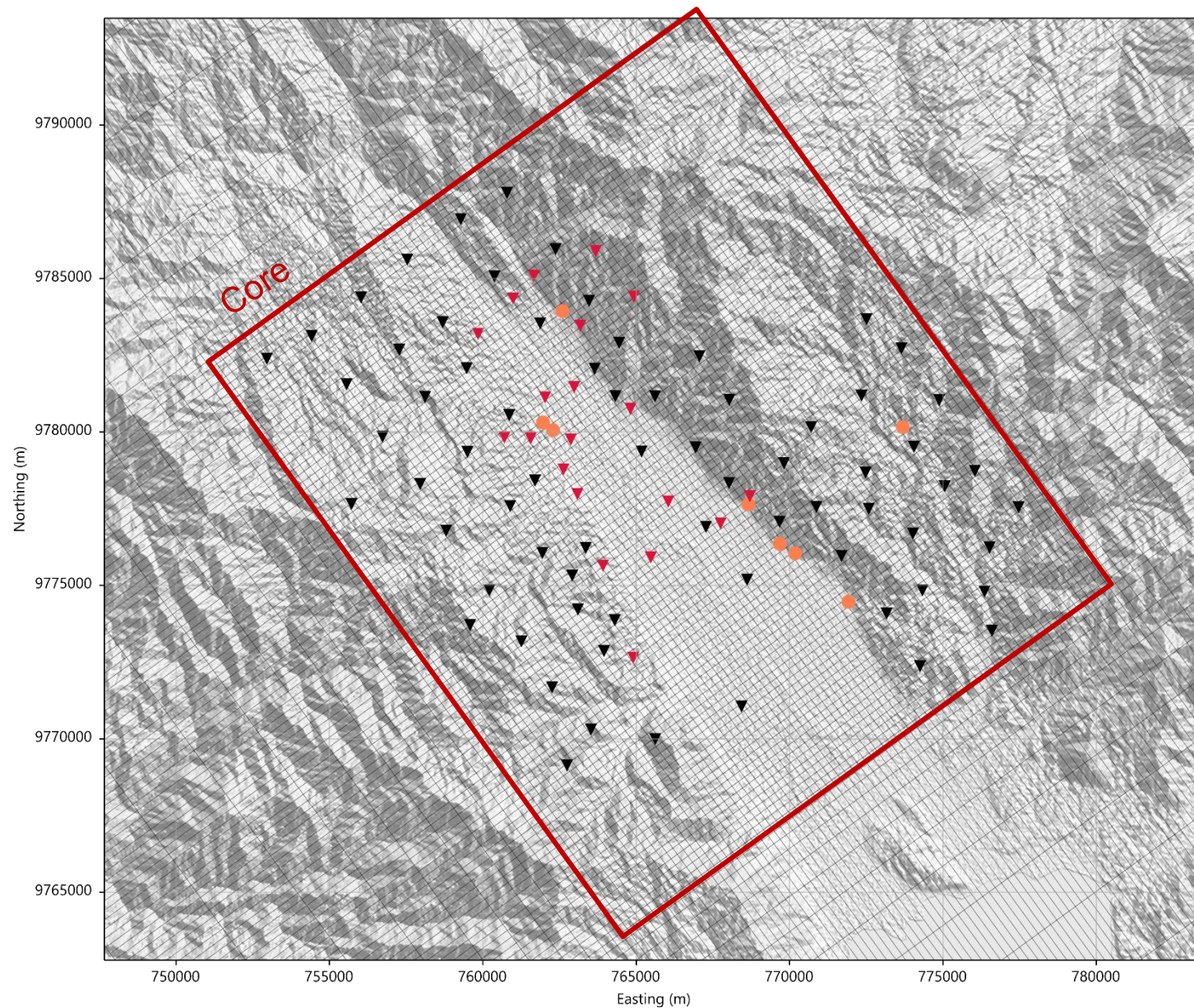
Error Floors: Z: 5%
Tz: 0.02 Absolute

Frequencies: 0.001 to 251 Hz (total 28)

Smoothing: horizontal (τ_{H}): 1
vertical (τ_{V}): 0.004 / 0.002 (MT02 / MT07)

Distortions: Weight: 1,000 Damping: 1

Data fit: rms = 1.18 (50 + 30 iterations)



3D Modeling – Gravity Inversion Parameters

Model:

Core cell size: 250m x 250m x 25m

Rotation: 36° counterclockwise from East
Cells: 1,917,201

Initial density: (2.2 g/cc) / -0.2 g/cc at surface
(2.6 g/cc) / +0.2 g/cc at -2,000m depth
Reference density: 2.4 g/cc

Topography from DEM SRTM1, 30m
Bathymetry from DEM SRTM15

Gravity 3D Inversion parameters (GR13):

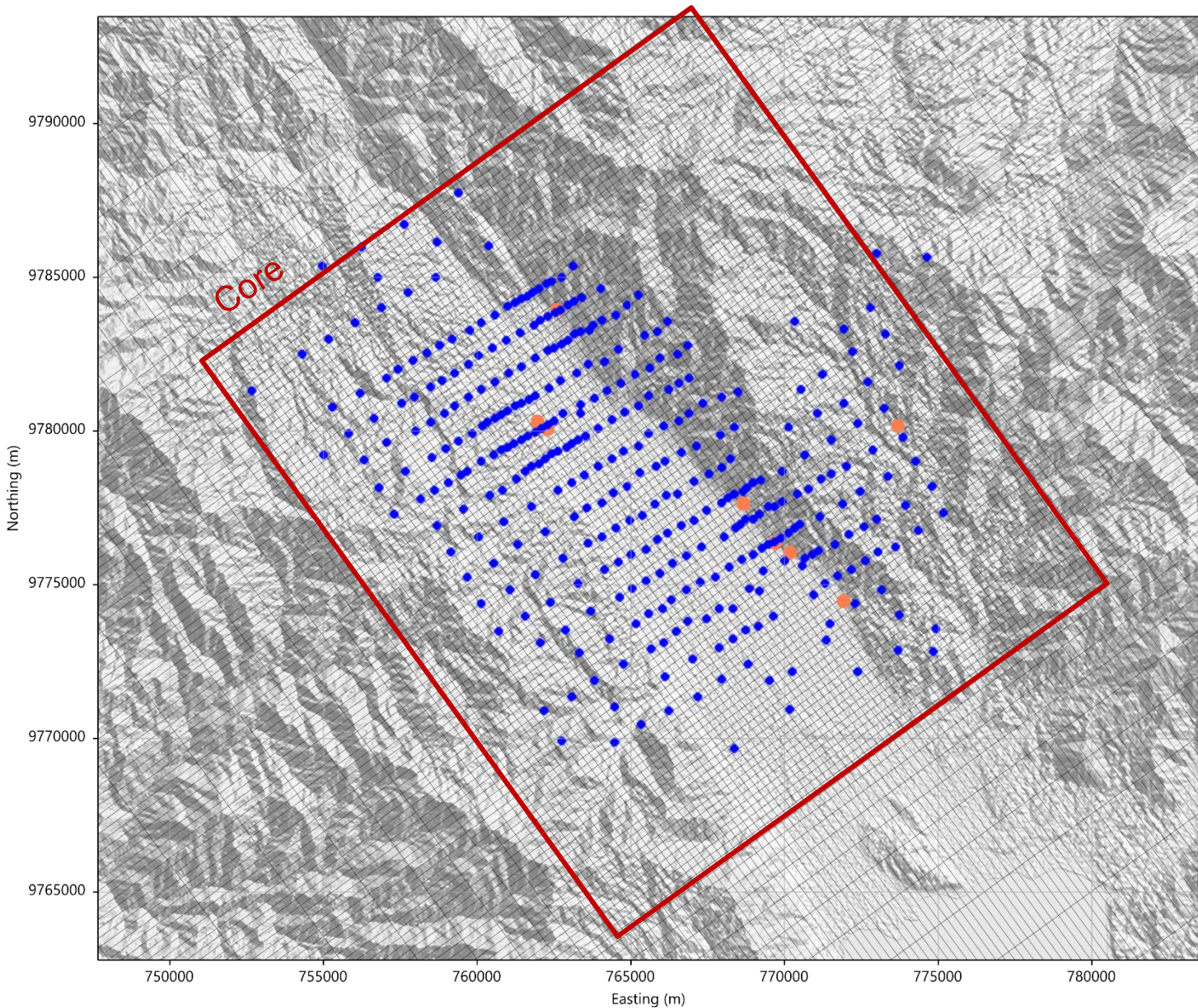
Data inverted: # 357 measurement points

Error Floors: Absolute error: 0.3 mGal

Smoothing: horizontal (τ_H): 0.2
vertical (τ_V): 0.003

Li&Oldenburg: Beta: 1.8
 z_0 : 500m

Data fit: rms = 1.16 (100 iterations)



3D Modeling – JI Inversion Parameters (JI03)



Models:

Starting resistivity and density models identical to the models used for single domain inversions.

MT +Gravity 3D Inversion parameters (JI03):

MT Data: # 90 sites
Full tensor complex Impedances and Magnetic transfer functions

Error Floors: Z: 5%
Tz: 0.02 Absolute

Frequencies: 0.001 to 251 Hz (total 28)

Smoothing: horizontal (τ_{H}): 1
vertical (τ_{V}): 0.002

Distortions: Weight: 1,000 Damping: 1

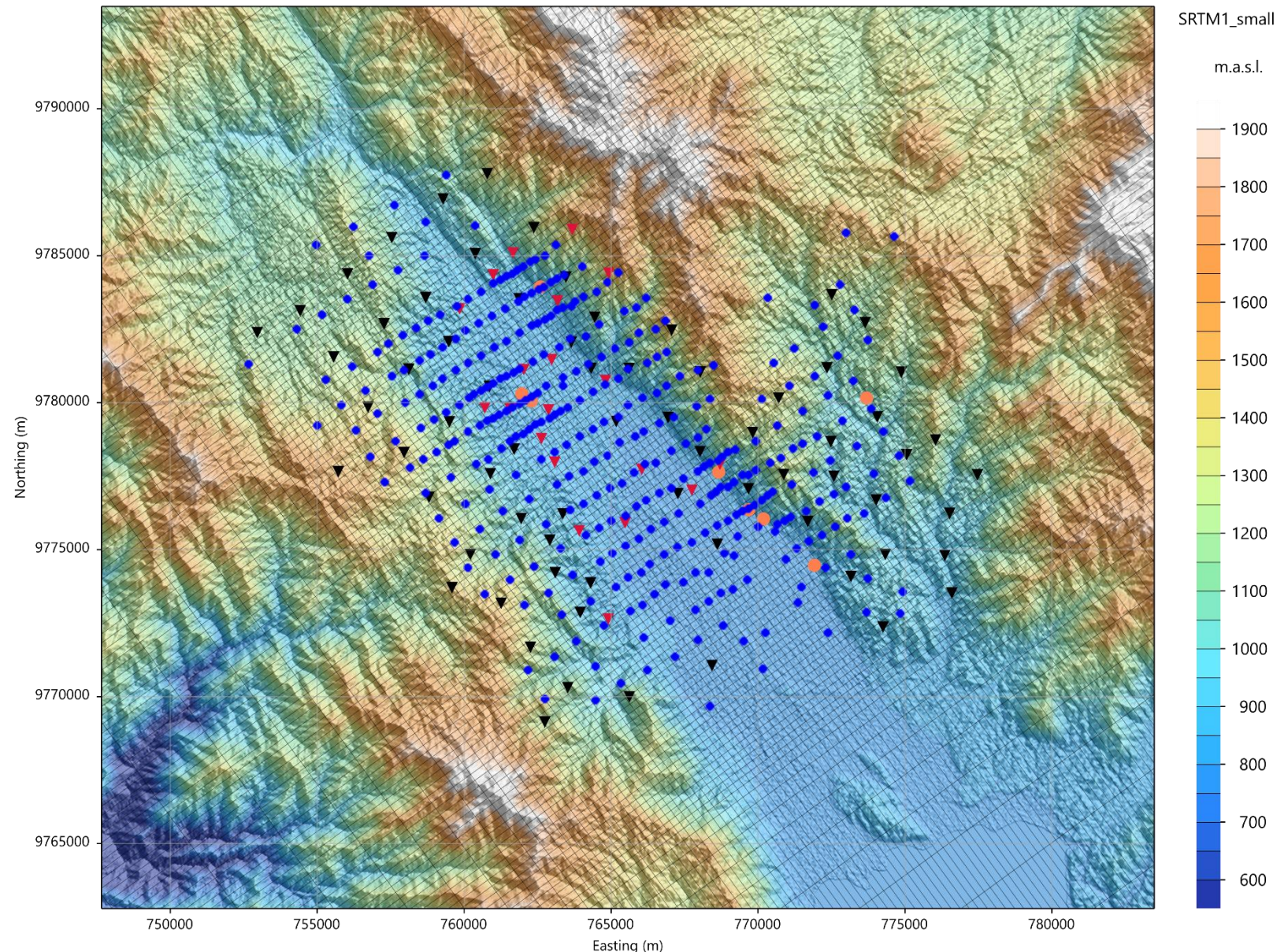
GR Data: # 357 measurement points
CBA @ 2.4 g/cc

GR Error: Absolute error: 0.3 mGal

Smoothing: horizontal (τ_{H}): 0.2
vertical (τ_{V}): 0.003

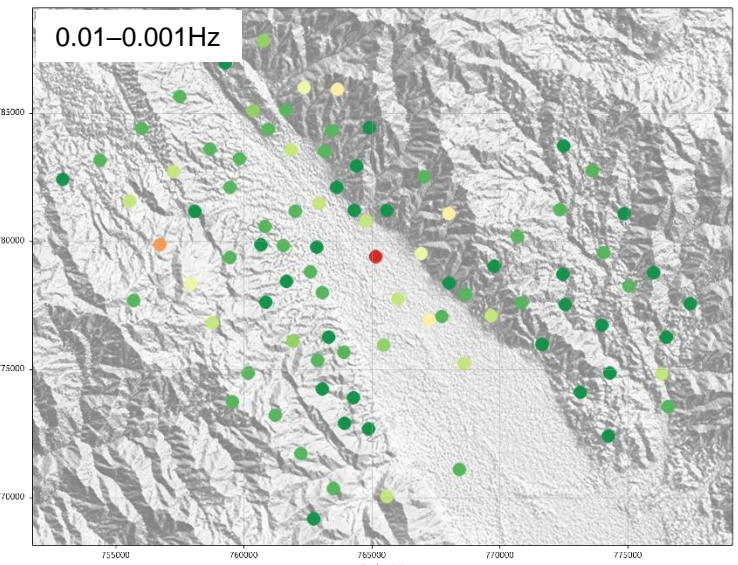
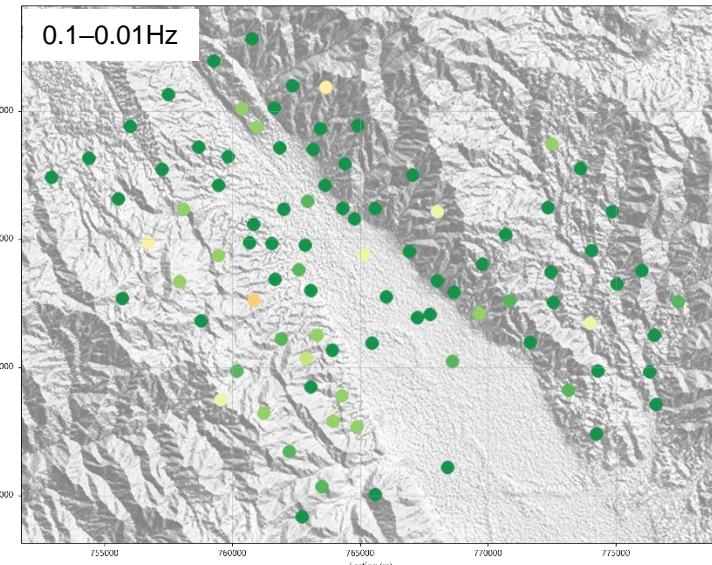
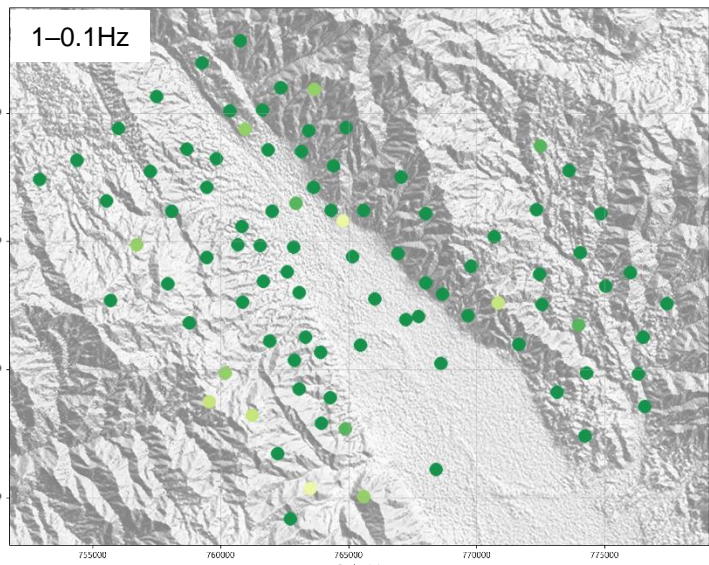
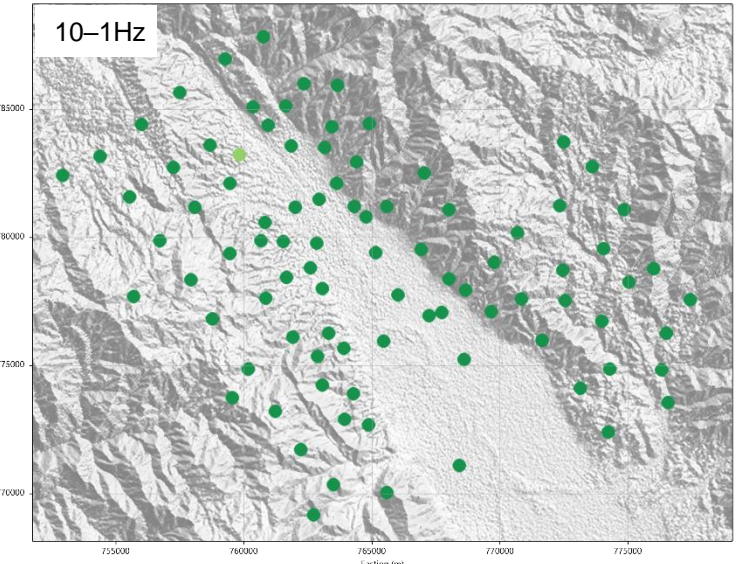
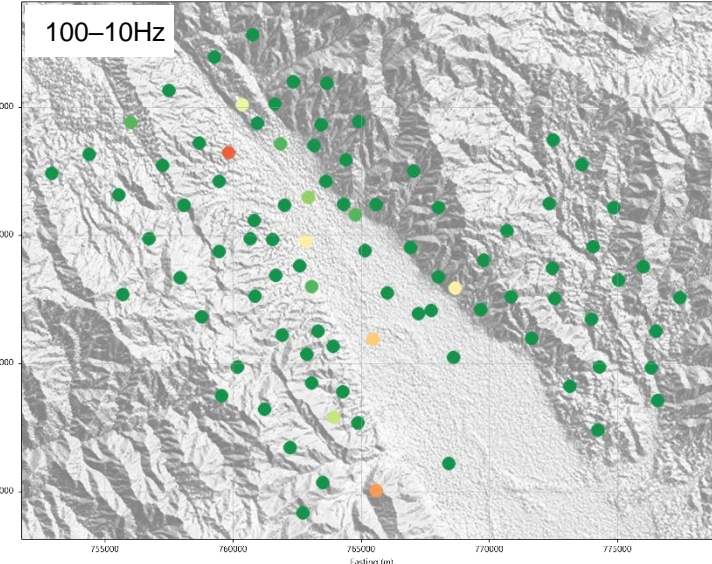
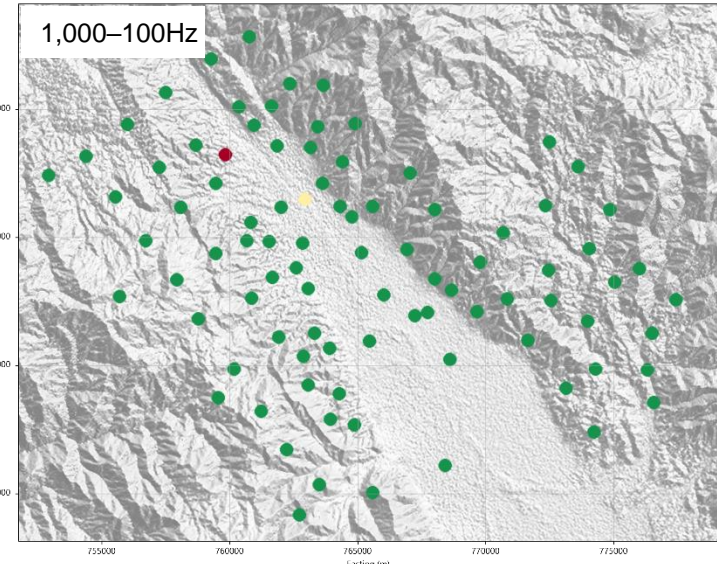
Smooth depth weighting: tau: 1, zmax: 200m

Data fit: rms MT = 1.55 (150 iterations)
rms GR = 0.64 (150 iterations)



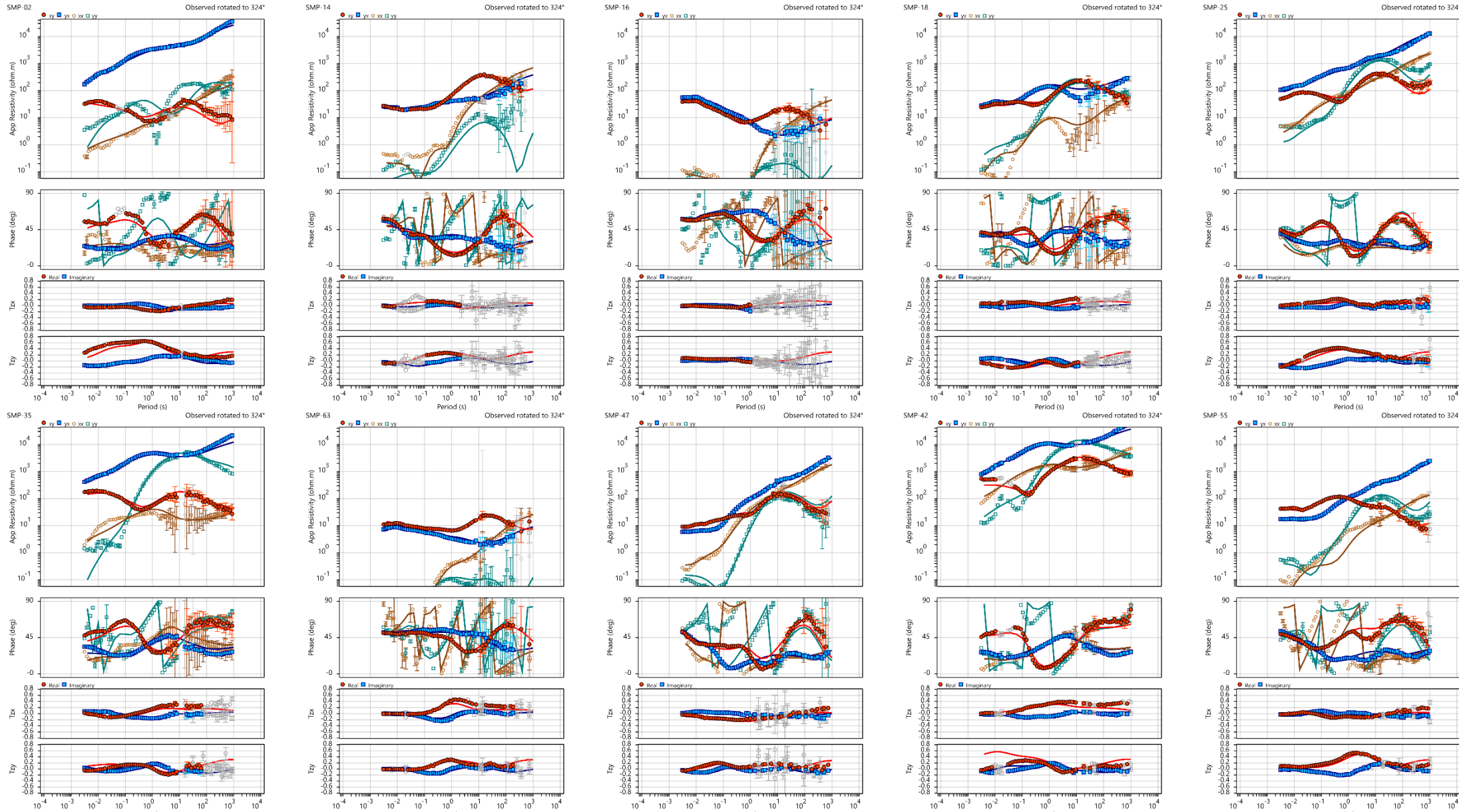


MT Data – Inclusion in 3D modeling



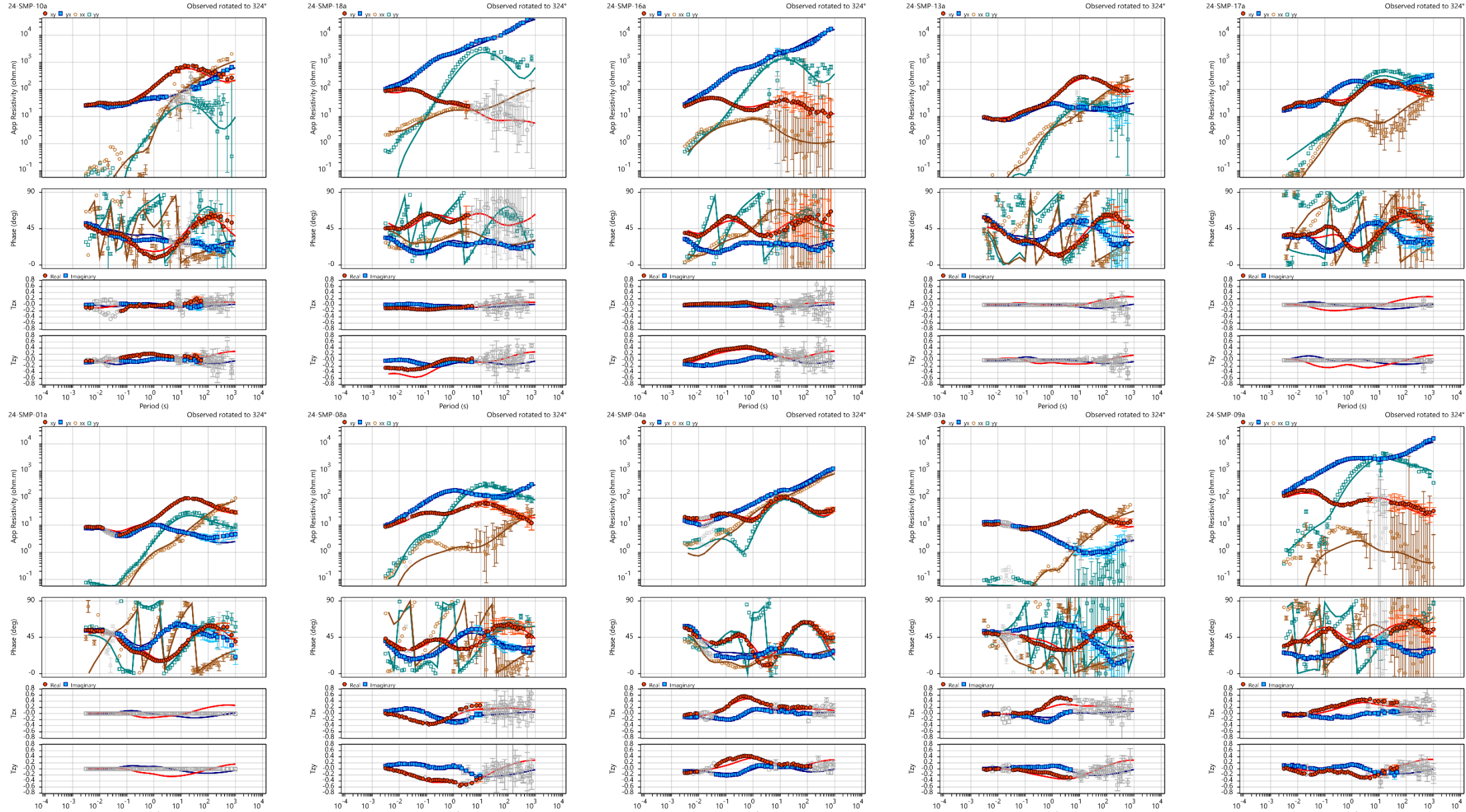
MT Datafit, 2022 dataset - MT07

Data Rotation: 324°



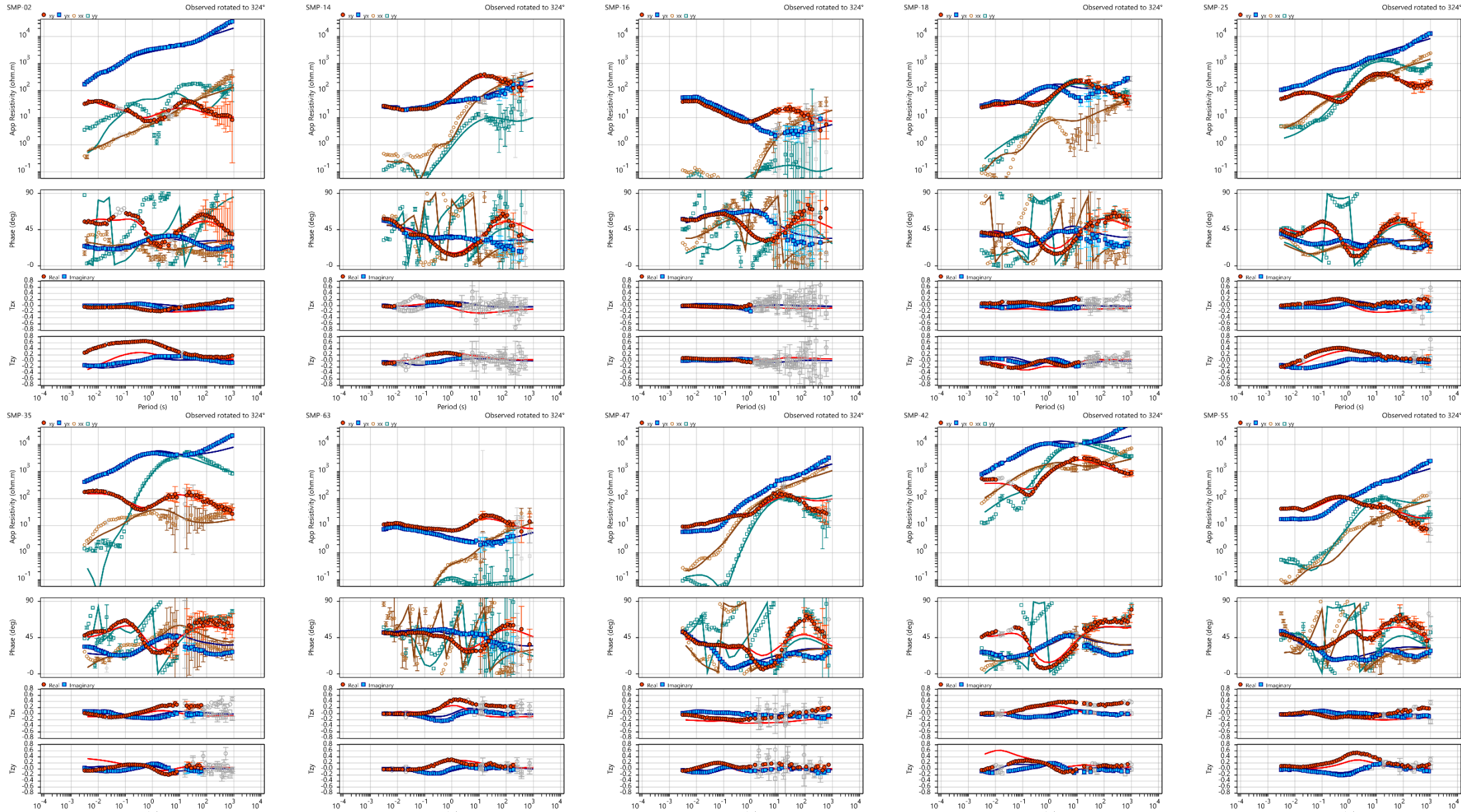


MT Datafit, 2024 dataset - MT07



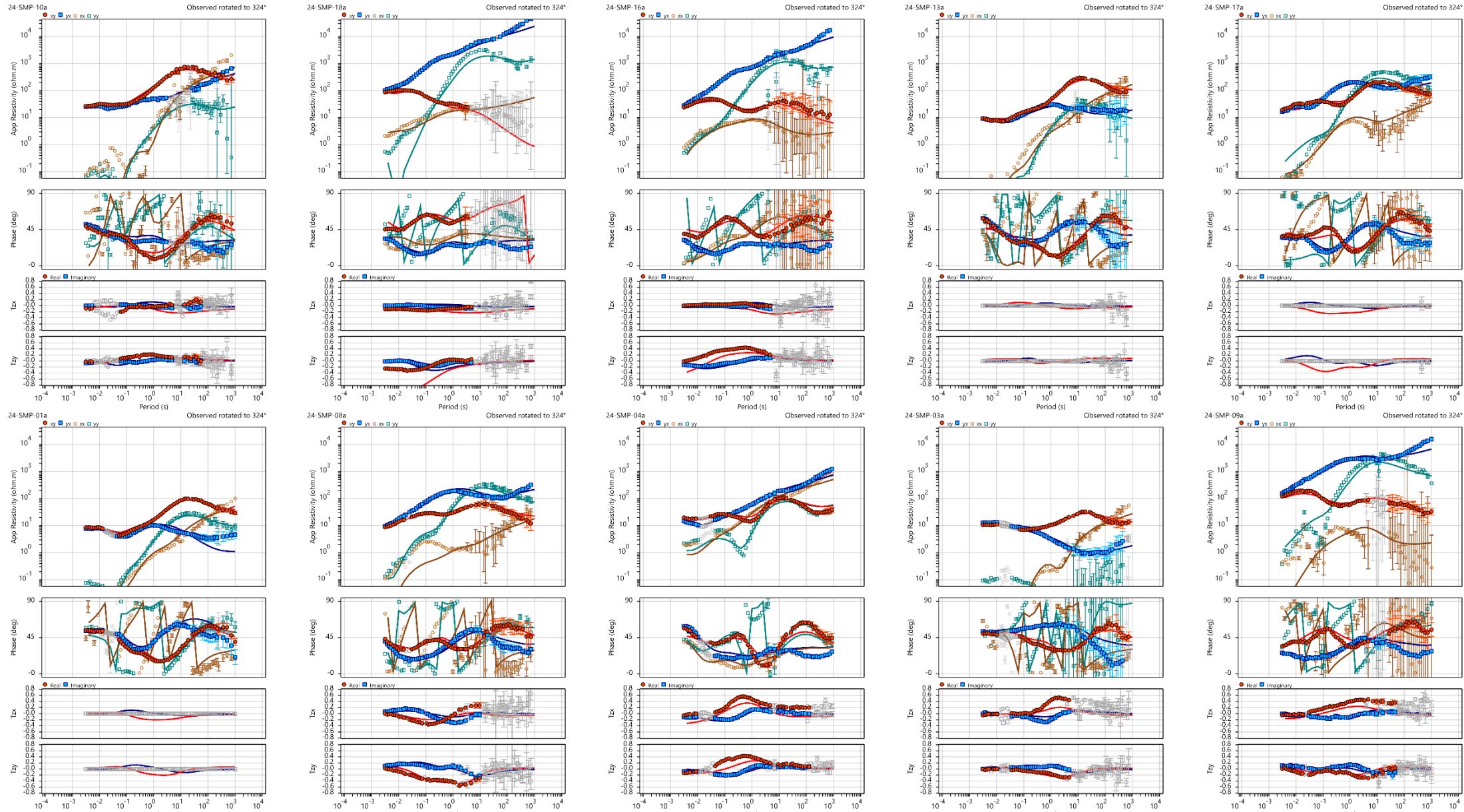
MT Datafit, 2022 dataset - JI03

Data Rotation: 324°





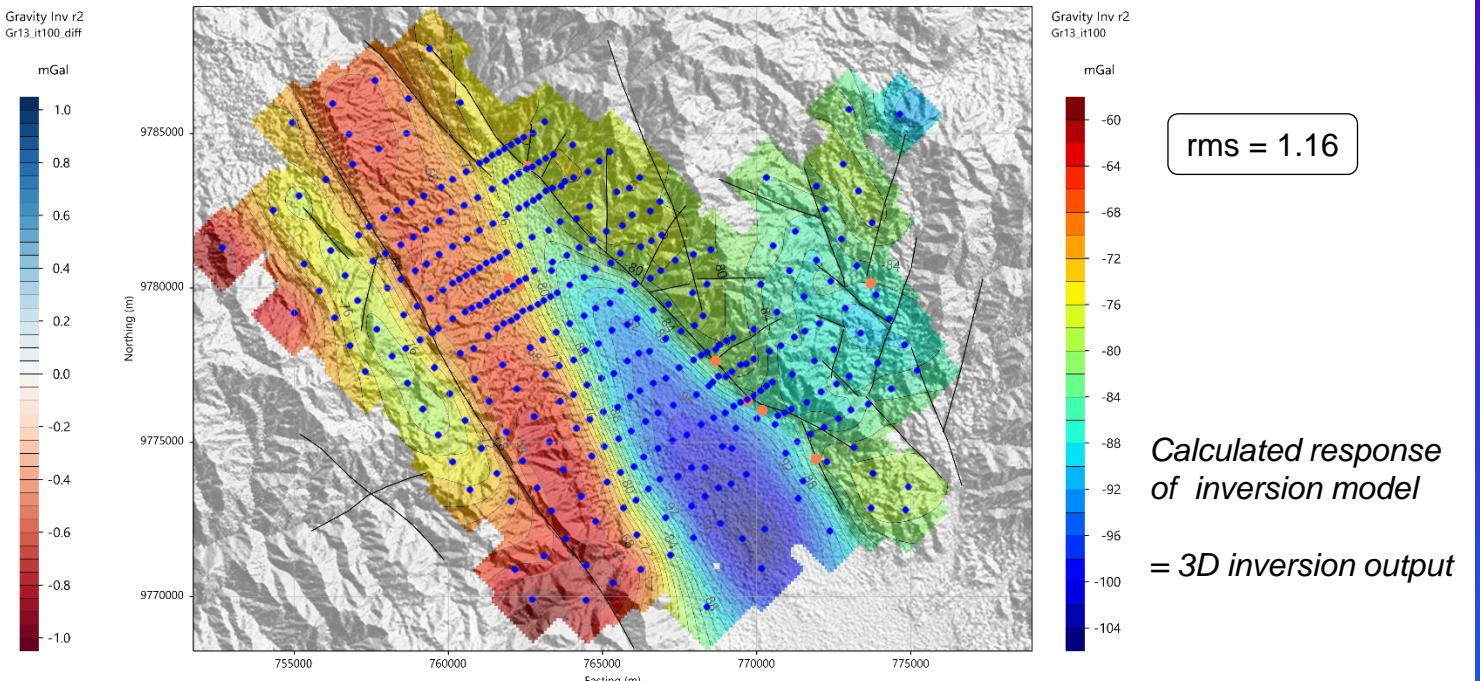
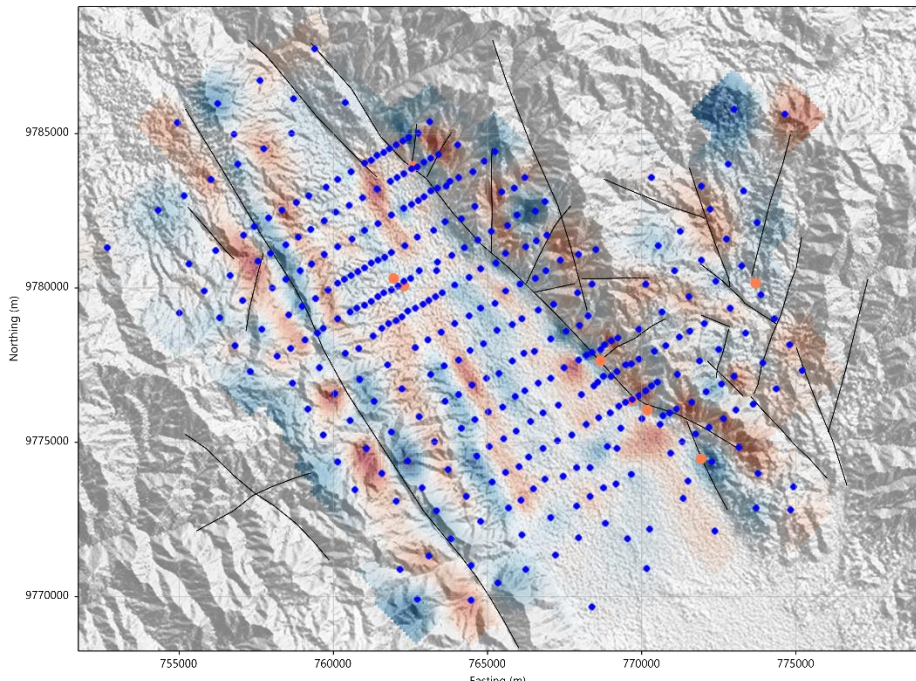
MT Datafit, 2024 dataset - JI03



Single domain Gravity Data Fit (GR13)

- The residual map shows mainly small-scale anomaly patterns, related to shallow density variations.

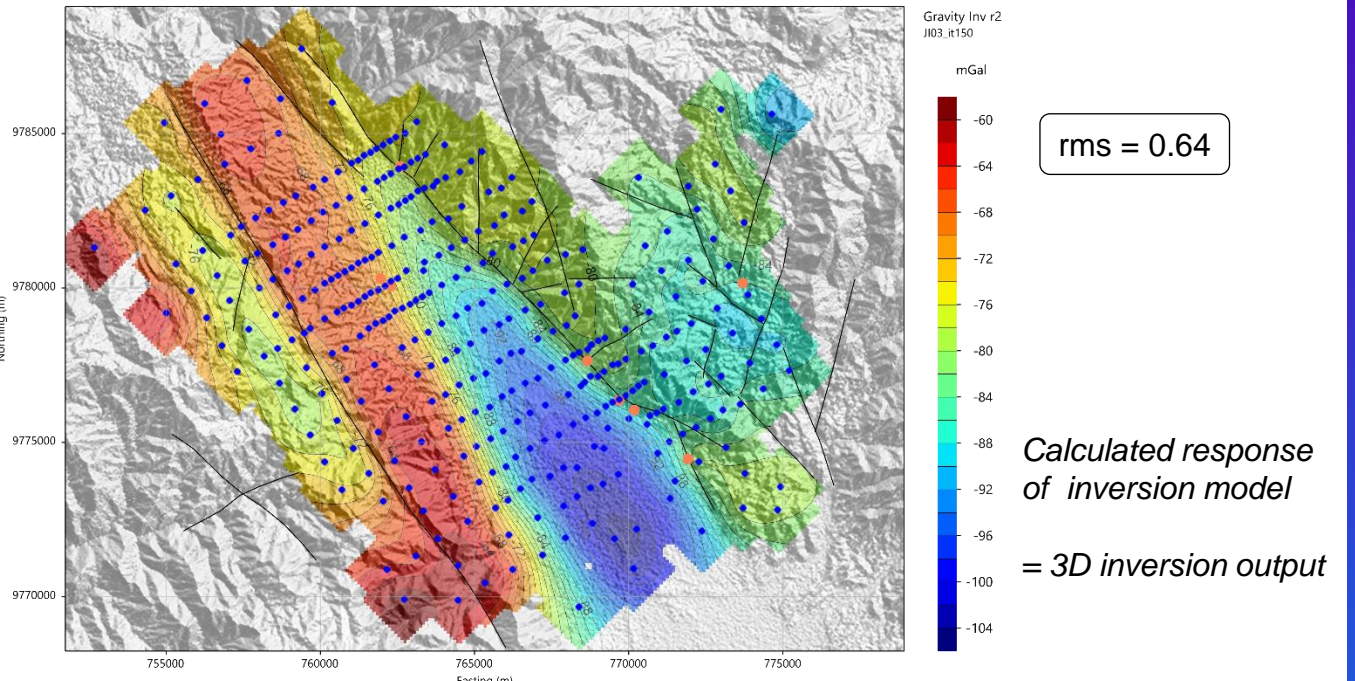
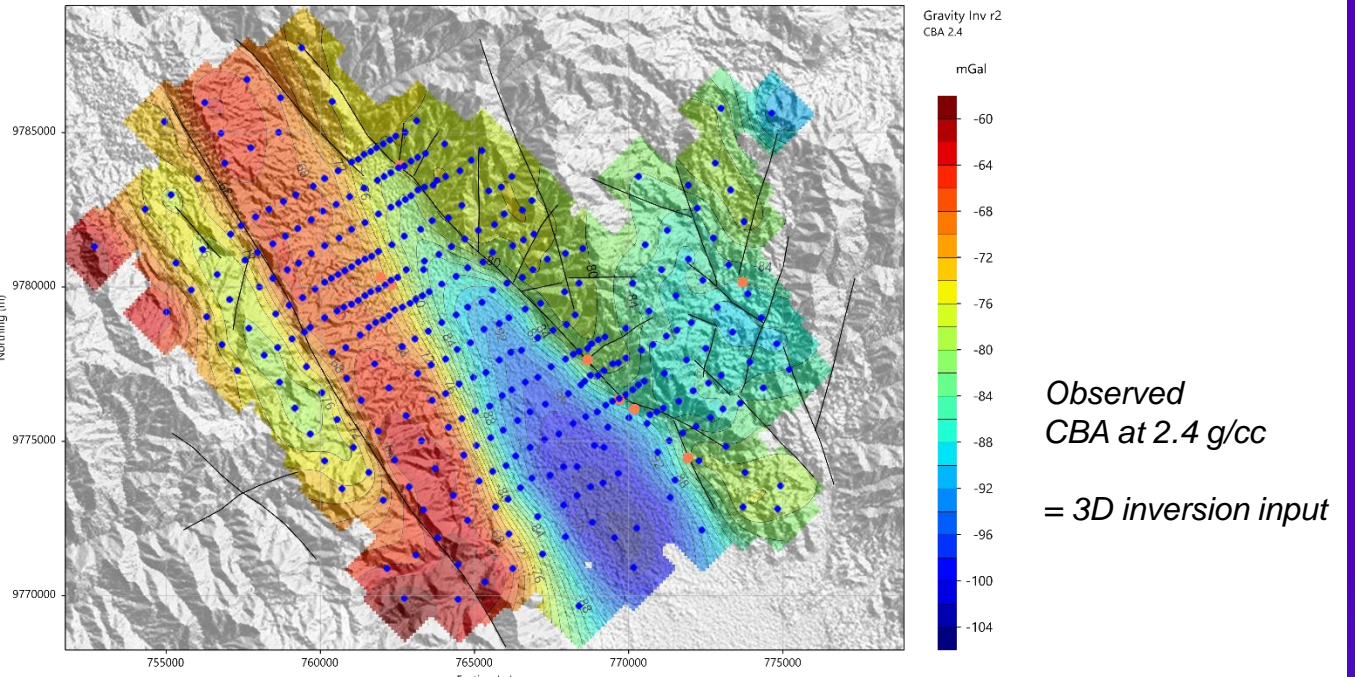
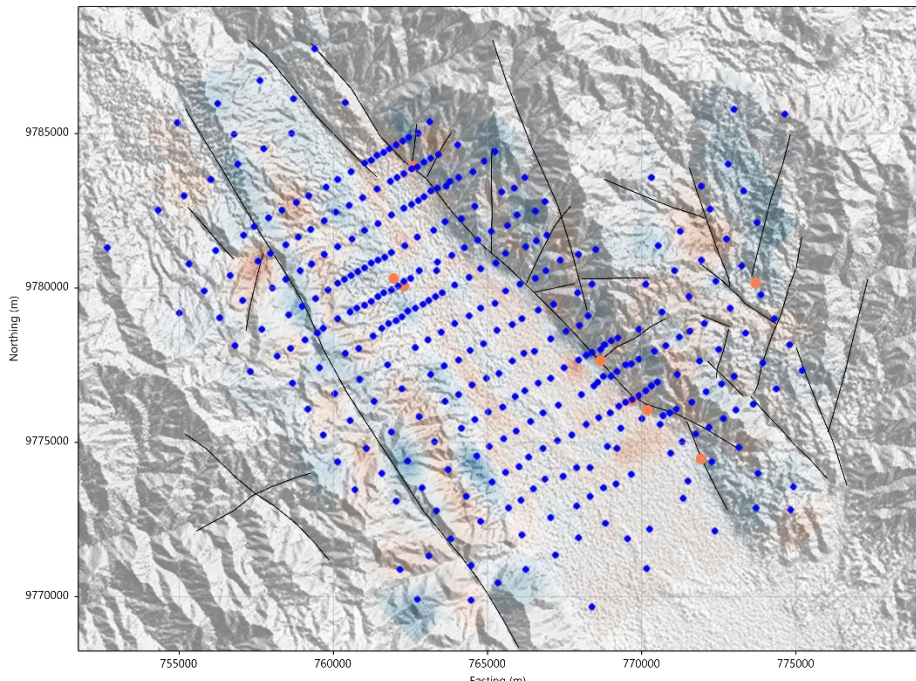
Residual = observed - calculated

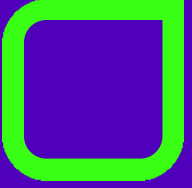


Joint inversion Gravity Data Fit (JI03)

- The residual map still shows mainly small-scale anomalies, but weaker with respect to the result from the single domain inversion. This has a correlation with the shallow anomalies introduced via structural constraint with the resistivity model and with the larger number of iterations performed (+50).

Residual = observed - calculated





3D Inversions – Single domain and Joint inversion results



Inversion sections and depth slices

- In the following slides will be shown sections from the following inversions:
 - MT single domain (MT07)
 - Gravity single domain (GR13)
 - JI MT with Gravity (JI03)

and maps at fixed elevation from the Joint Inversion #JI03.

- The joint inversion approach used is cross-gradients.
- This approach stimulates structural similarity.

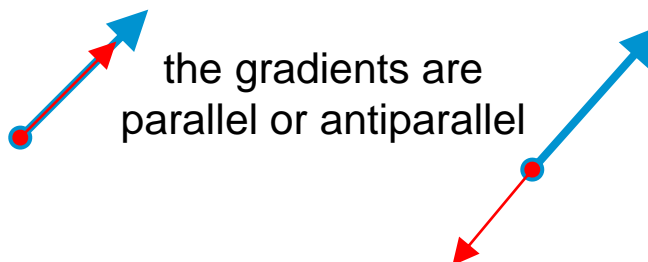
Cross-Gradients \equiv Stimulation of structural similarity

Introduced by Gallardo and Meju (2003, 2011) for joint inversions, the cross-gradient term $\Phi_{\text{res,den}}$ is added to the total cost function Ψ :

$$\Phi_{\text{res,den}}^{xg}(\vec{m}) = \int_V \underbrace{\|\nabla \vec{m}_{\text{res}} \times \nabla \vec{m}_{\text{den}}\|^2}$$

Cross-product of gradient fields from two properties (e.g. resistivity and density)

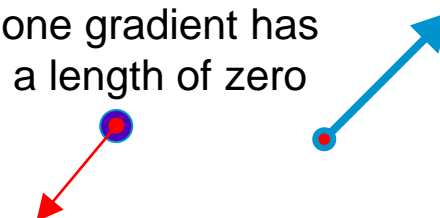
The X-gradient term is zero if:



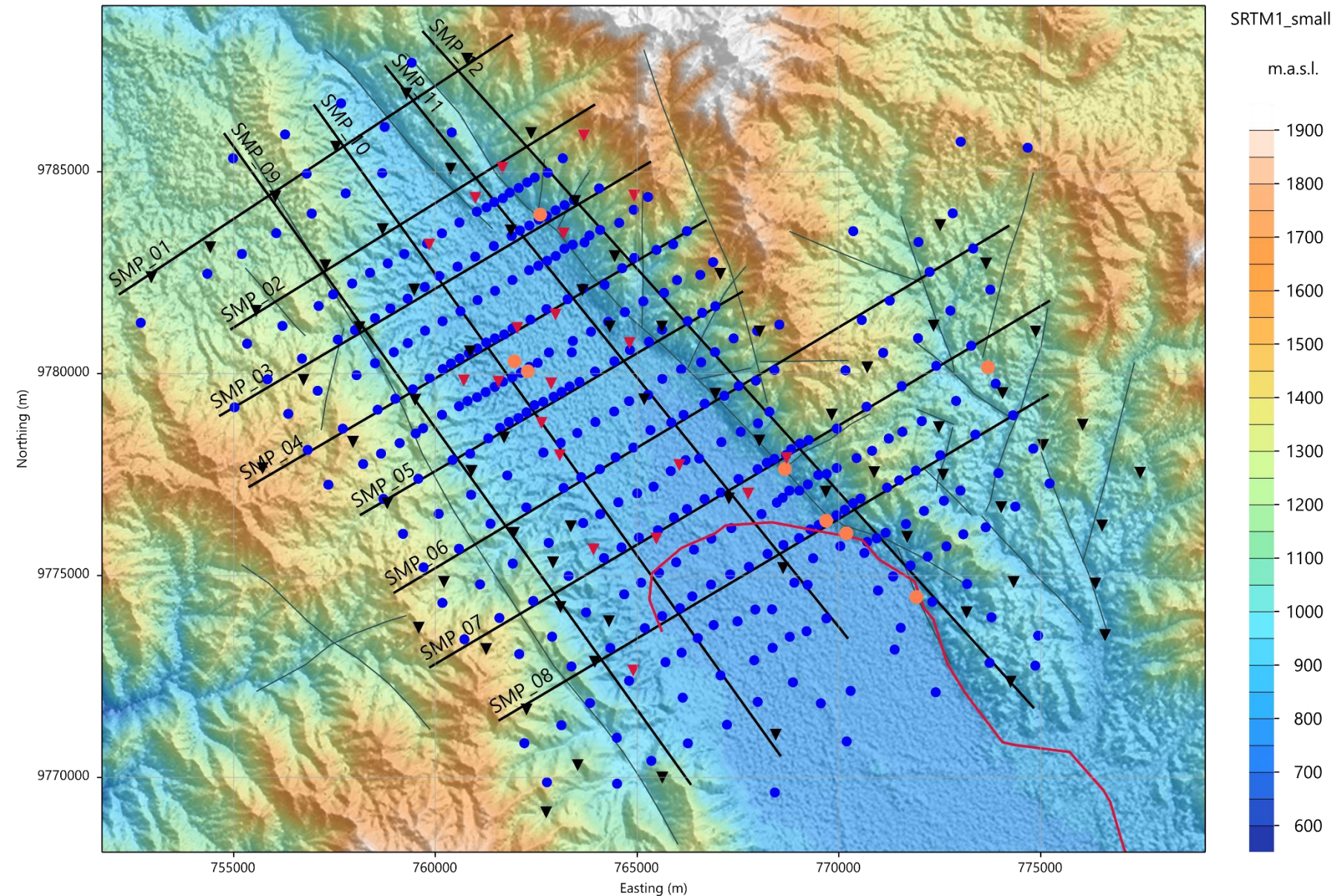
the gradients are
parallel or antiparallel

or

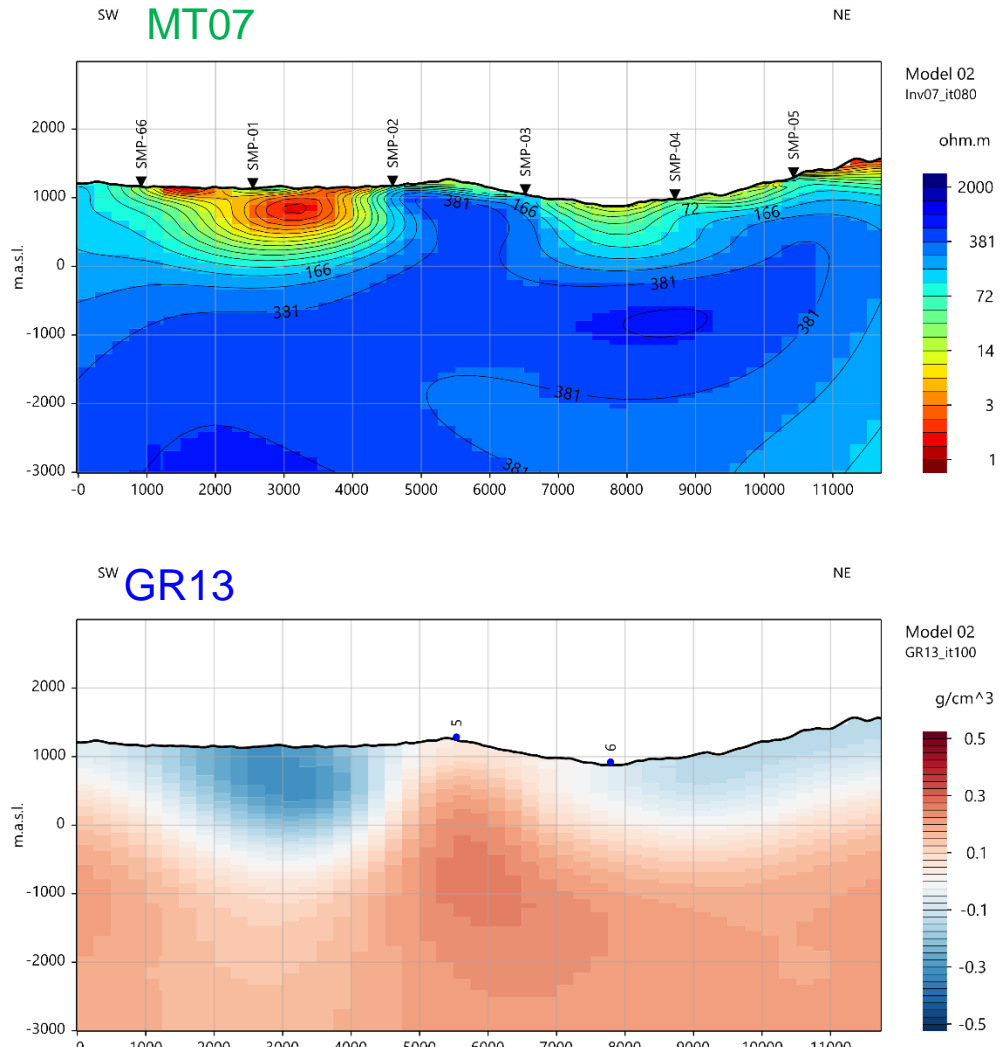
one gradient has
a length of zero



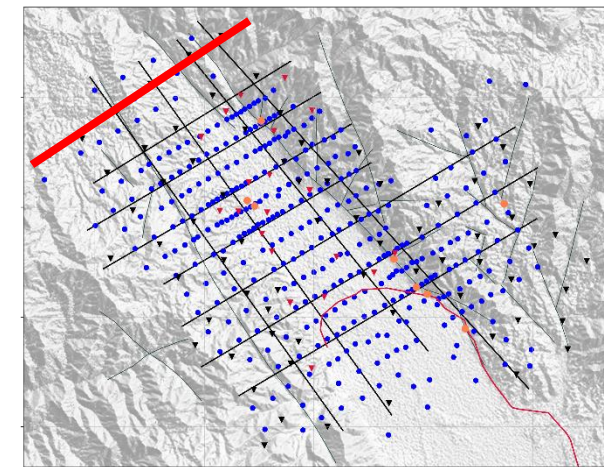
Profiles



Profile SMP_01 (MT07 / GR13)



Single domain
inversions



MT 2024



MT 2022



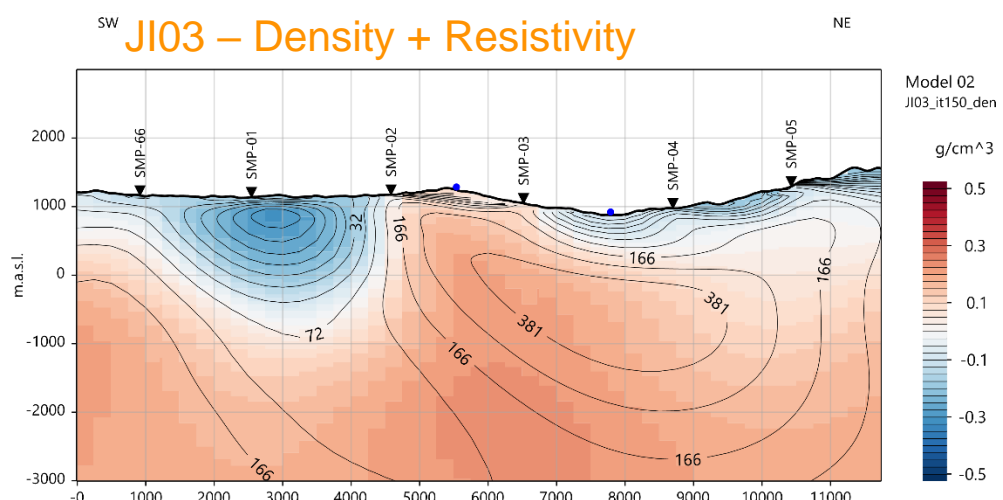
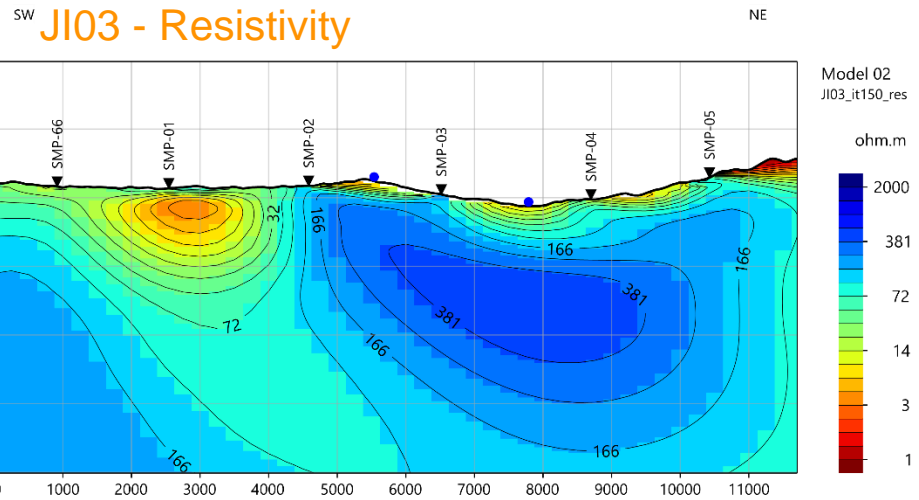
Gravity



Manifestations

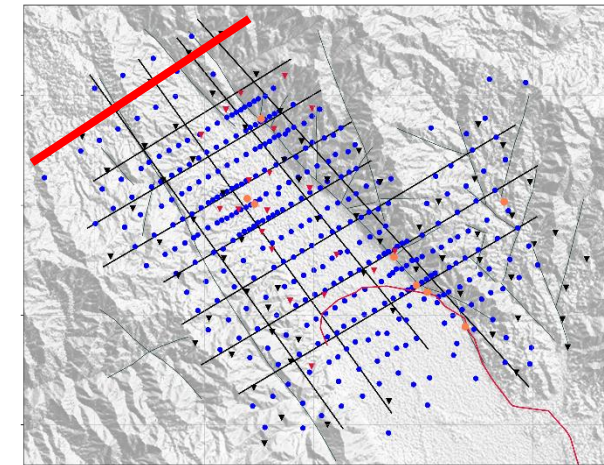


Profile SMP_01 (JI03)



*Color: density
Contour: resistivity*

**MT + Gravity
joint inversion**



MT 2024



MT 2022



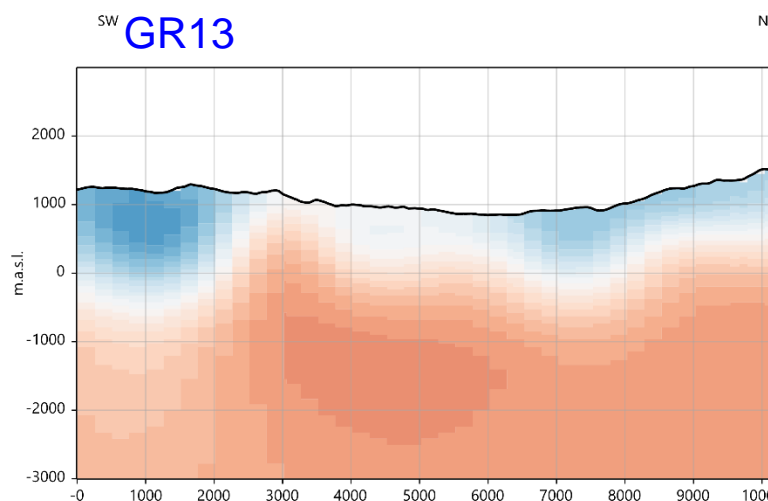
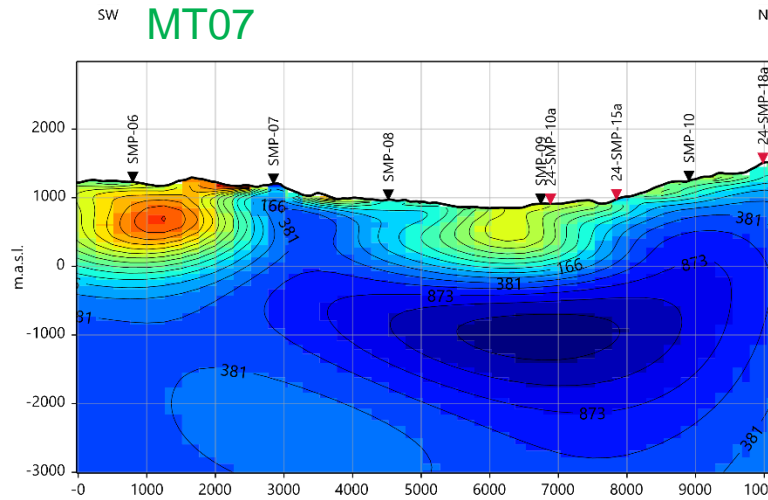
Gravity



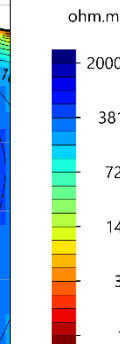
Manifestations



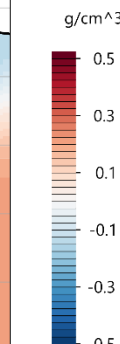
Profile SMP_02 (MT07 / GR13)



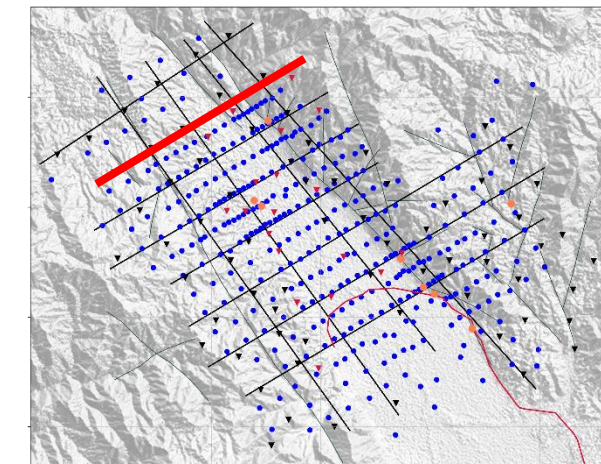
Model 02
Inv07_it080



Model 02
GR13_it100



Single domain
inversions



MT 2024



MT 2022



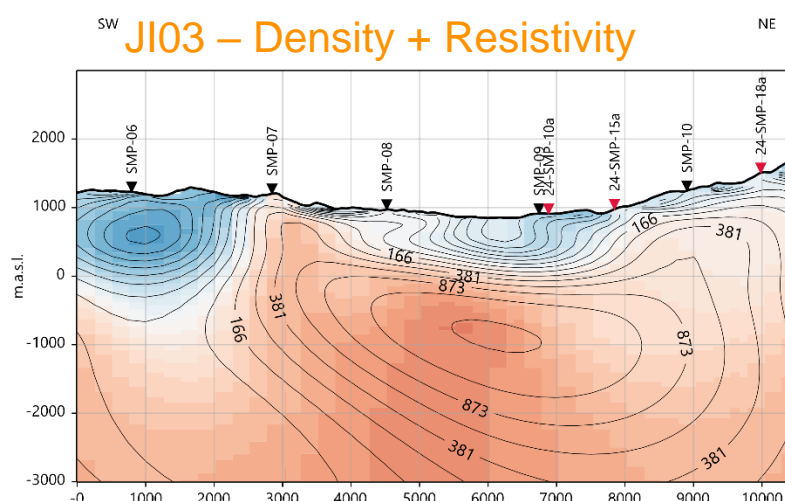
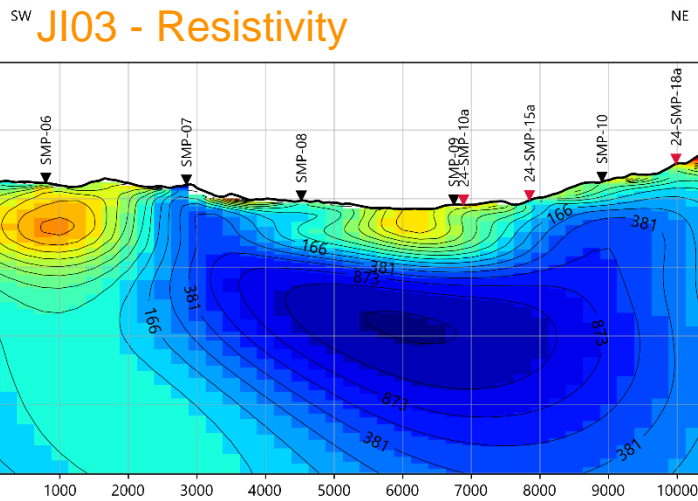
Gravity



Manifestations

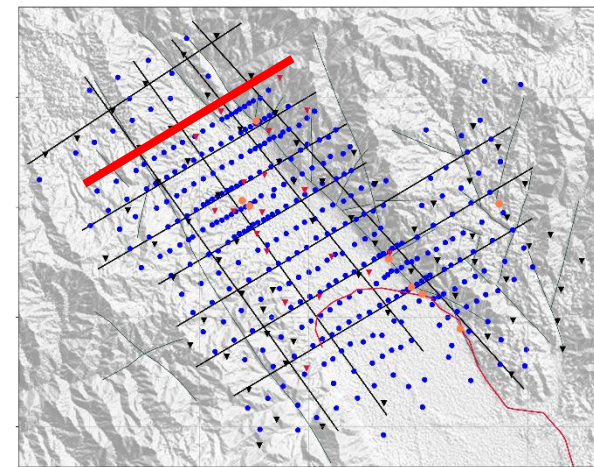


Profile SMP_02 (JI03)



Color: density
Contour: resistivity

MT + Gravity
joint inversion



MT 2024



MT 2022



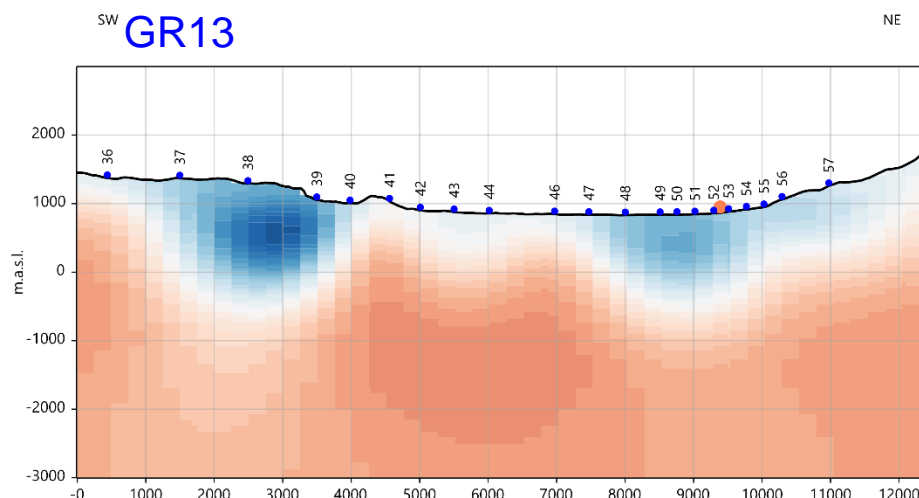
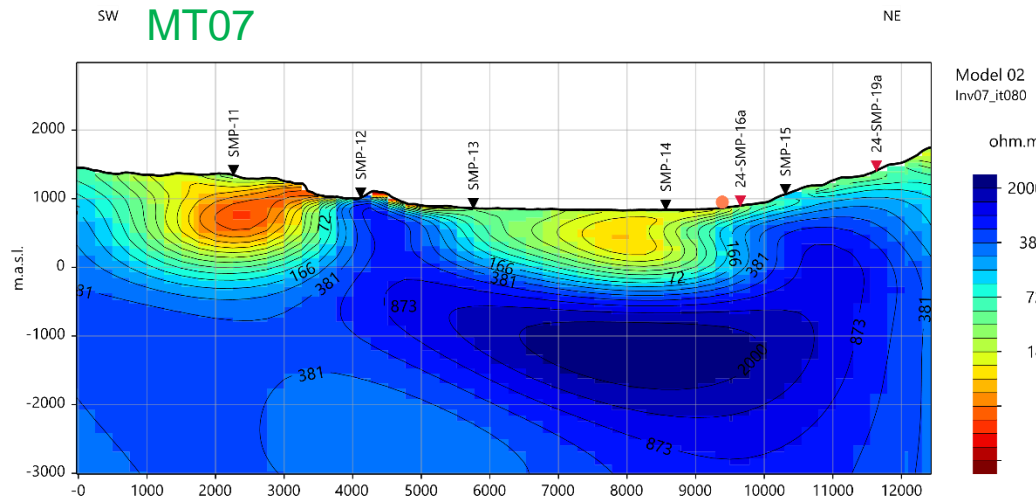
Gravity



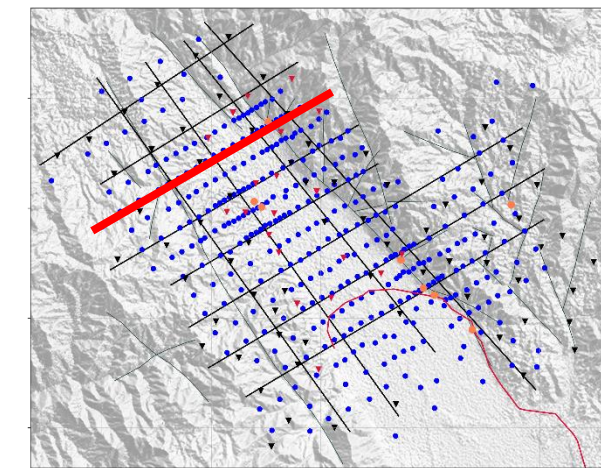
Manifestations



Profile SMP_03 (MT07 / GR13)



Single domain inversions



MT 2024

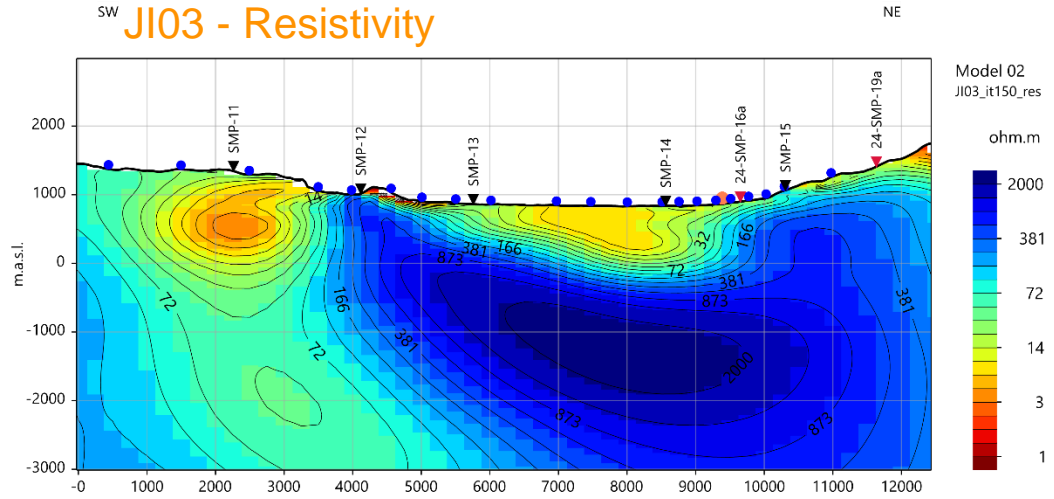
MT 202

Gravity

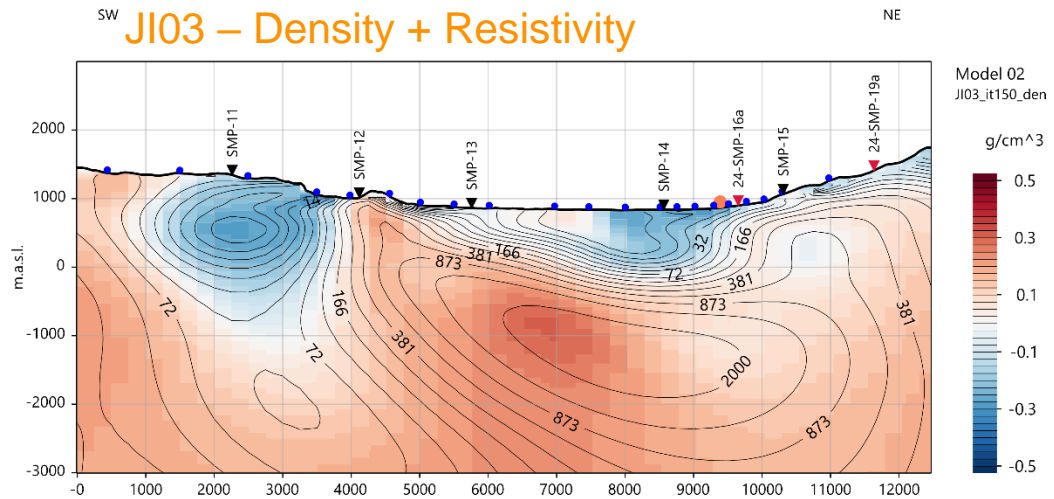
Manifestation

Profile SMP_03 (JI03)

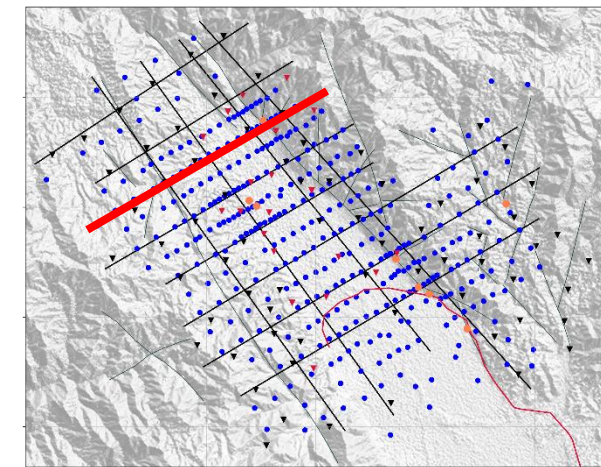
SW JI03 - Resistivity



SW JI03 – Density + Resistivity



MT + Gravity
joint inversion



MT 2024



MT 2022



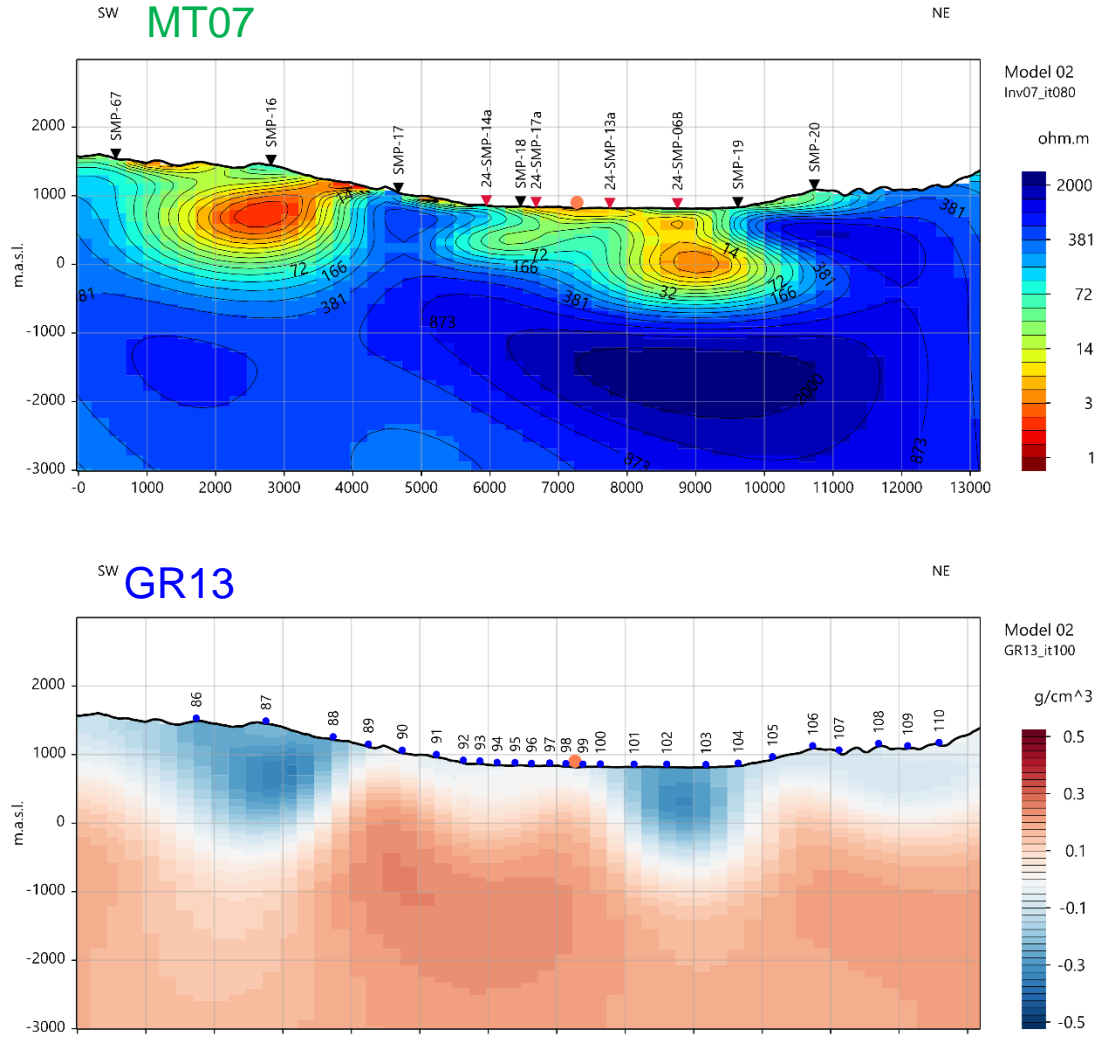
Gravity



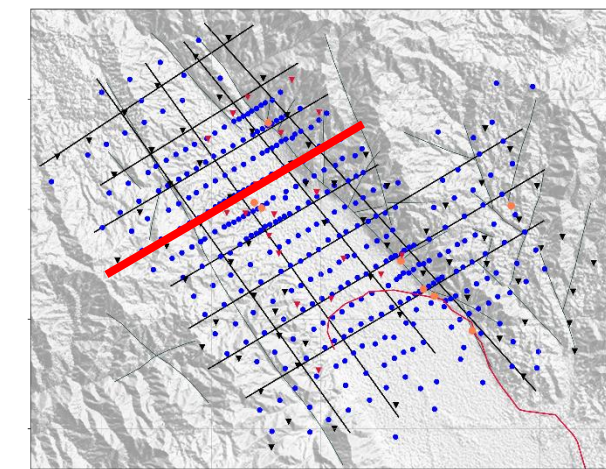
Manifestations



Profile SMP_04 (MT07 / GR13)



Single domain
inversions



MT 2024



MT 2022



Gravity

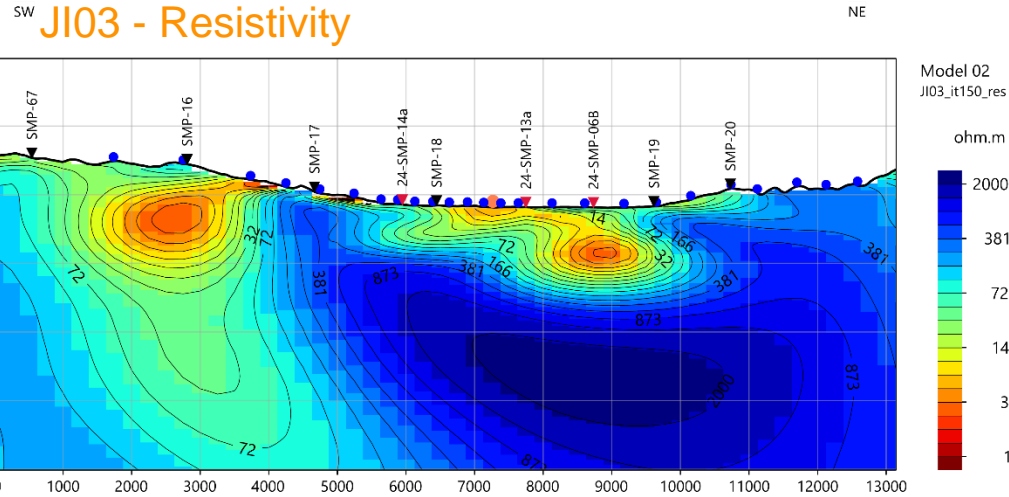


Manifestations





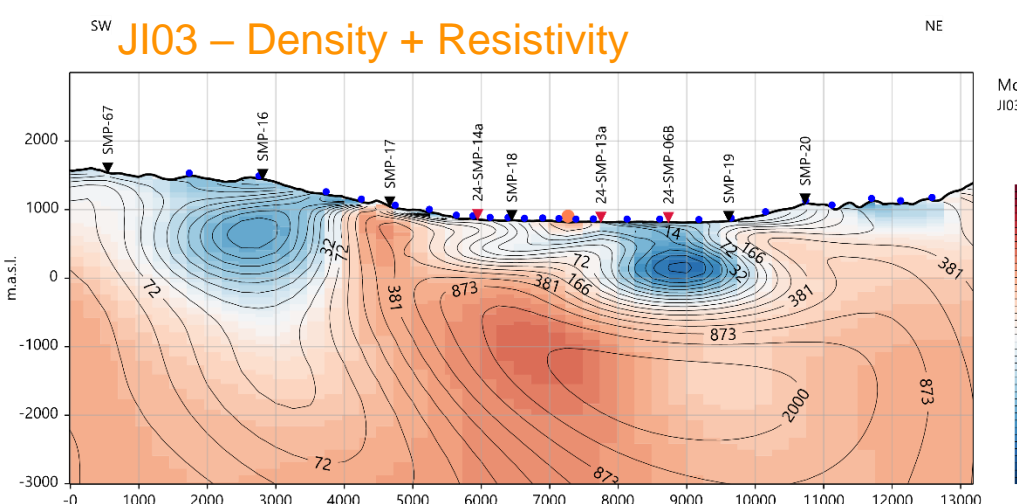
Profile SMP_04 (JI03)



Model 02
JI03_it150_res

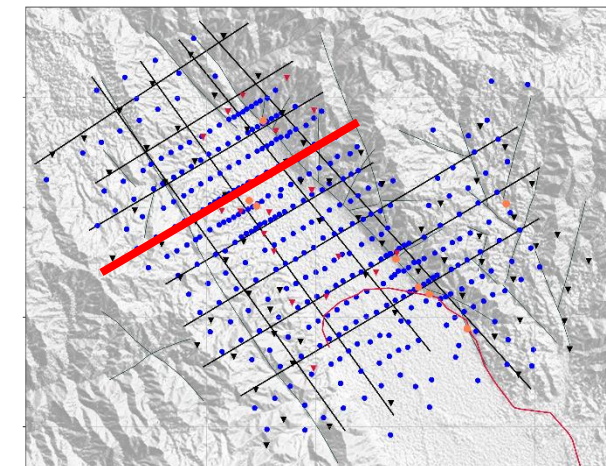
ohm.m

2000
381
72
14
3
1



Color: density
Contour: resistivity

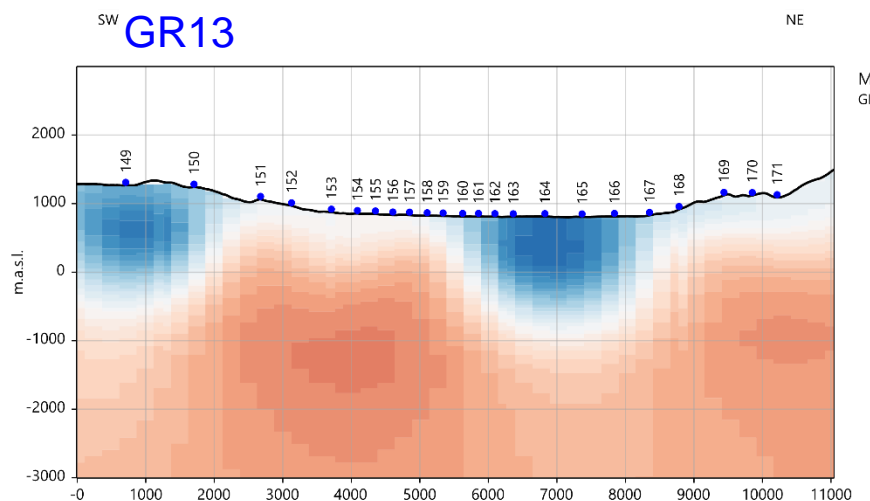
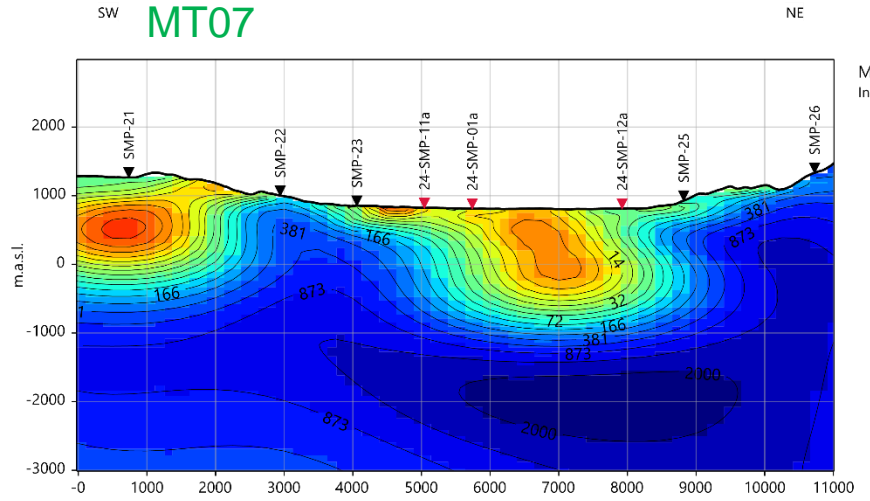
MT + Gravity
joint inversion



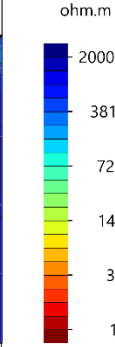
MT 2024
MT 2022
Gravity
Manifestations



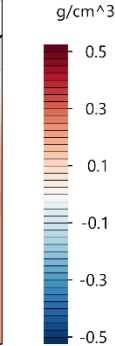
Profile SMP_05 (MT07 / GR13)



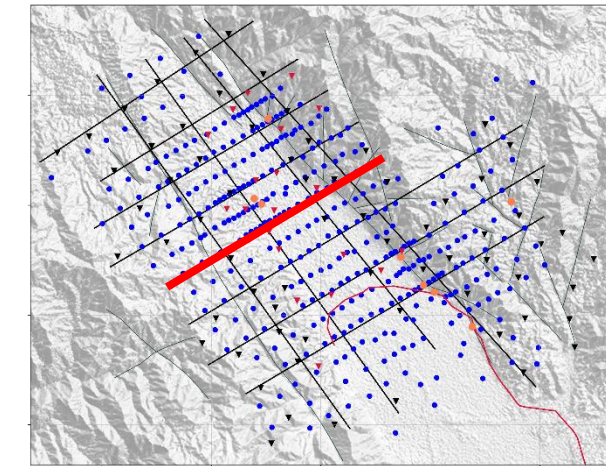
Model 02
Inv07_it080



Model 02
GR13_it100



Single domain
inversions



MT 2024



MT 2022



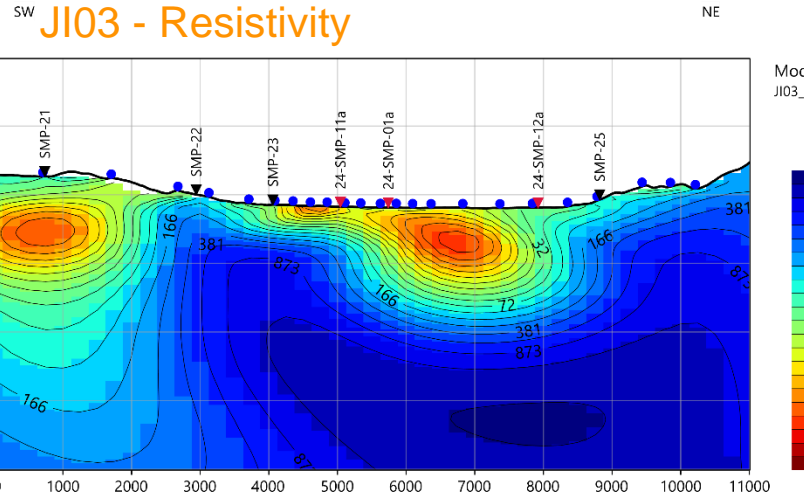
Gravity



Manifestations

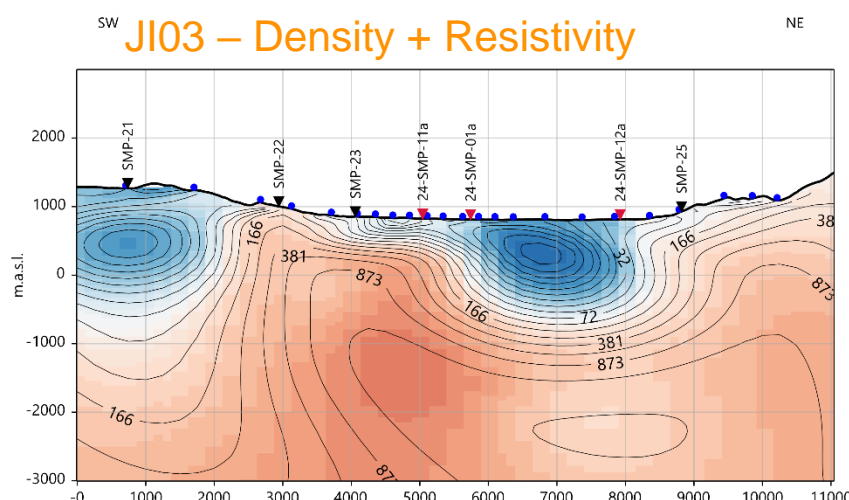


Profile SMP_05 (JI03)



Model 02
JI03_it150_res

ohm.m
2000
381
72
14
3
1

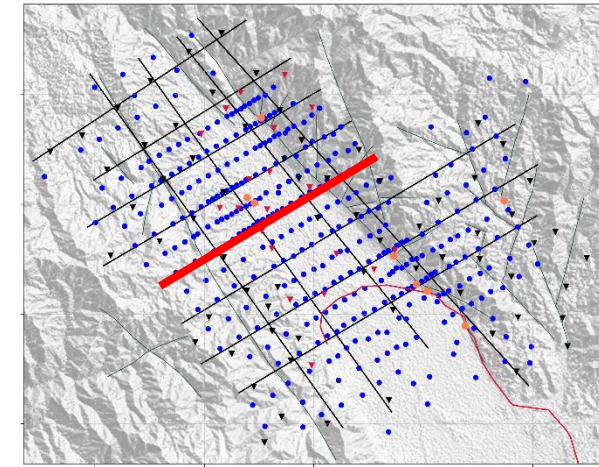


Model 02
JI03_it150_den

g/cm³
0.5
0.3
0.1
-0.1
-0.3
-0.5

Color: density
Contour: resistivity

**MT + Gravity
joint inversion**



MT 2024



MT 2022



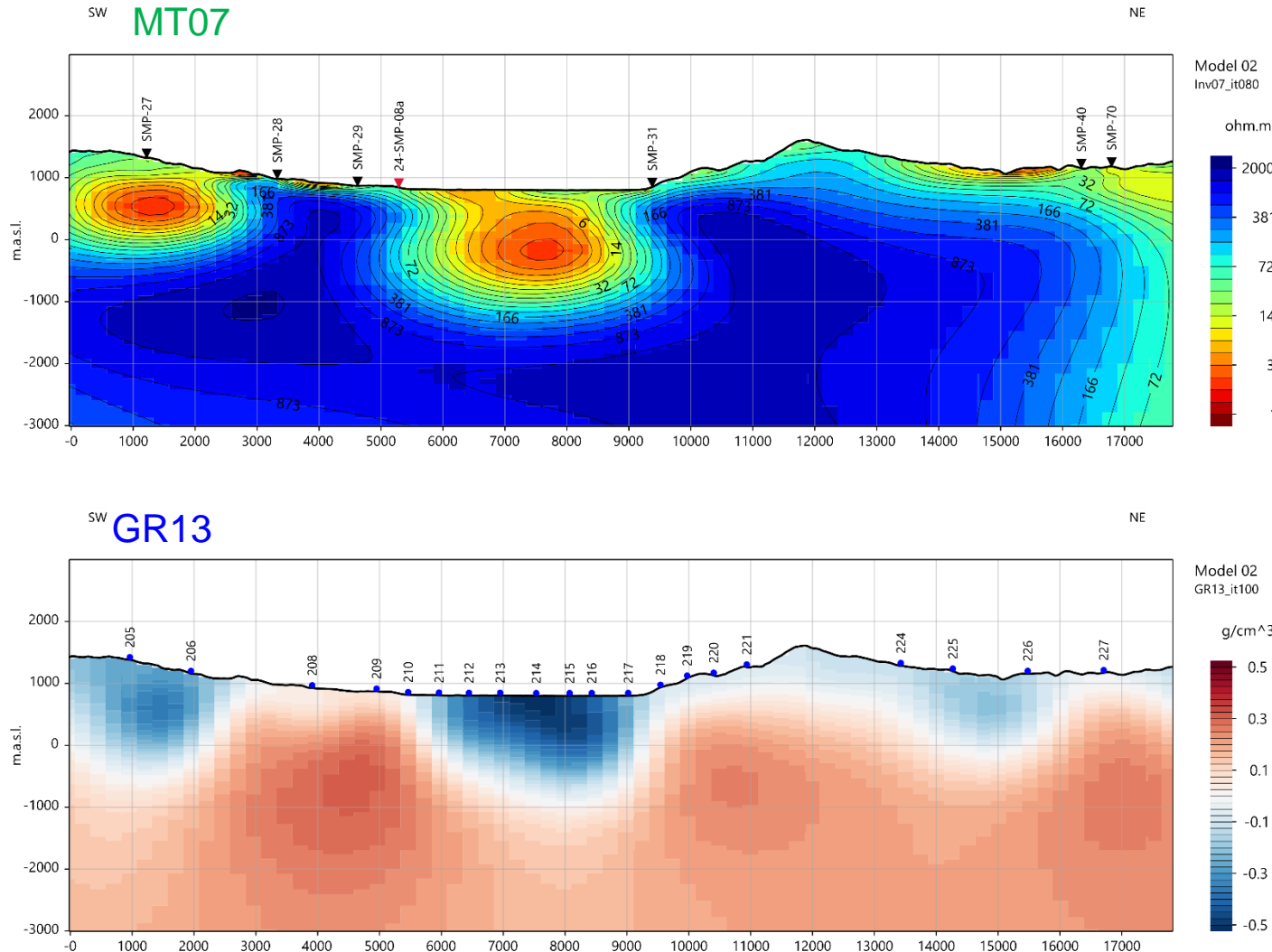
Gravity



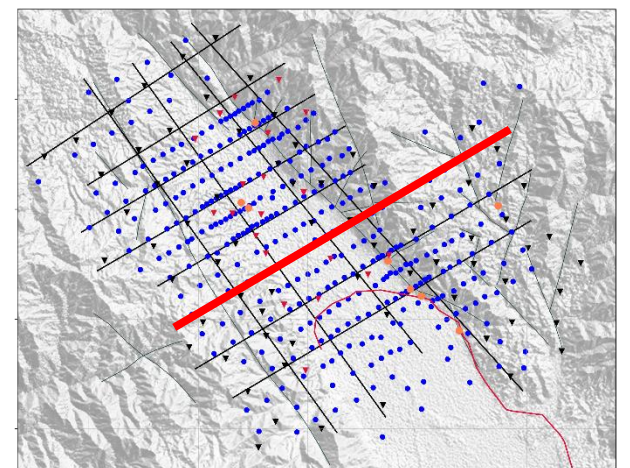
Manifestations



Profile SMP_06 (MT07 / GR13)

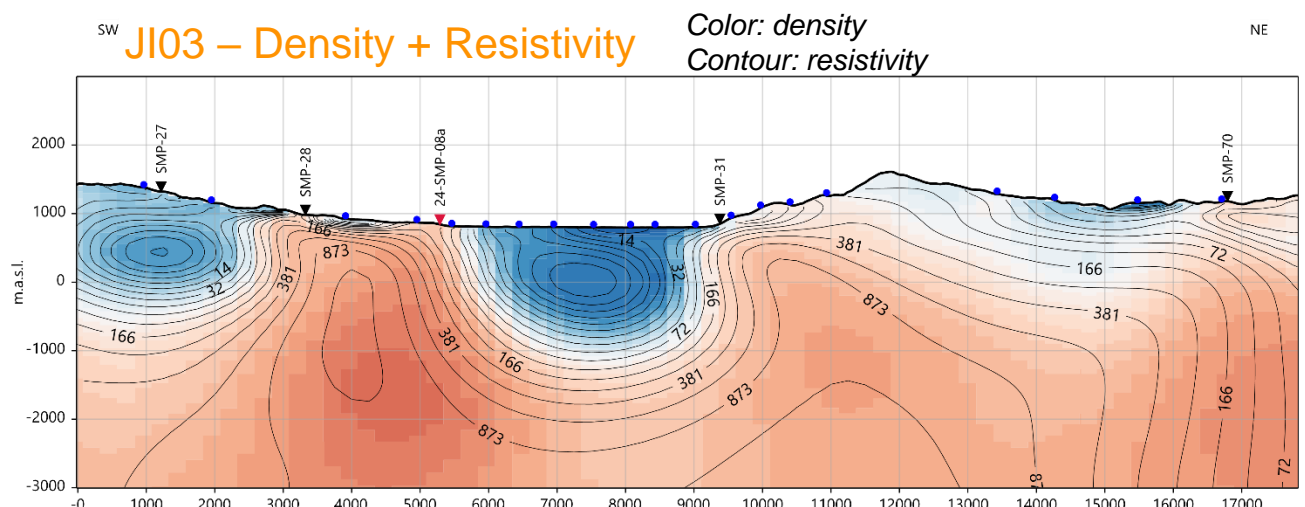
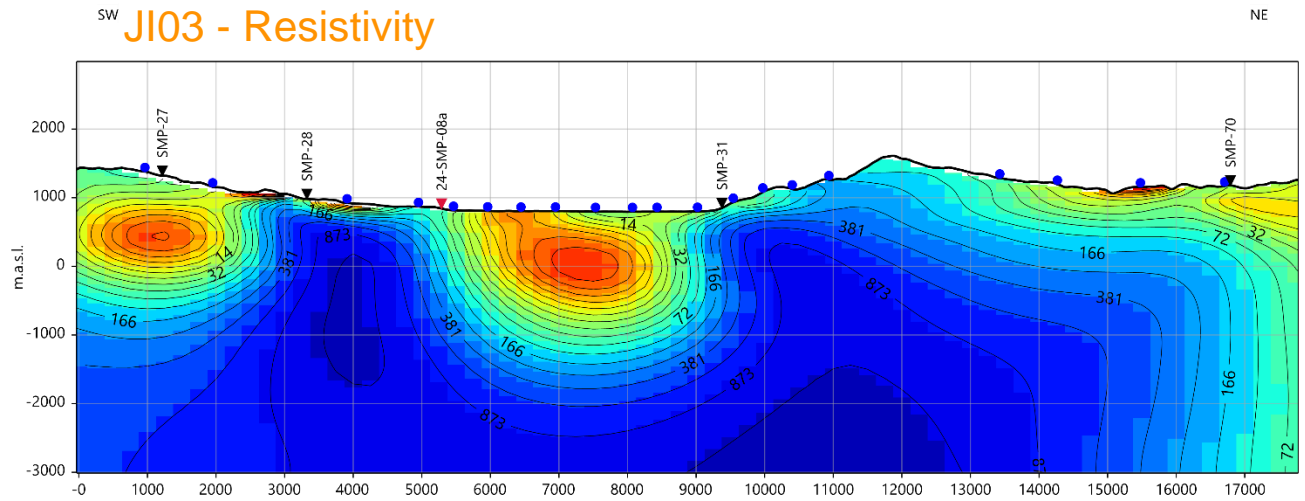


Single domain
inversions

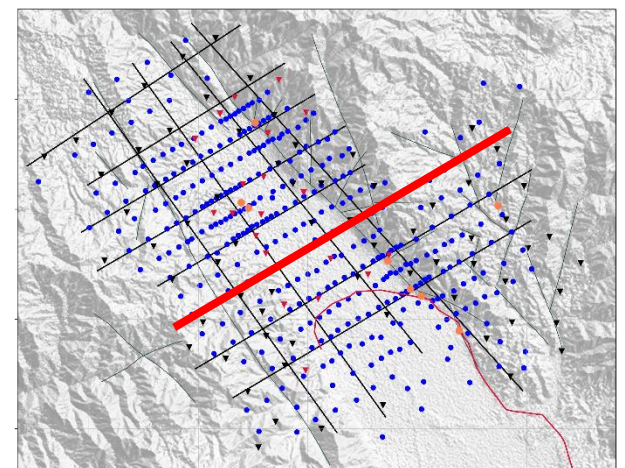


- MT 2024
- MT 2022
- Gravity
- Manifestations

Profile SMP_06 (JI03)



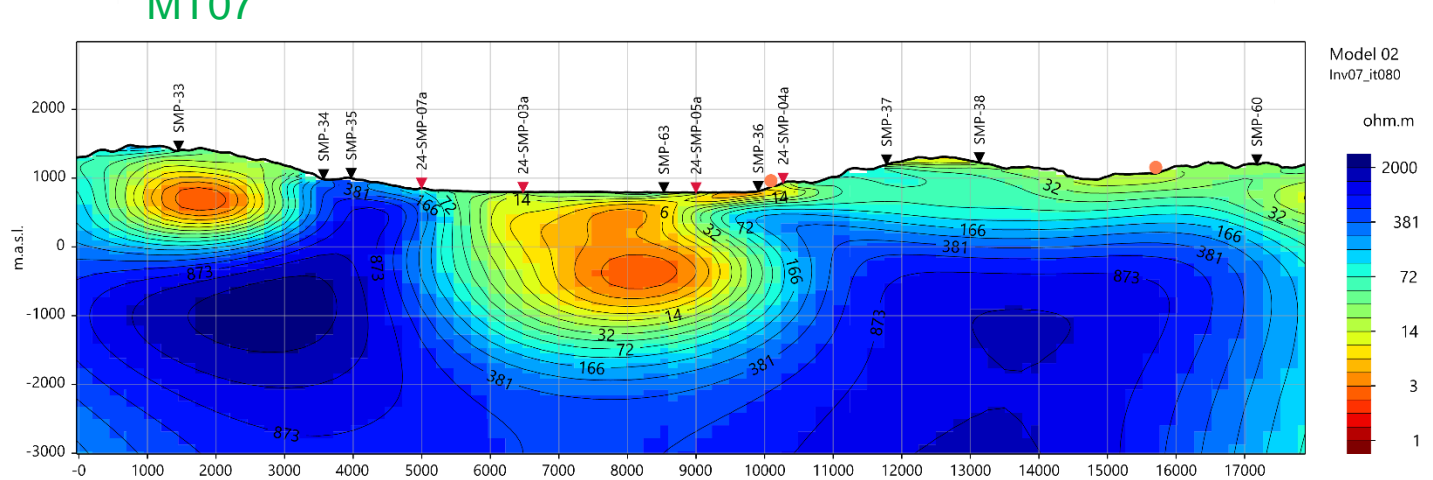
**MT + Gravity
joint inversion**



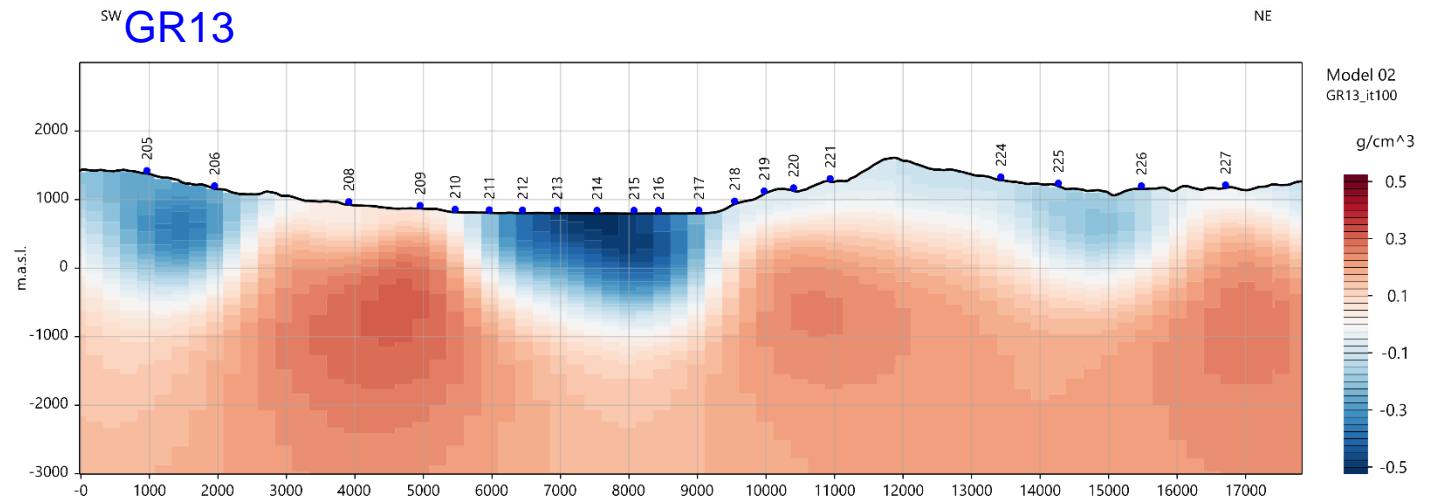
- MT 2024
- MT 2022
- Gravity
- Manifestations

Profile SMP_07 (MT07 / GR13)

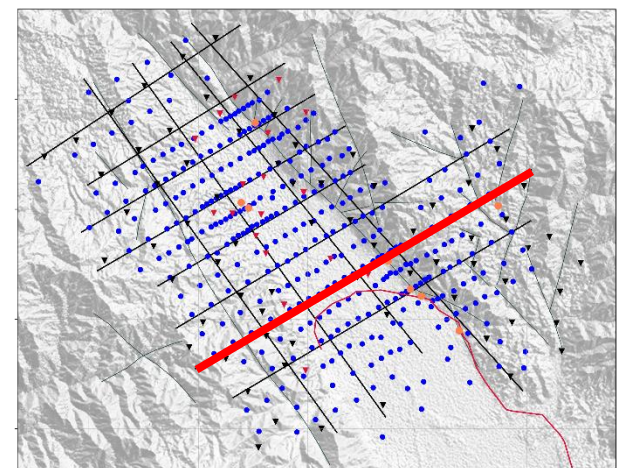
MT07



GR13



Single domain inversions



MT 2024



MT 2022



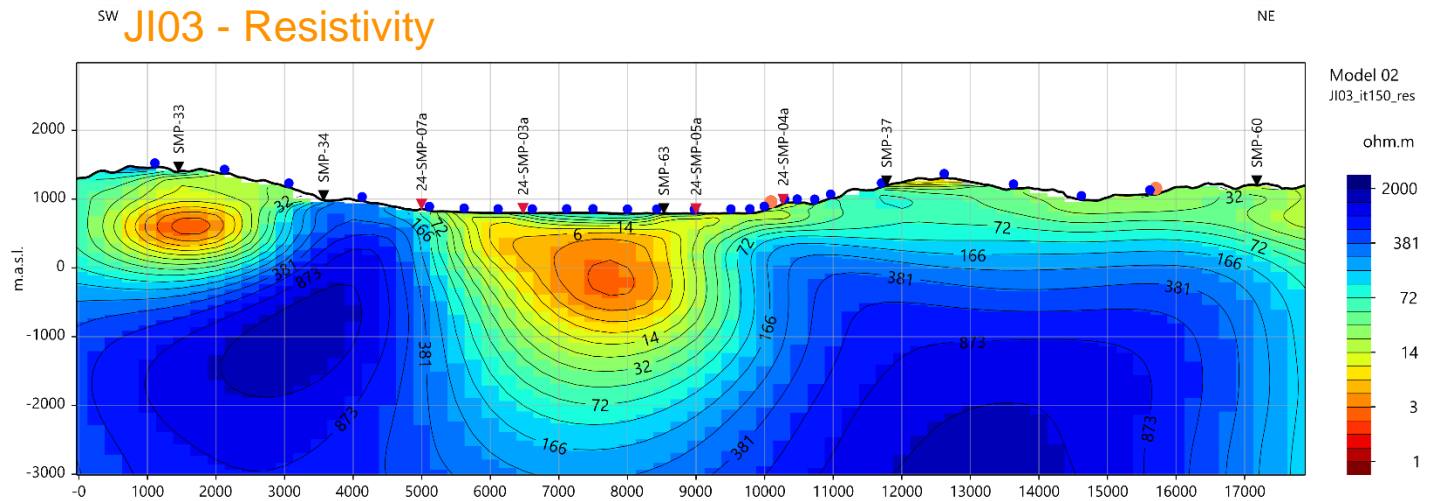
Gravity



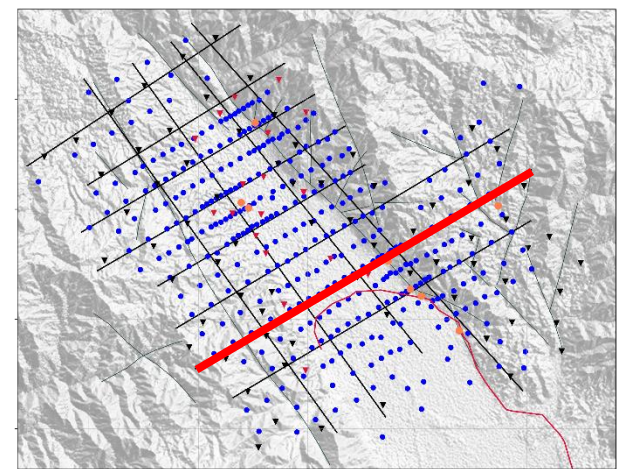
Manifestations



Profile SMP_07 (JI03)



MT + Gravity joint inversion

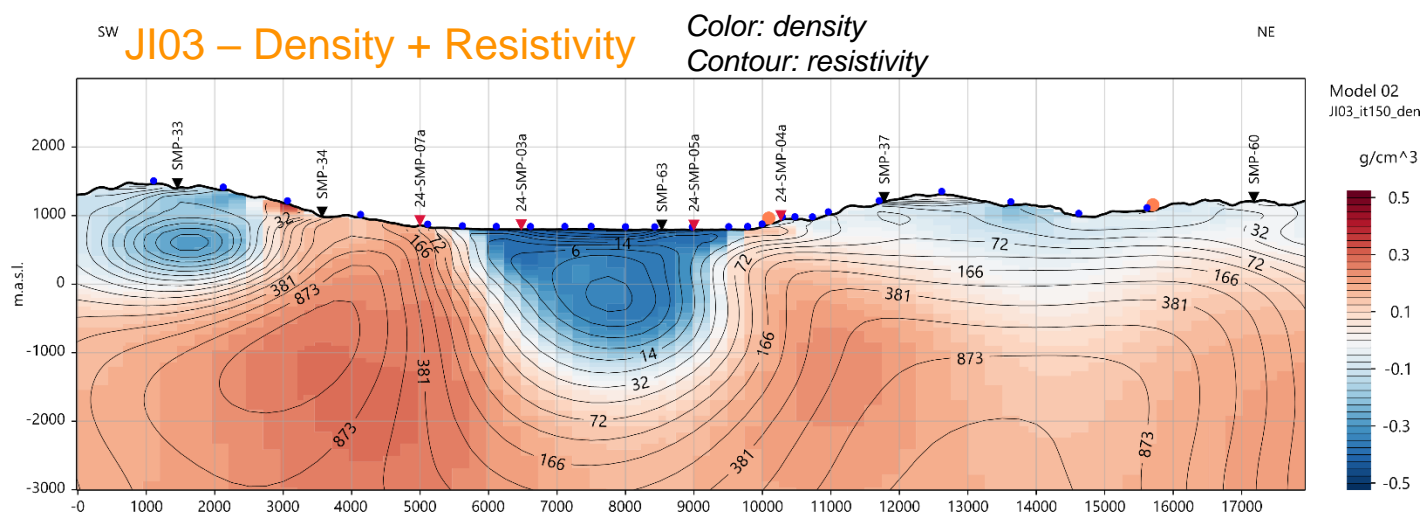


MT 2024

MT 2022

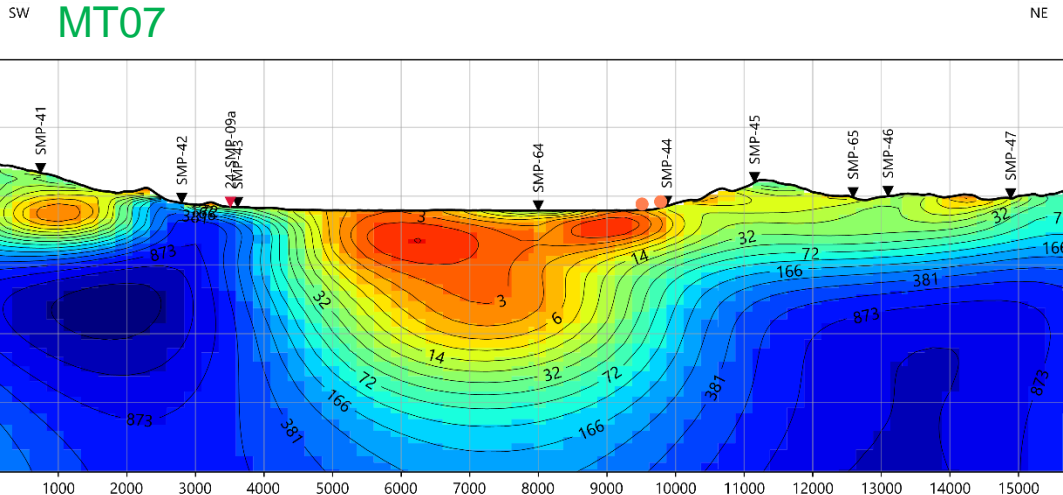
Gravity

Manifestations





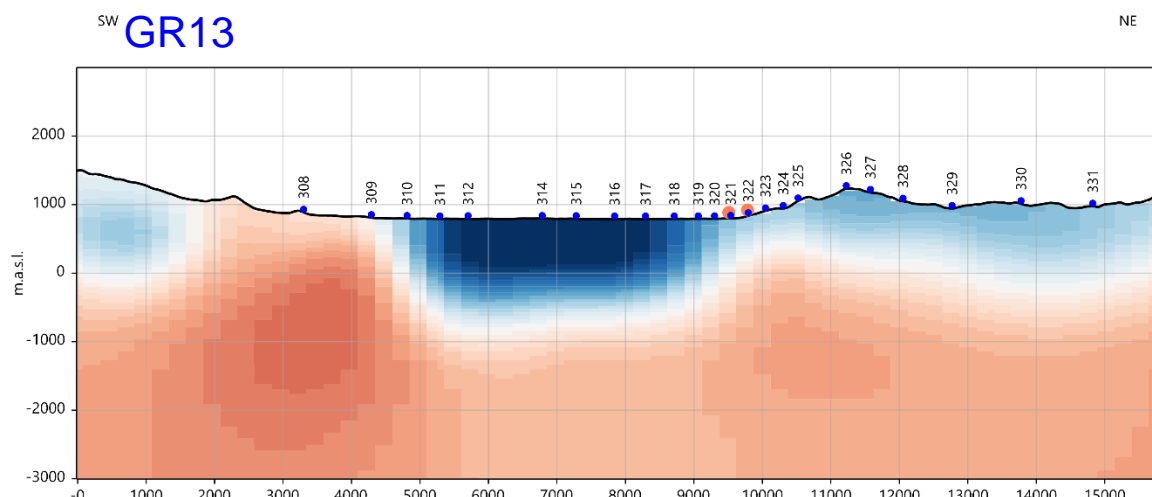
Profile SMP_08 (MT07 / GR13)



Model 02
Inv07_it080

ohm.m

2000
381
72
14
3
1

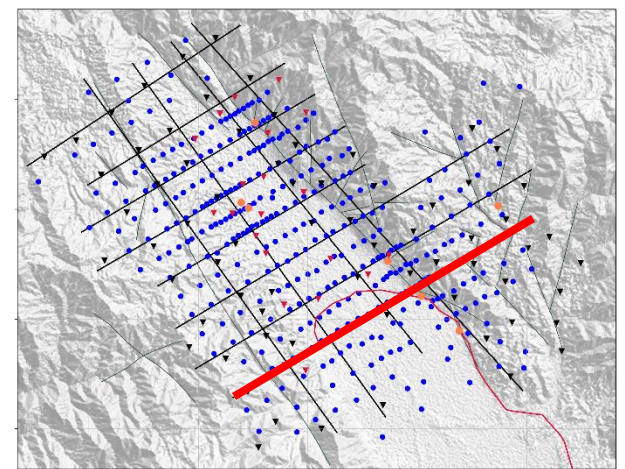


Model 02
GR13_it100

g/cm³

0.5
0.3
0.1
-0.1
-0.3
-0.5

Single domain
inversions



MT 2024



MT 2022



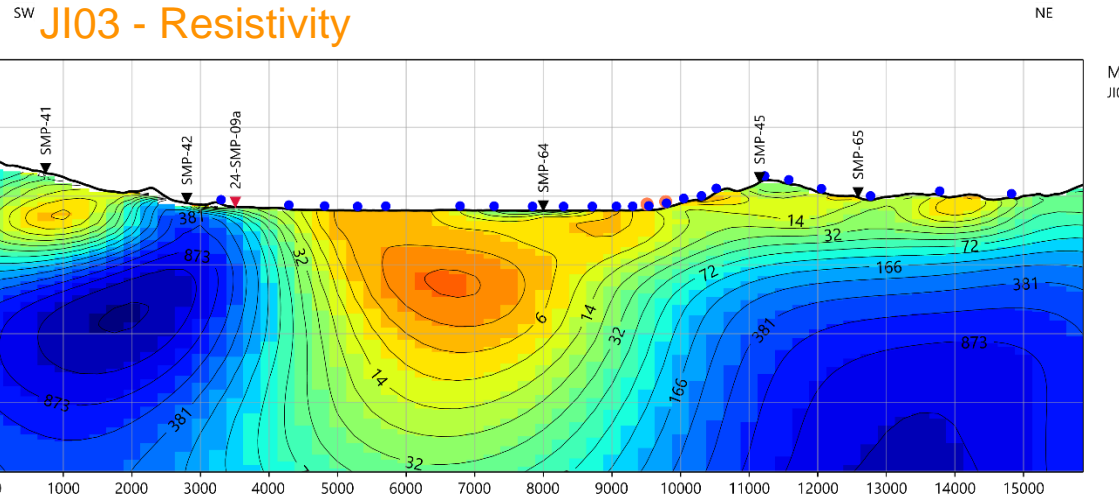
Gravity



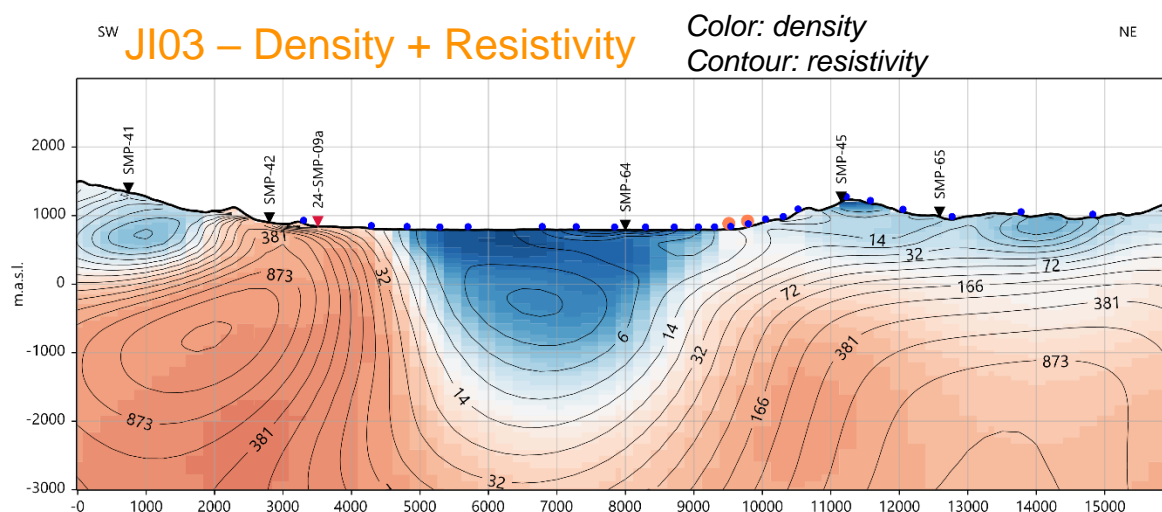
Manifestations



Profile SMP_08 (JI03)

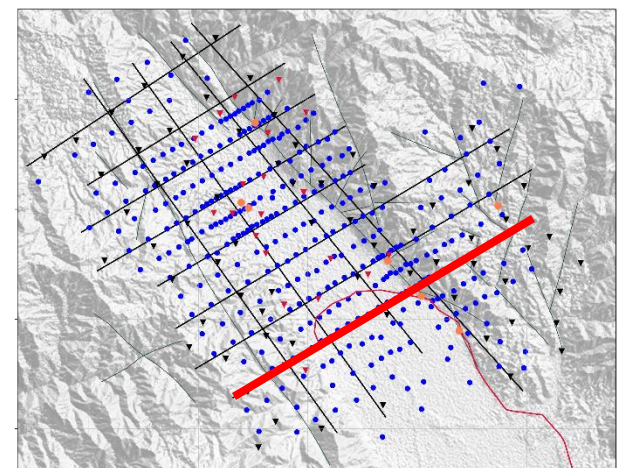


Model 02
JI03_it150_res
ohm.m



Model 02
JI03_it150_den
g/cm³

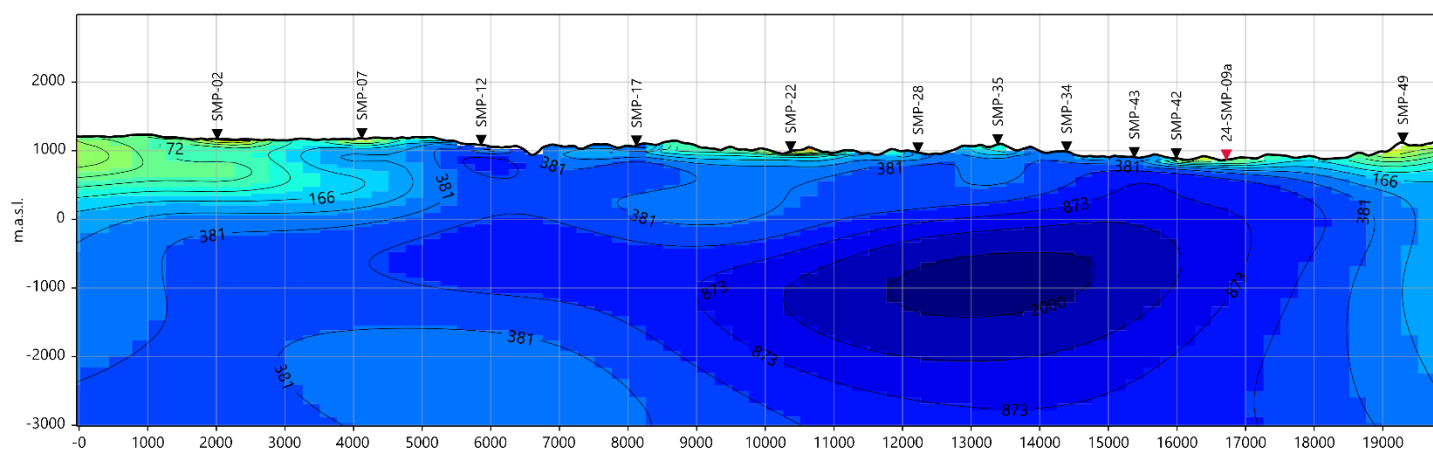
MT + Gravity
joint inversion



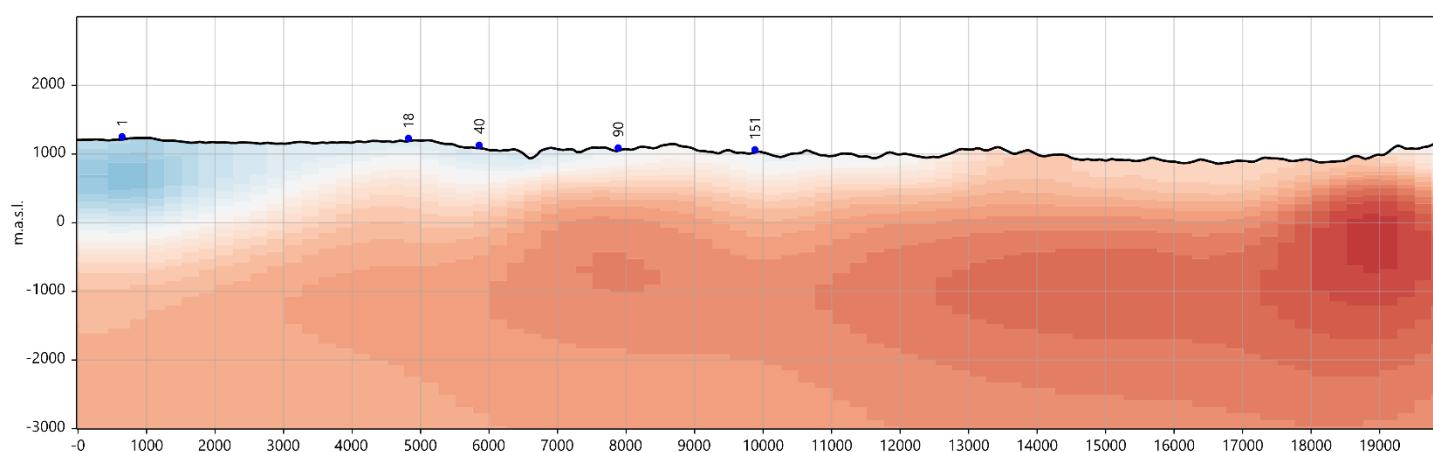
- MT 2024 ▼
- MT 2022 ▲
- Gravity ●
- Manifestations ○

Profile SMP_09 (MT07 / GR13)

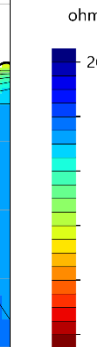
NW MT07



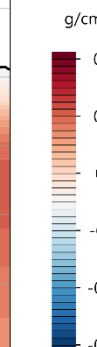
NW GR13



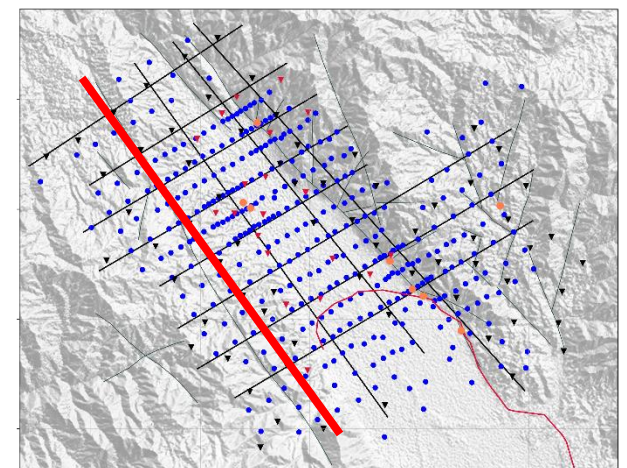
Model 02
Inv07_it080



Model 02
GR13_it100

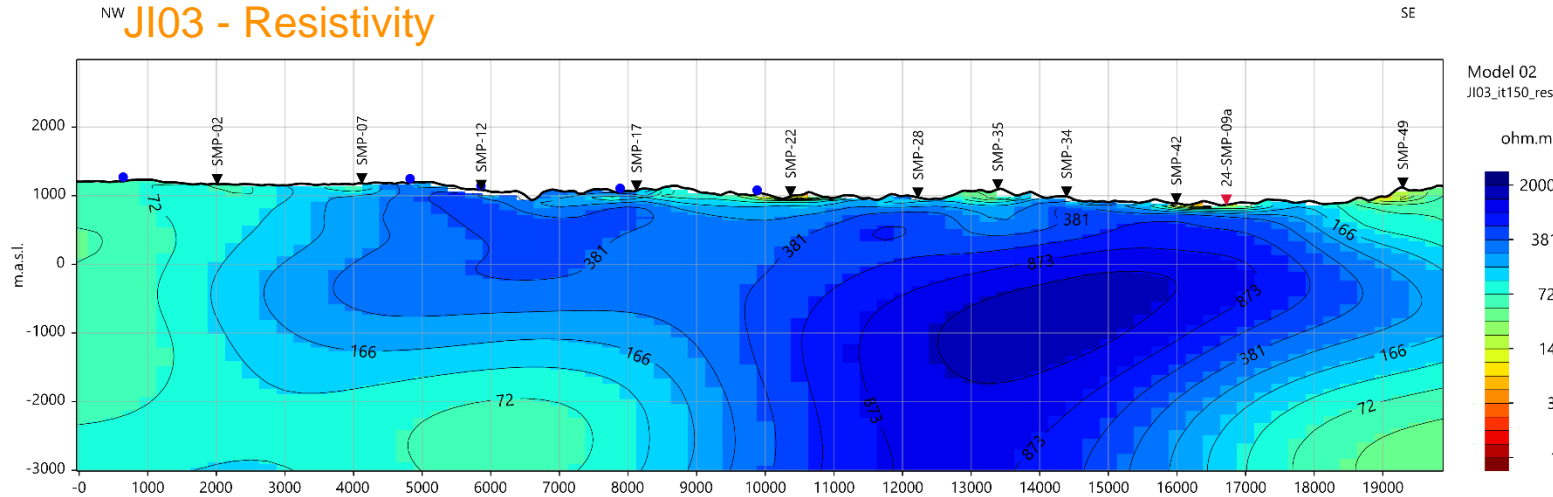


Single domain
inversions



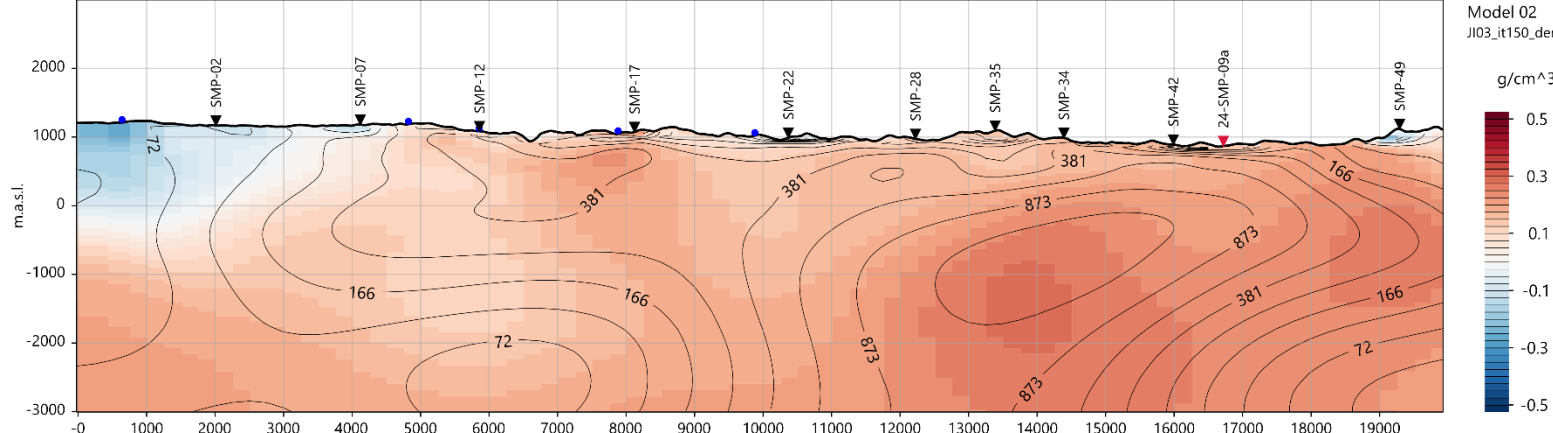
Profile SMP_09 (JI03)

NW JI03 - Resistivity

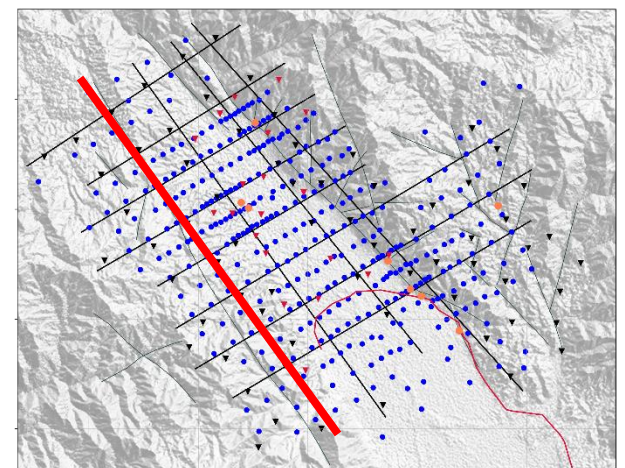


NW JI03 – Density + Resistivity

Color: density
Contour: resistivity



MT + Gravity
joint inversion



MT 2024



MT 2022



Gravity

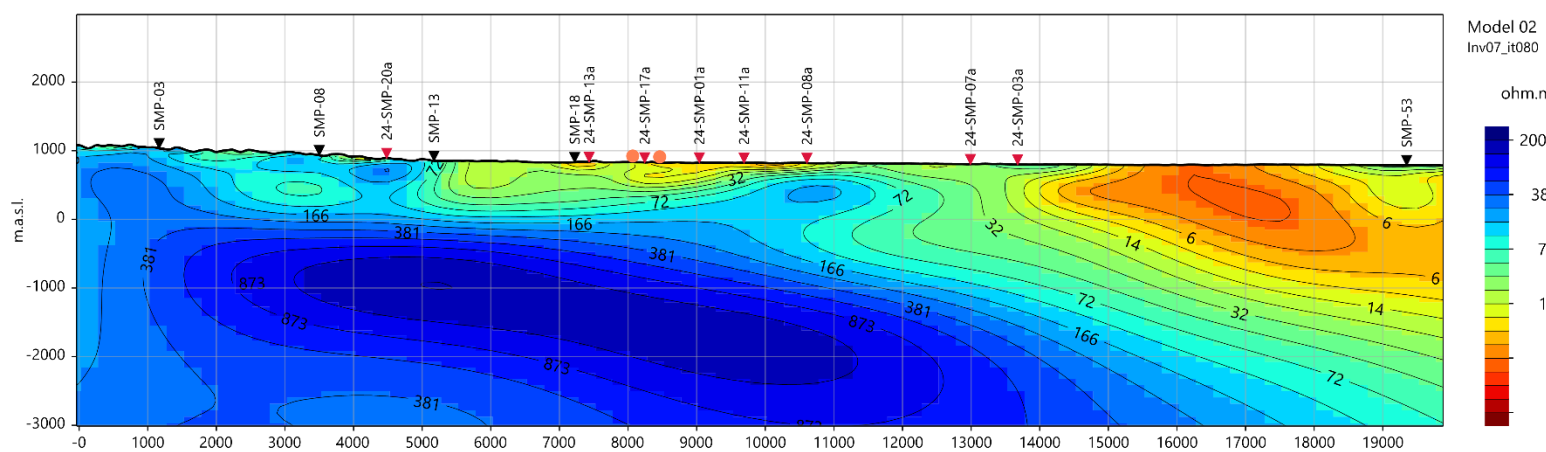


Manifestations

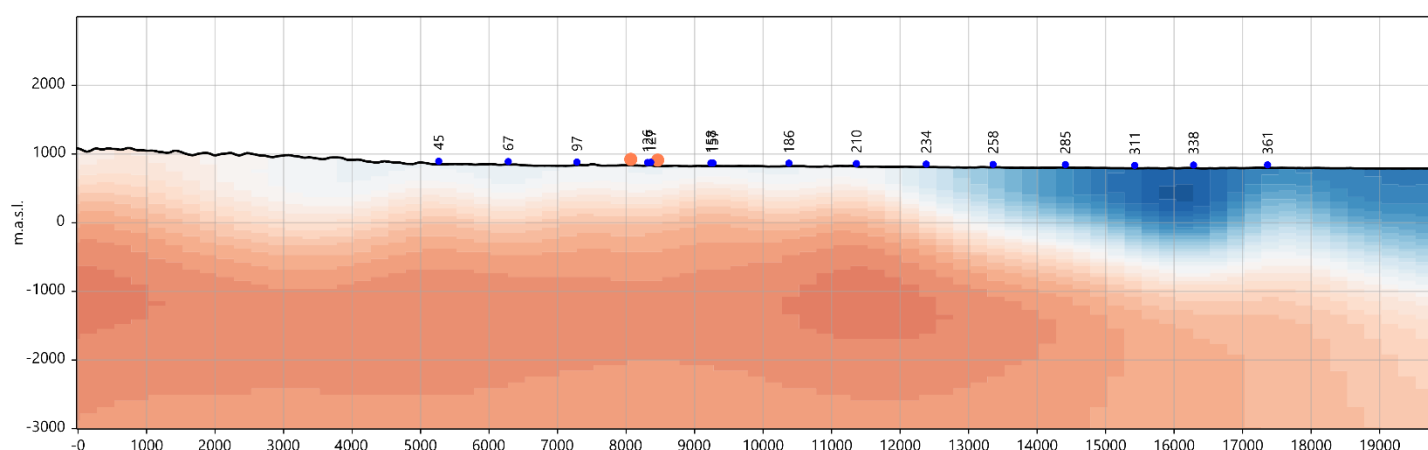


Profile SMP_10 (MT07 / GR13)

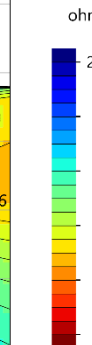
MT07



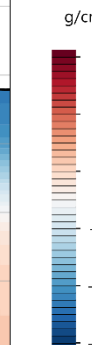
GR13



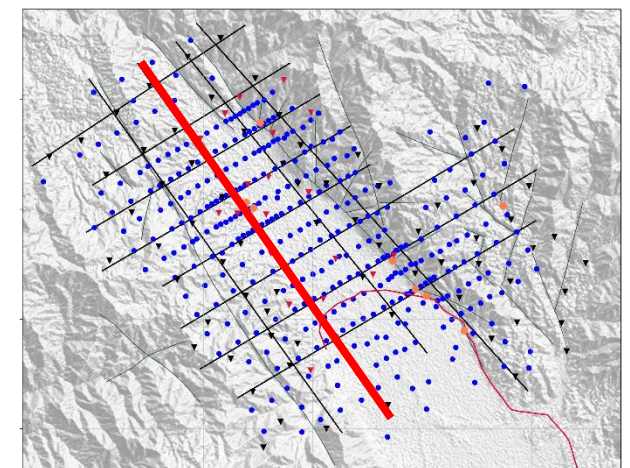
Model 02
Inv07_it080



Model 02
GR13_it100



Single domain
inversions



MT 2024



MT 2022



Gravity

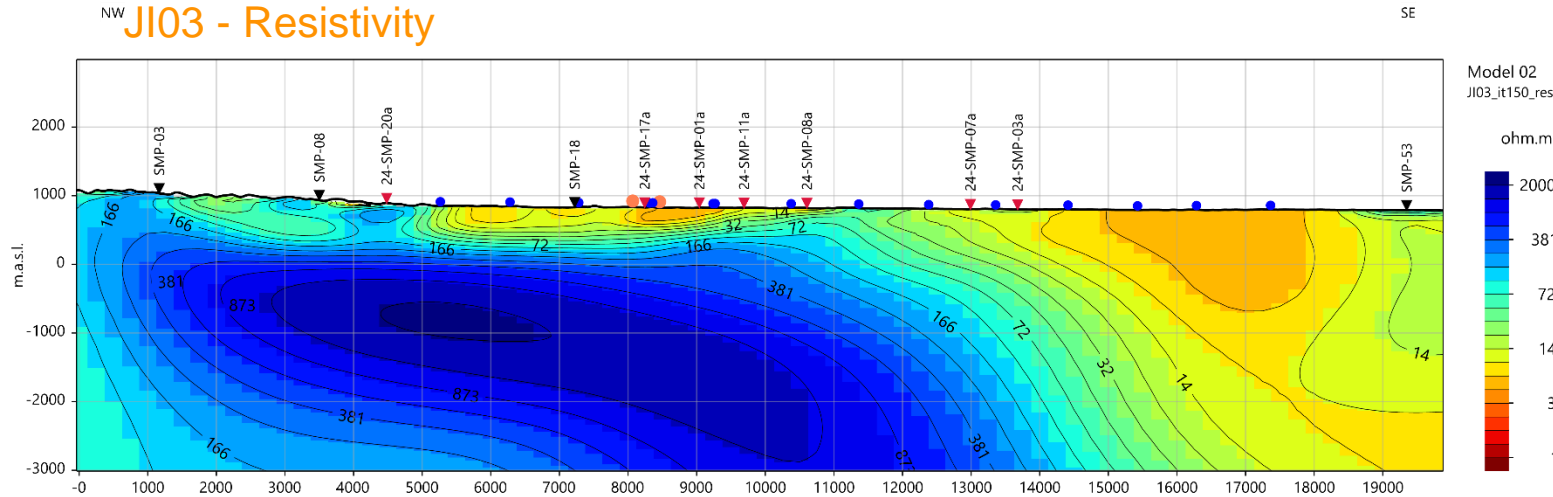


Manifestations



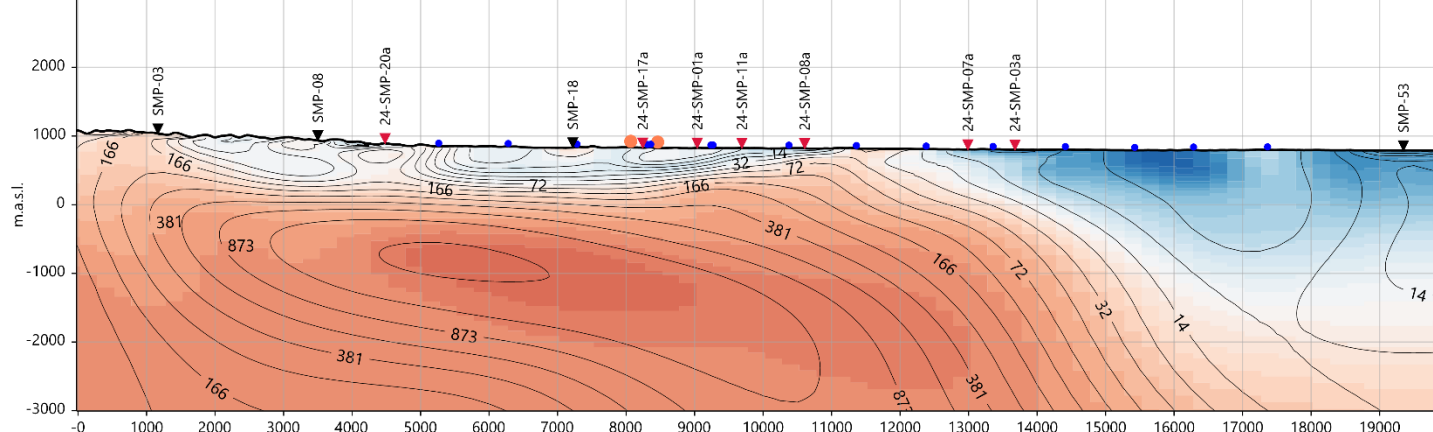
Profile SMP_10 (JI03)

NW JI03 - Resistivity

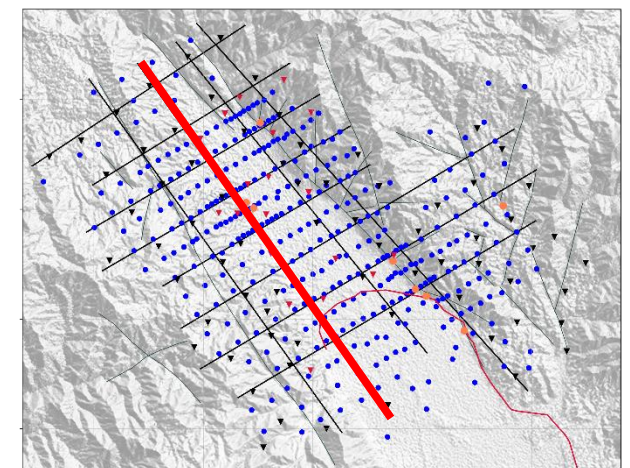


NW JI03 – Density + Resistivity

Color: density
Contour: resistivity



MT + Gravity
joint inversion



MT 2024



MT 2022



Gravity



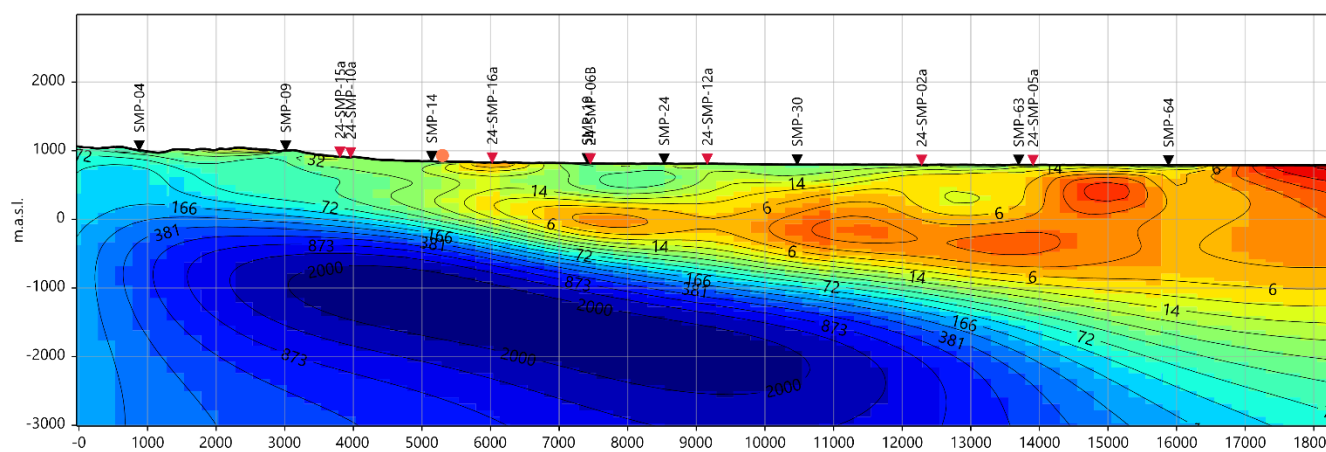
Manifestations



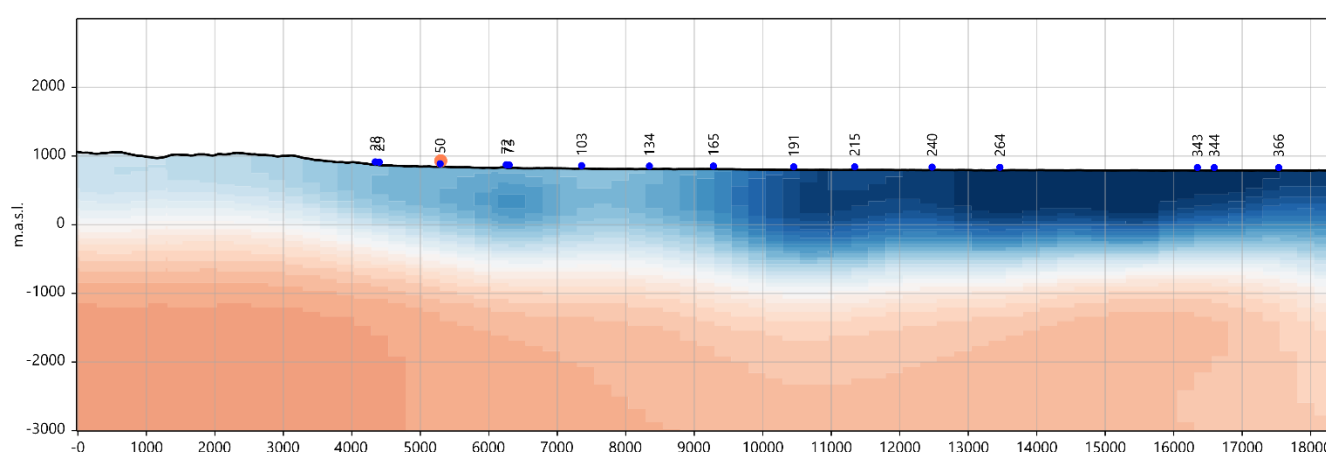


Profile SMP_11 (MT07 / GR13)

NW MT07

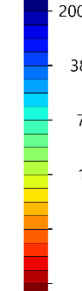


NW GR13



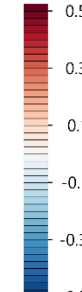
Model 02
Inv07_it080

ohm.m

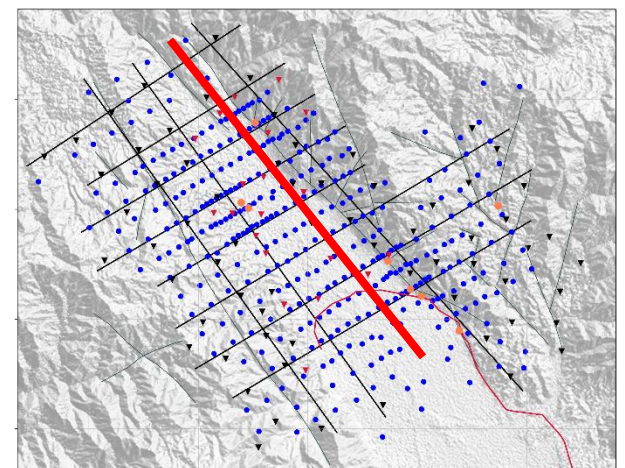


Model 02
GR13_it100

g/cm³



Single domain
inversions



MT 2024



MT 2022



Gravity



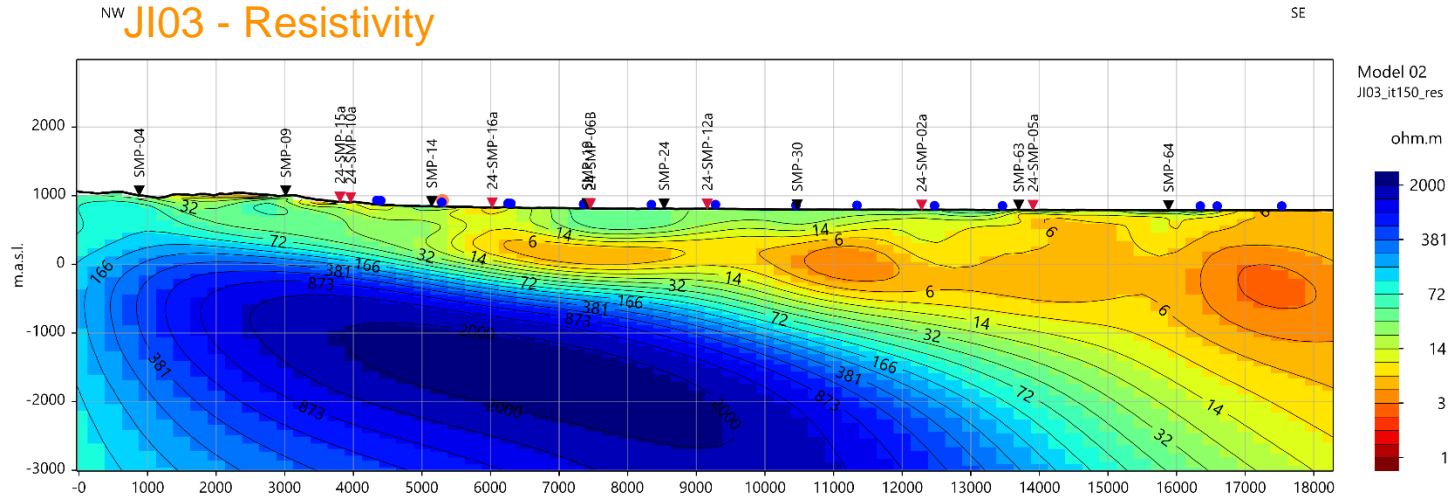
Manifestations



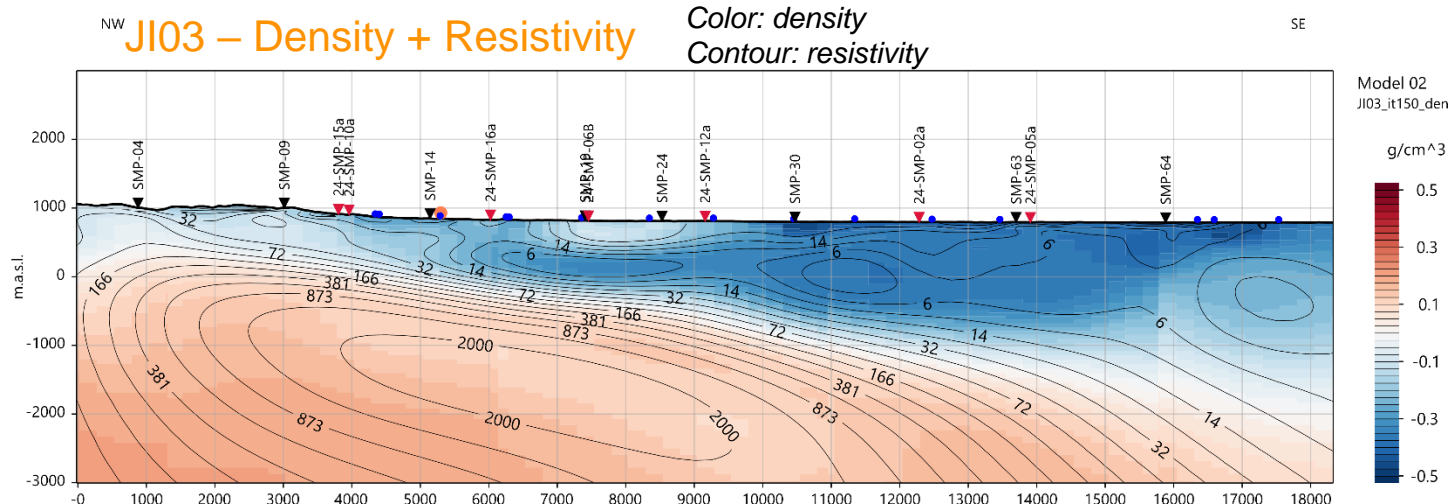


Profile SMP_11 (JI03)

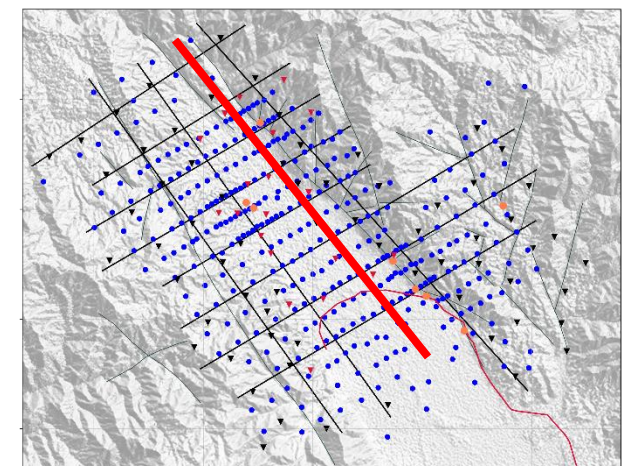
NW JI03 - Resistivity



NW JI03 – Density + Resistivity



MT + Gravity
joint inversion



MT 2024



MT 2022



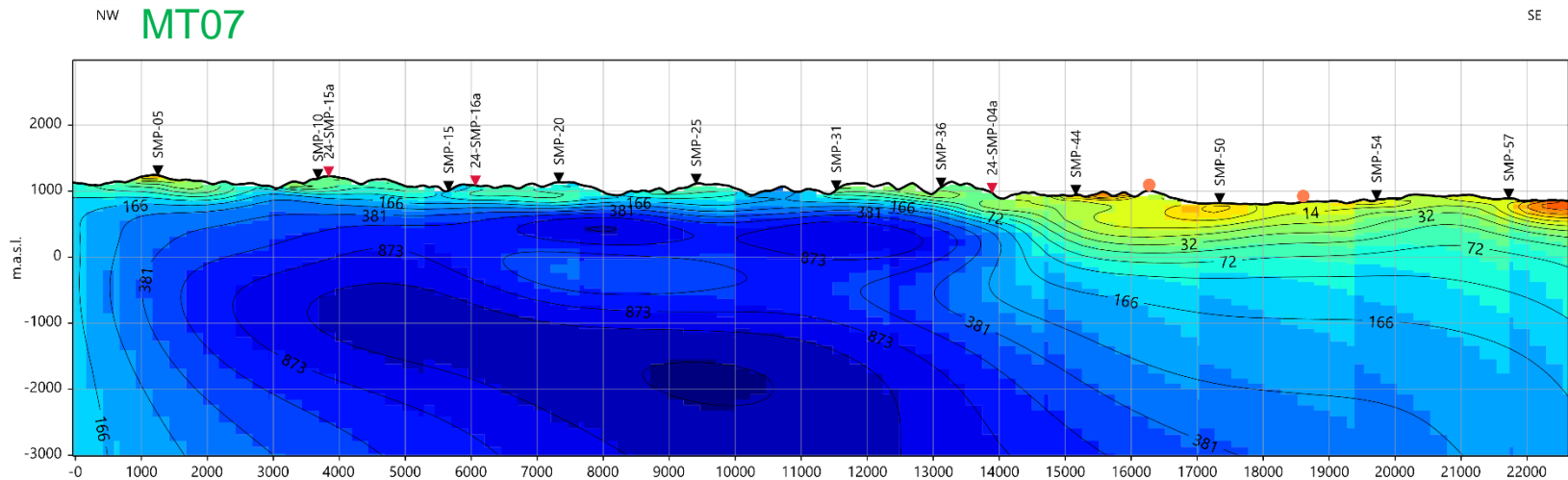
Gravity



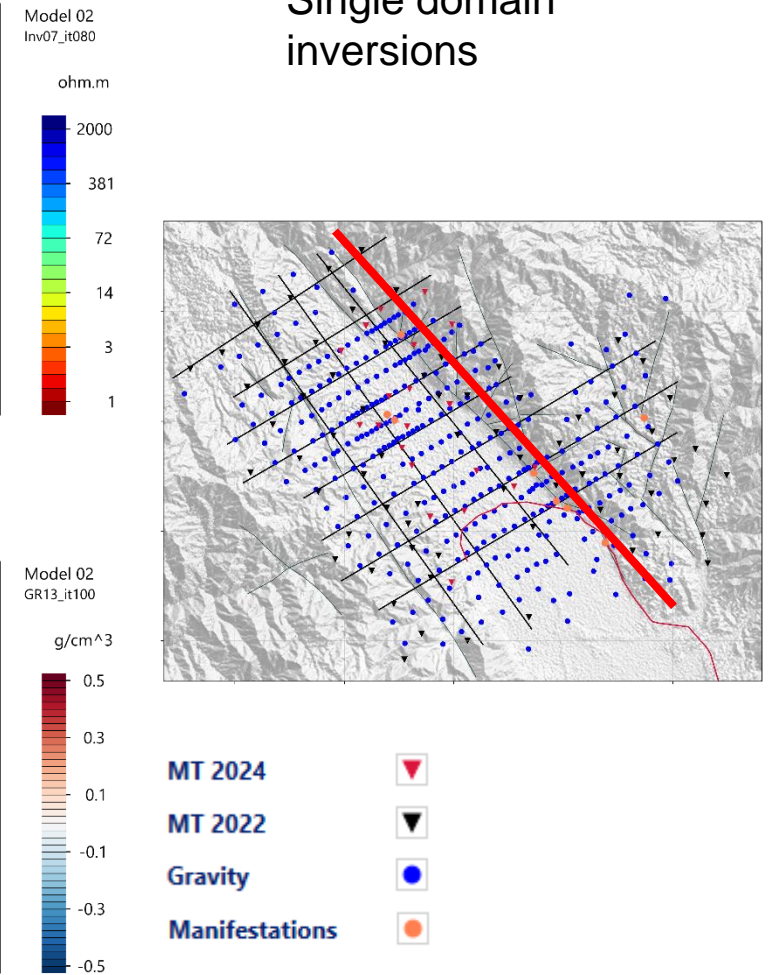
Manifestations



Profile SMP_12 (MT07 / GR13)

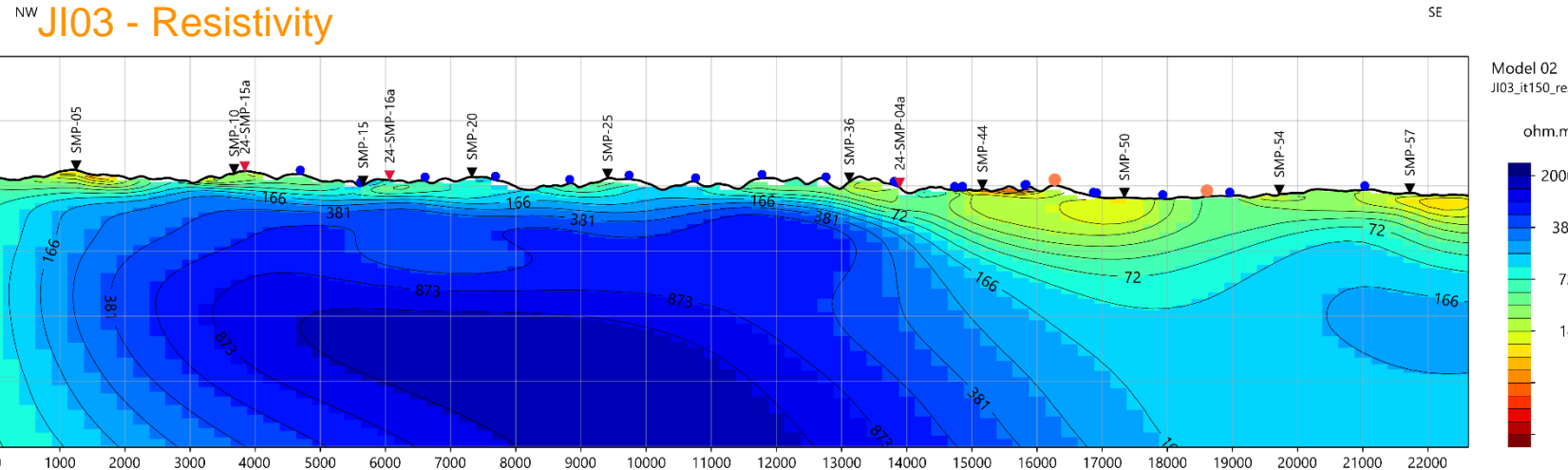


Single domain inversions

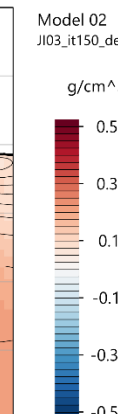
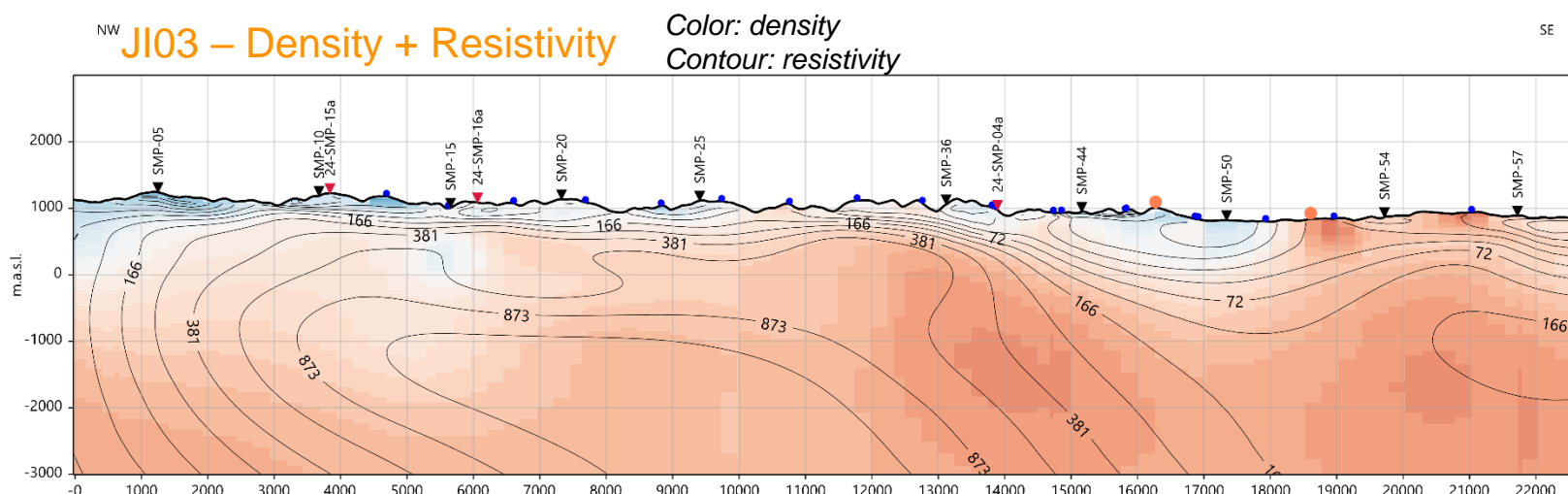
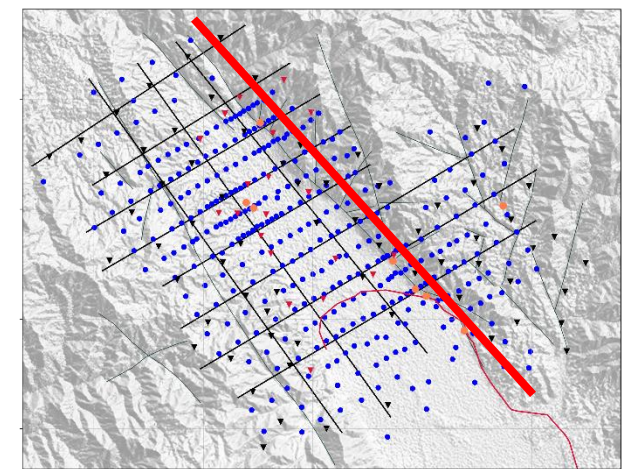
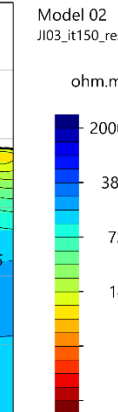




Profile SMP_12 (JI03)



MT + Gravity
joint inversion

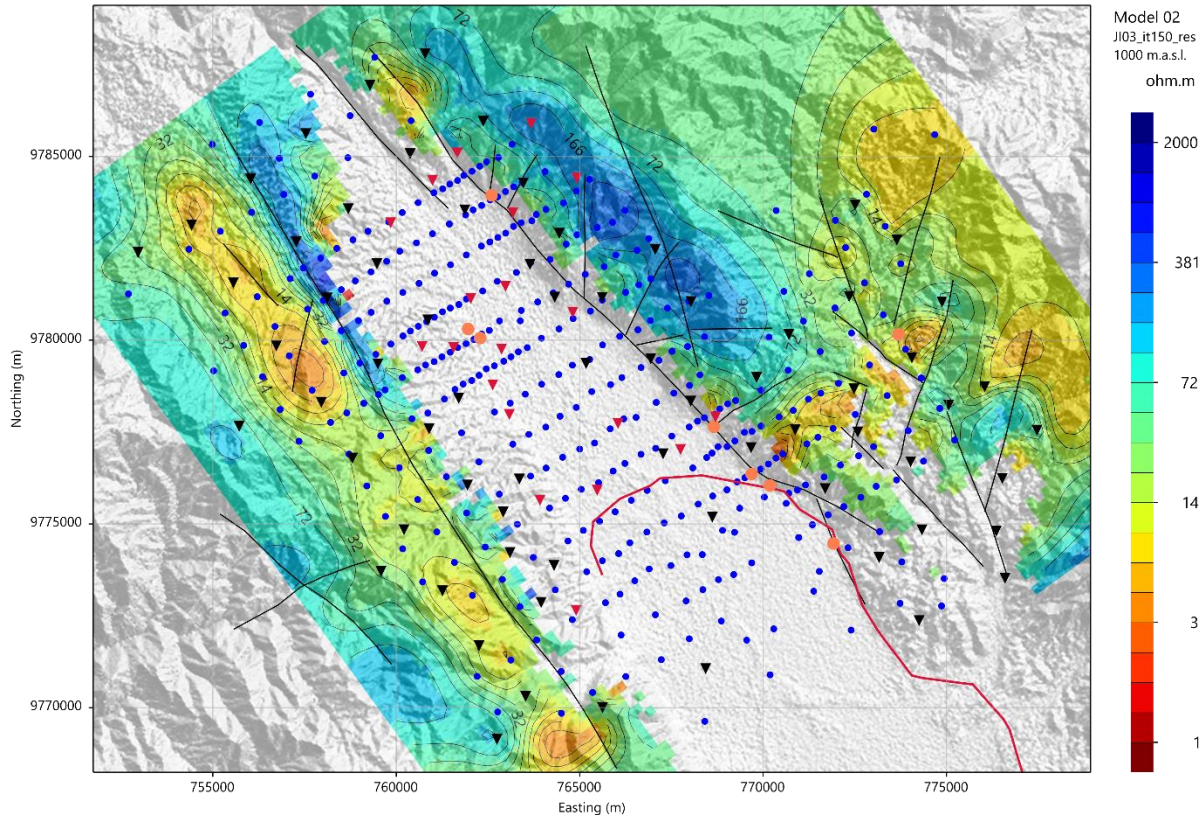


- MT 2024
- MT 2022
- Gravity
- Manifestations

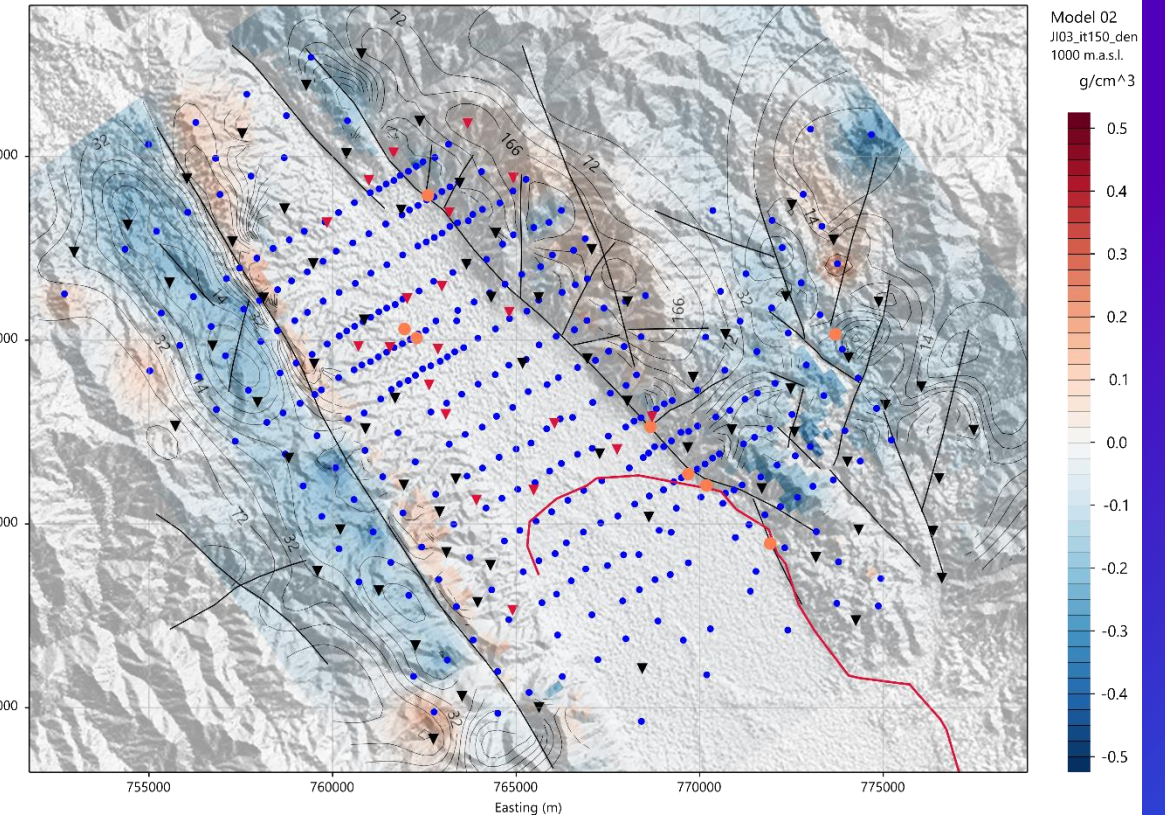
Maps at 1,000m asl (JI03)



JI03 - Resistivity



JI03 - Density

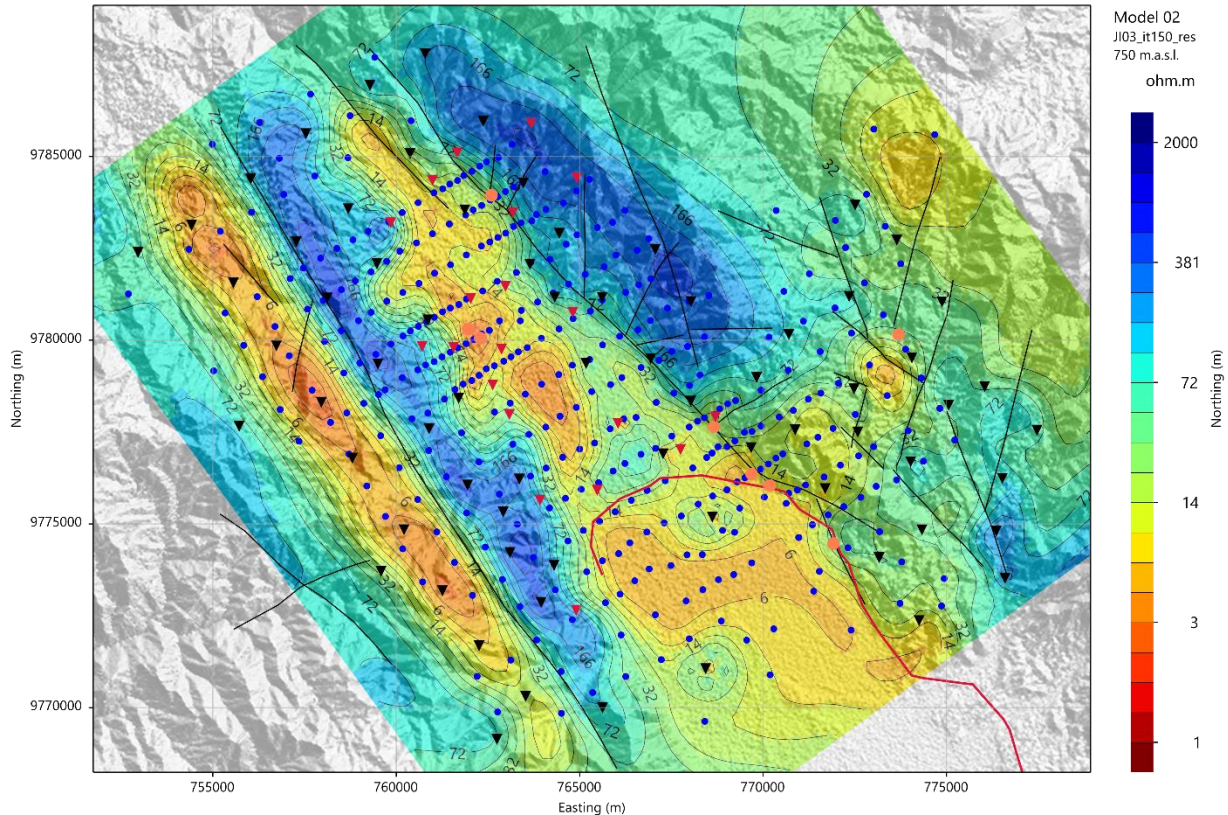


Color: density
Contour: resistivity

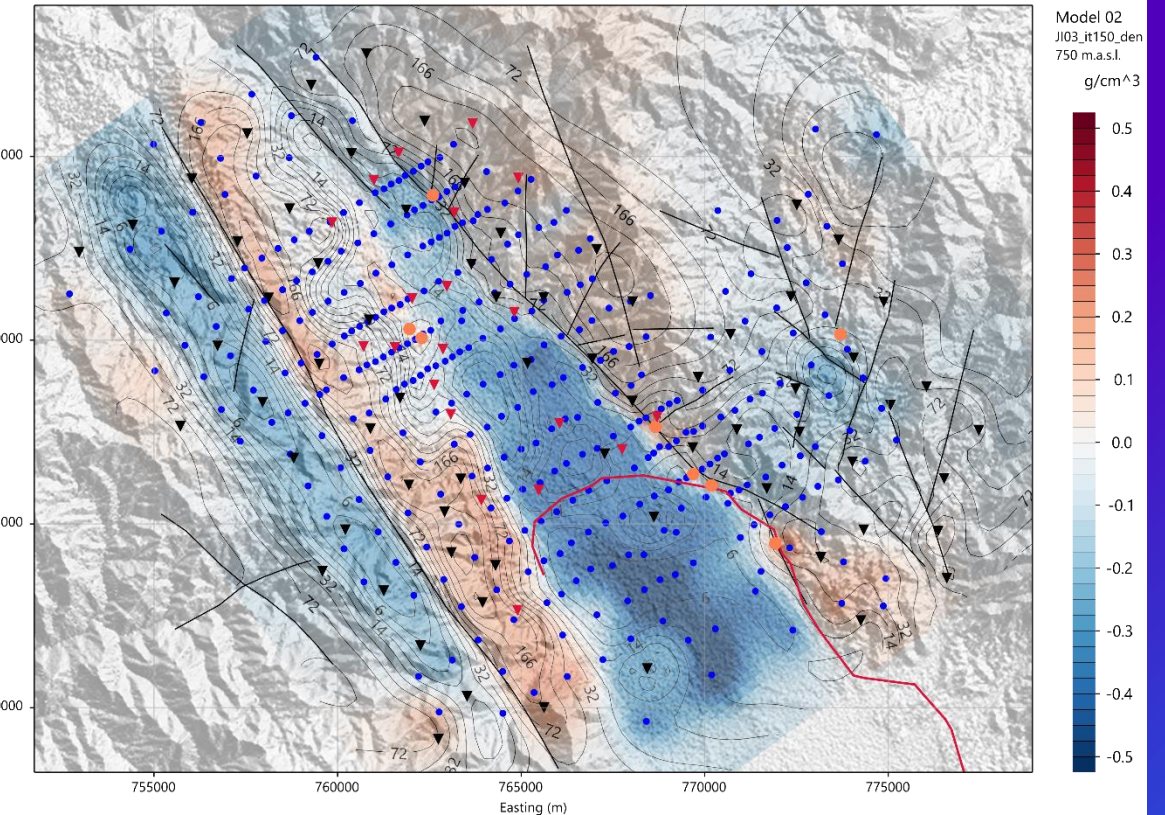
Maps at 750m asl (JI03)



JI03 - Resistivity

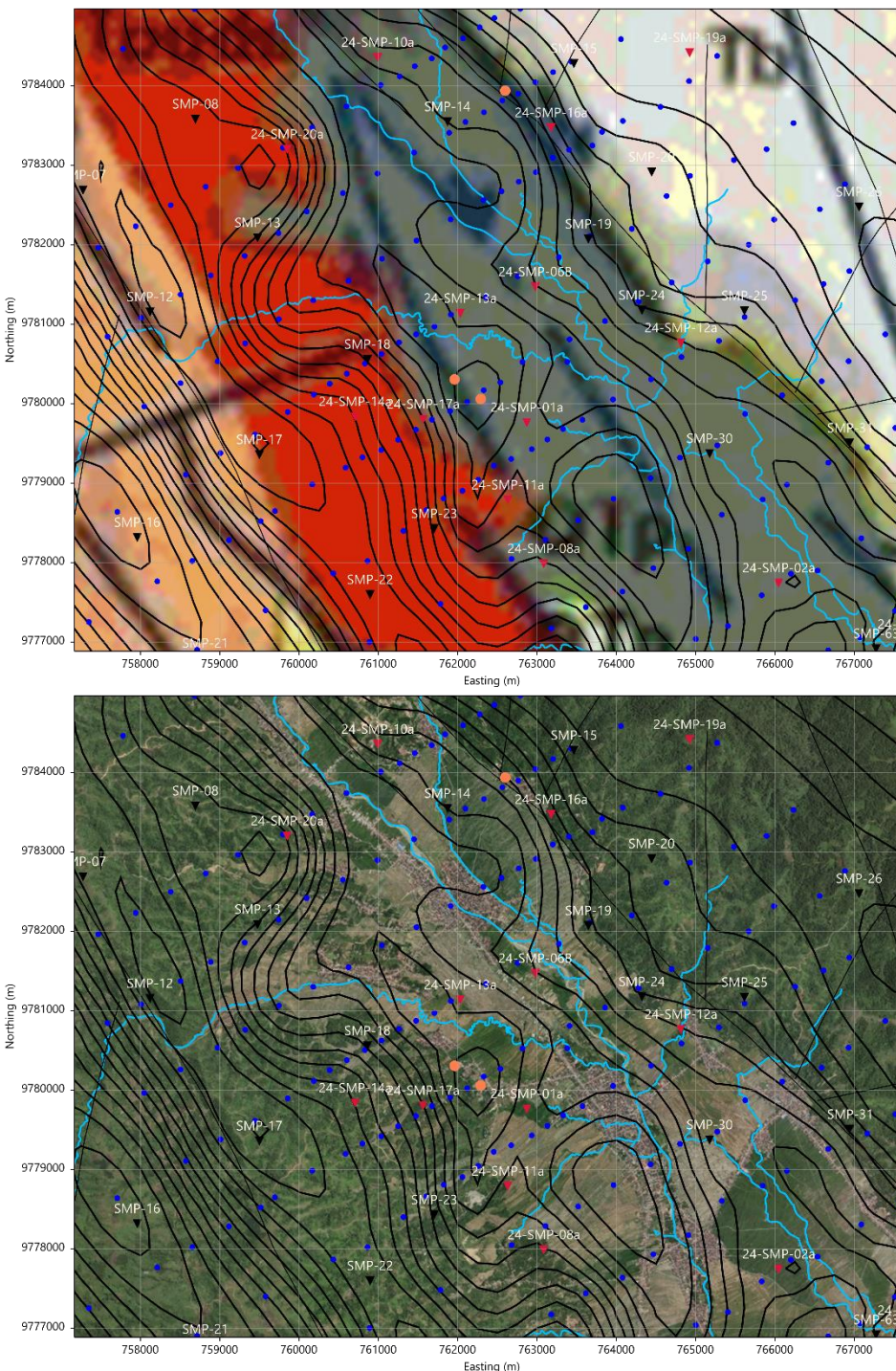
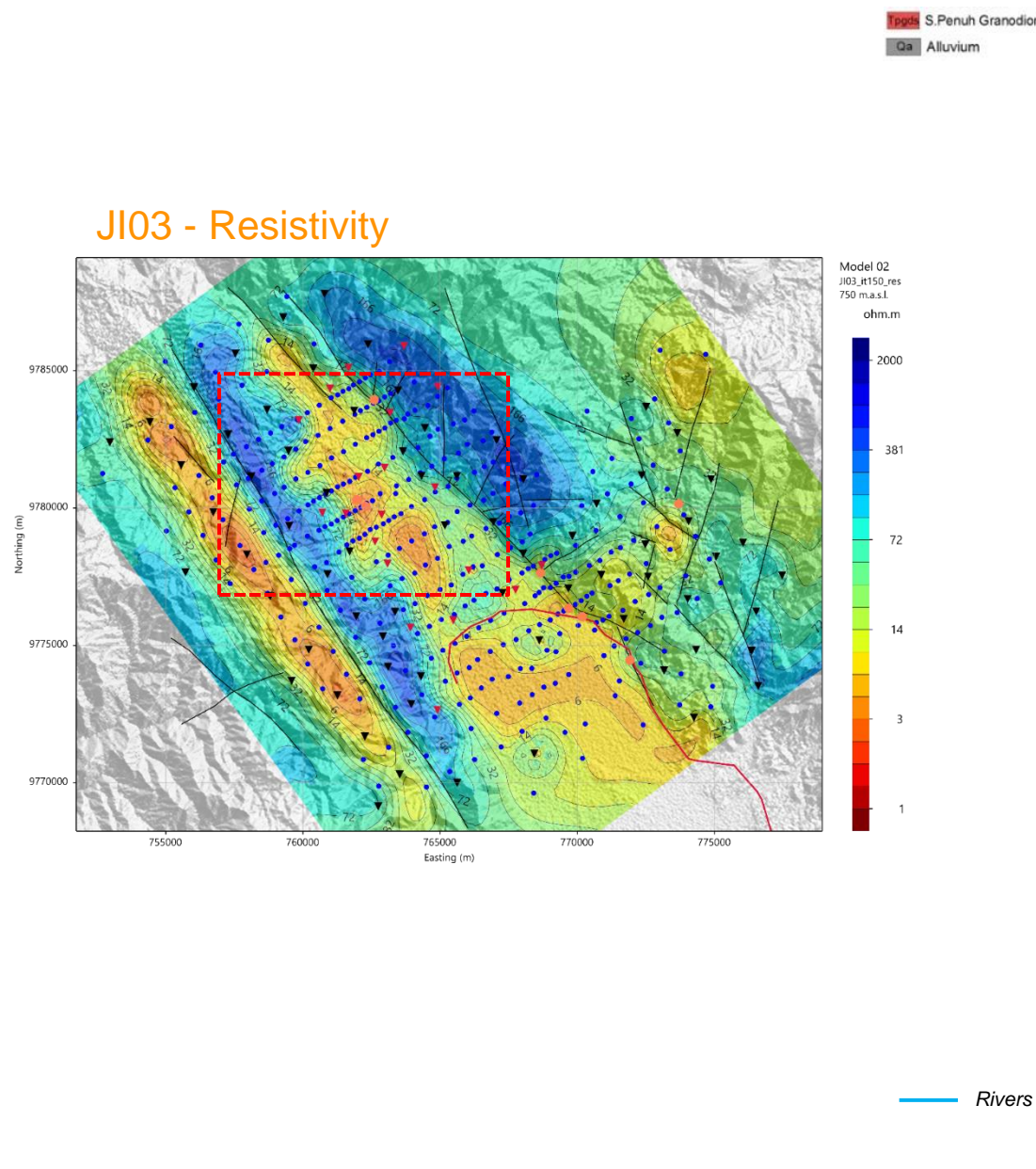


JI03 - Density



Color: density
Contour: resistivity

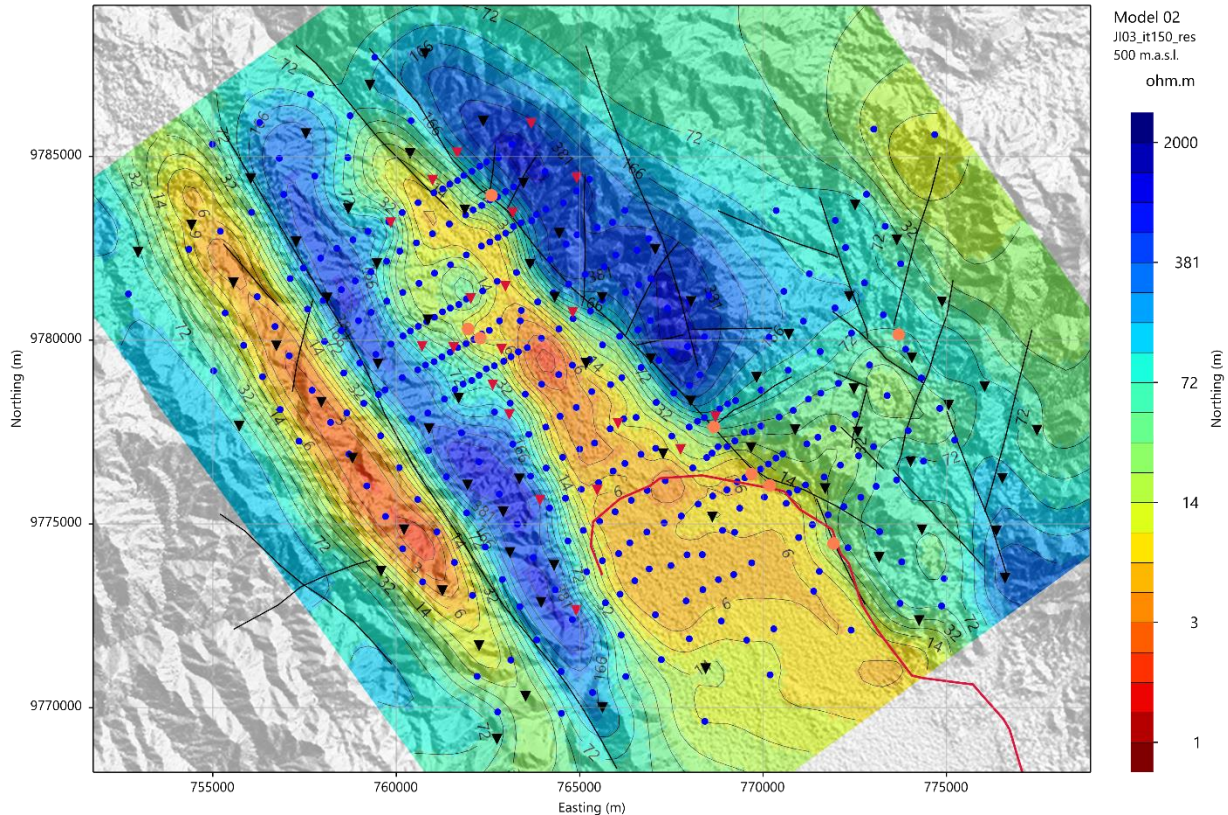
Maps at 750m asl (JI03)



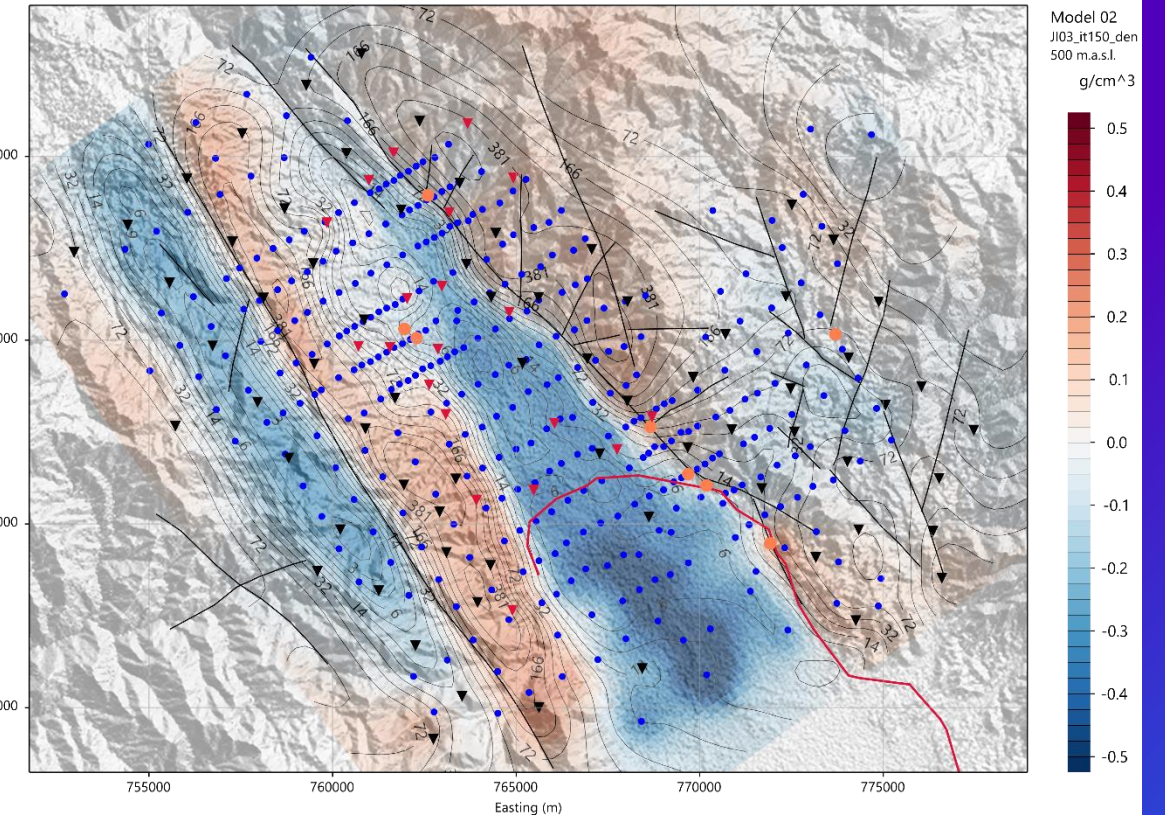
Maps at 500m asl (JI03)



JI03 - Resistivity



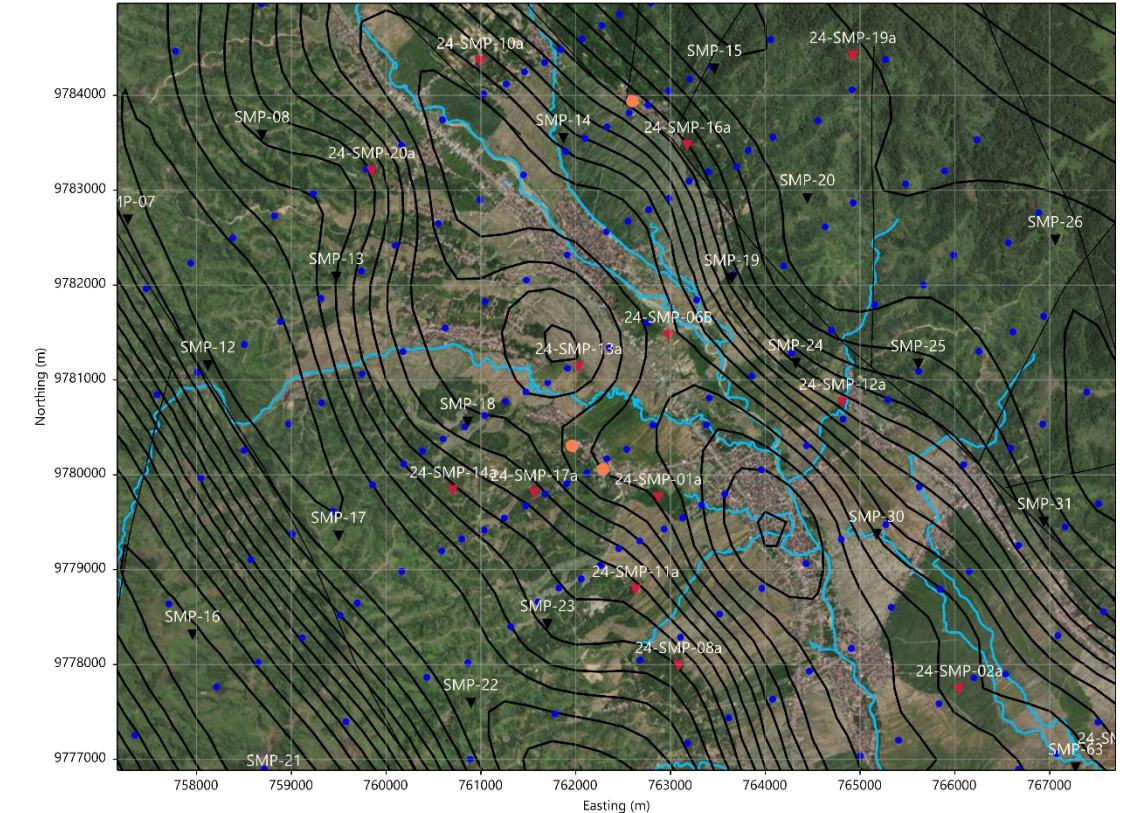
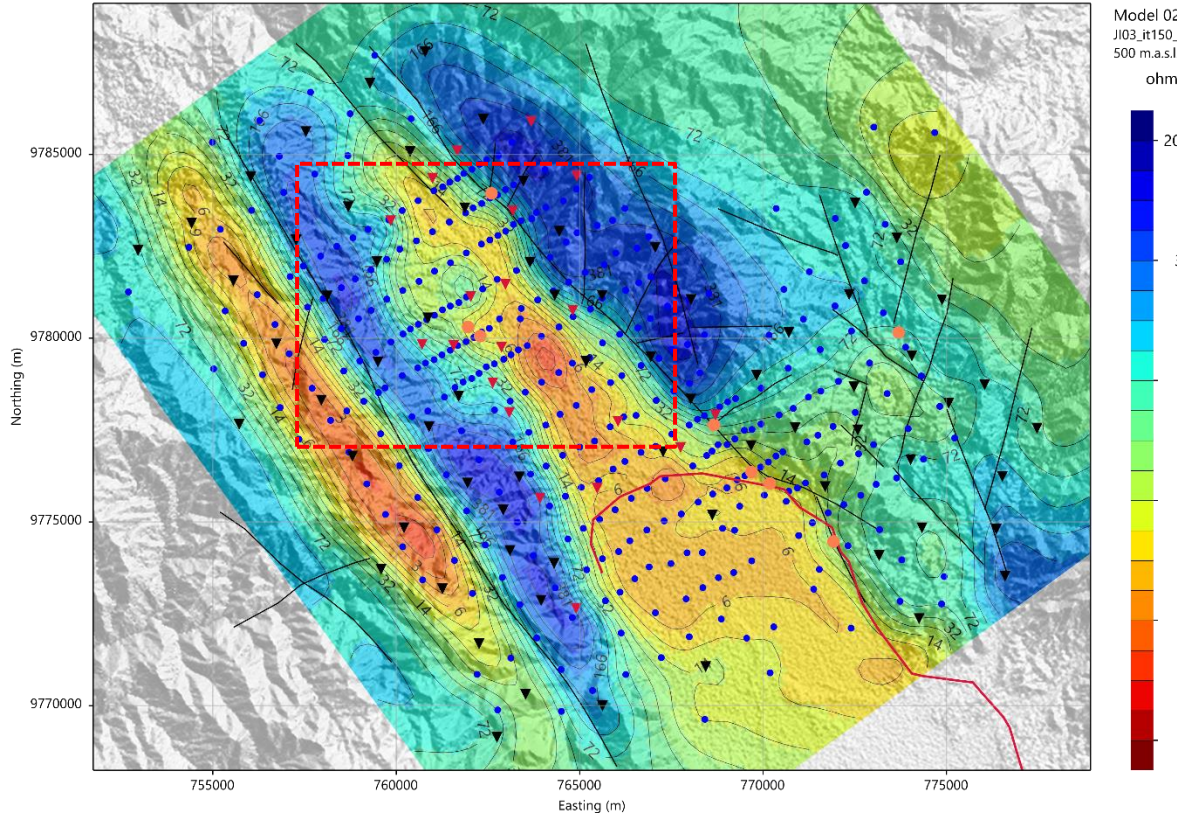
JI03 - Density



Maps at 500m asl (JI03)



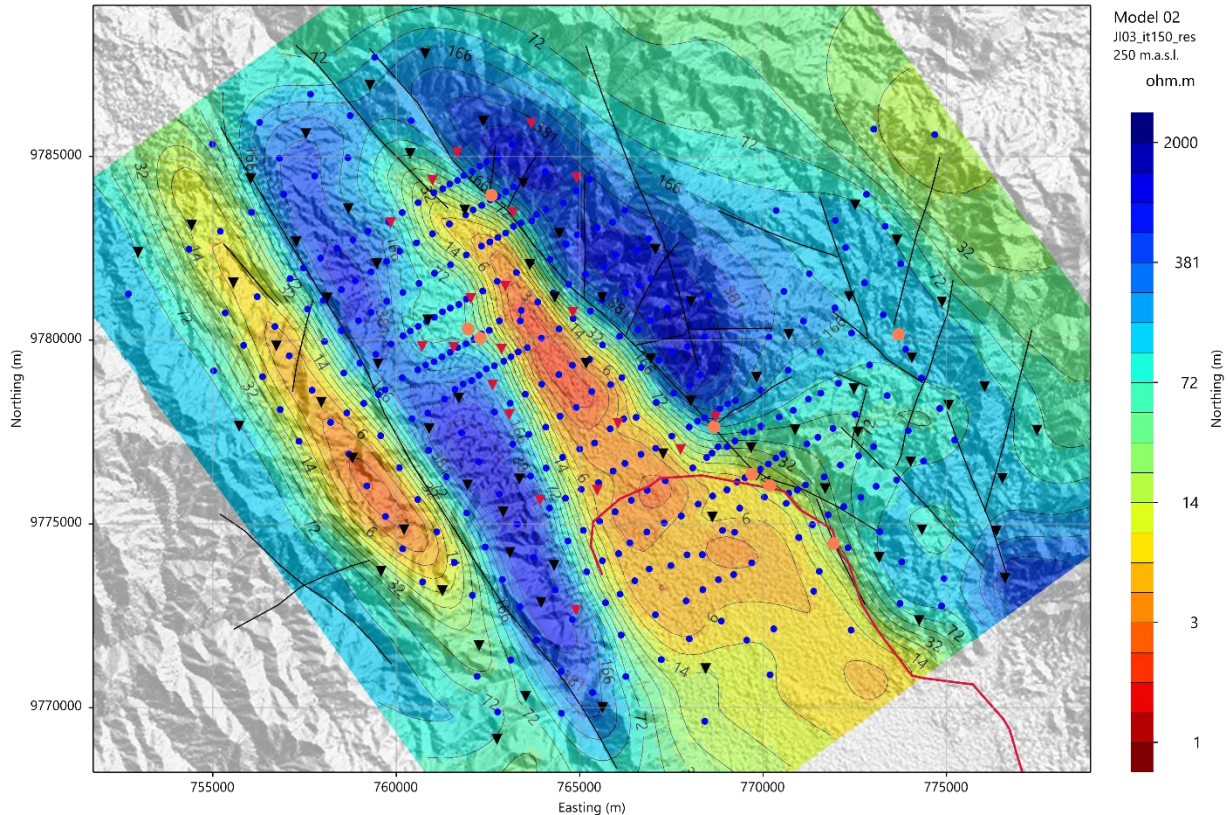
JI03 - Resistivity



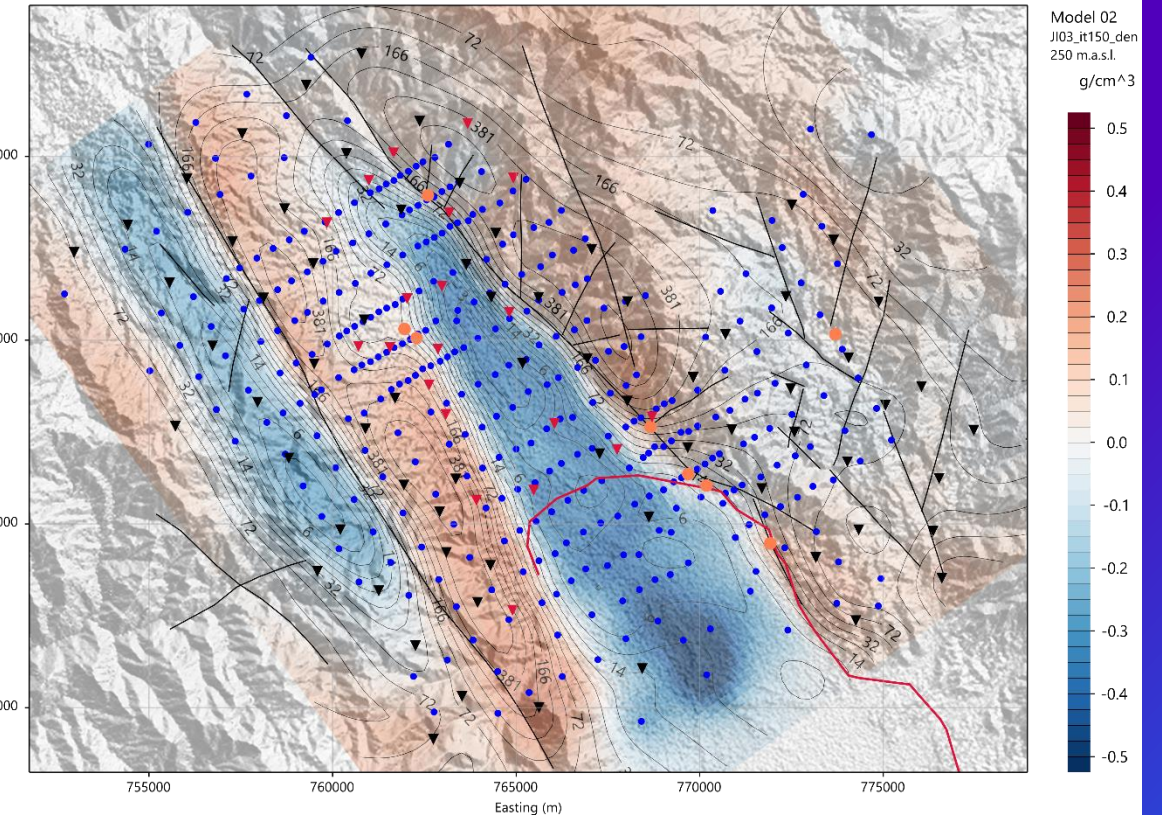
Maps at 250m asl (JI03)



JI03 - Resistivity



JI03 - Density

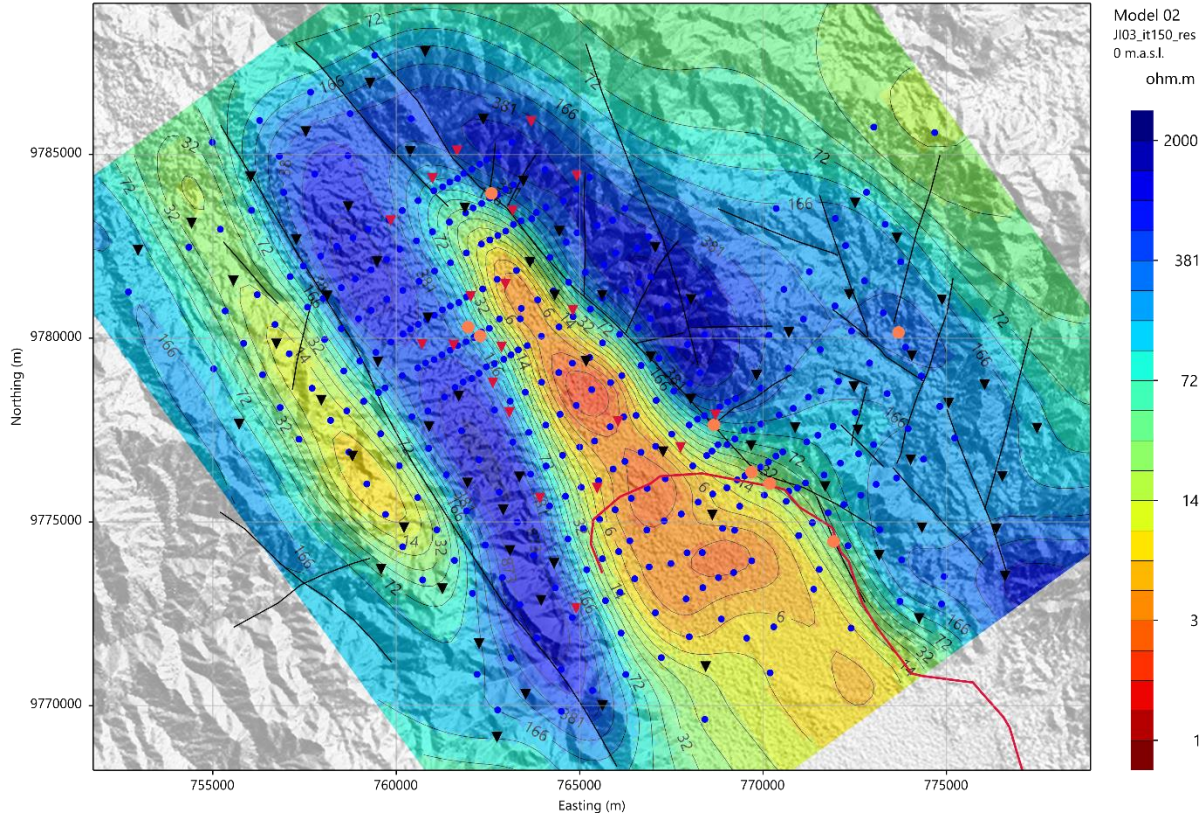


Color: density
Contour: resistivity

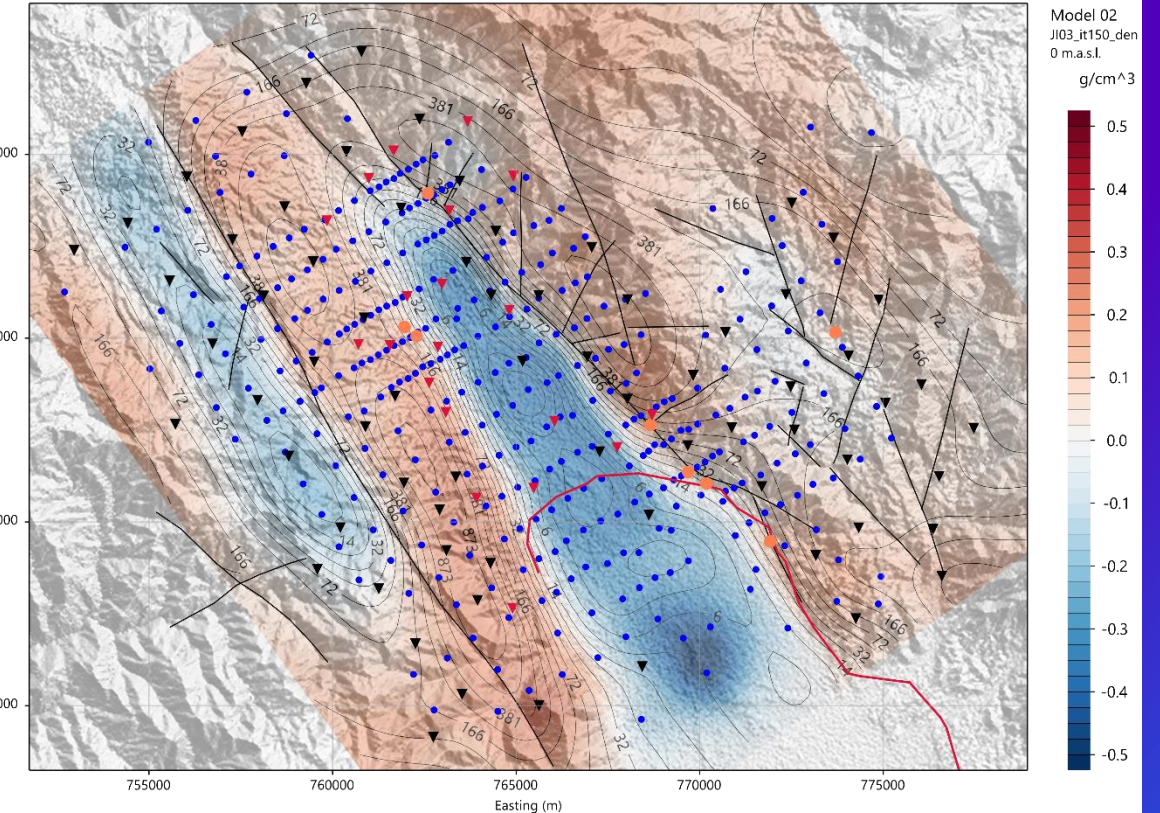
Maps at 0m asl (JI03)



JI03 - Resistivity



JI03 - Density

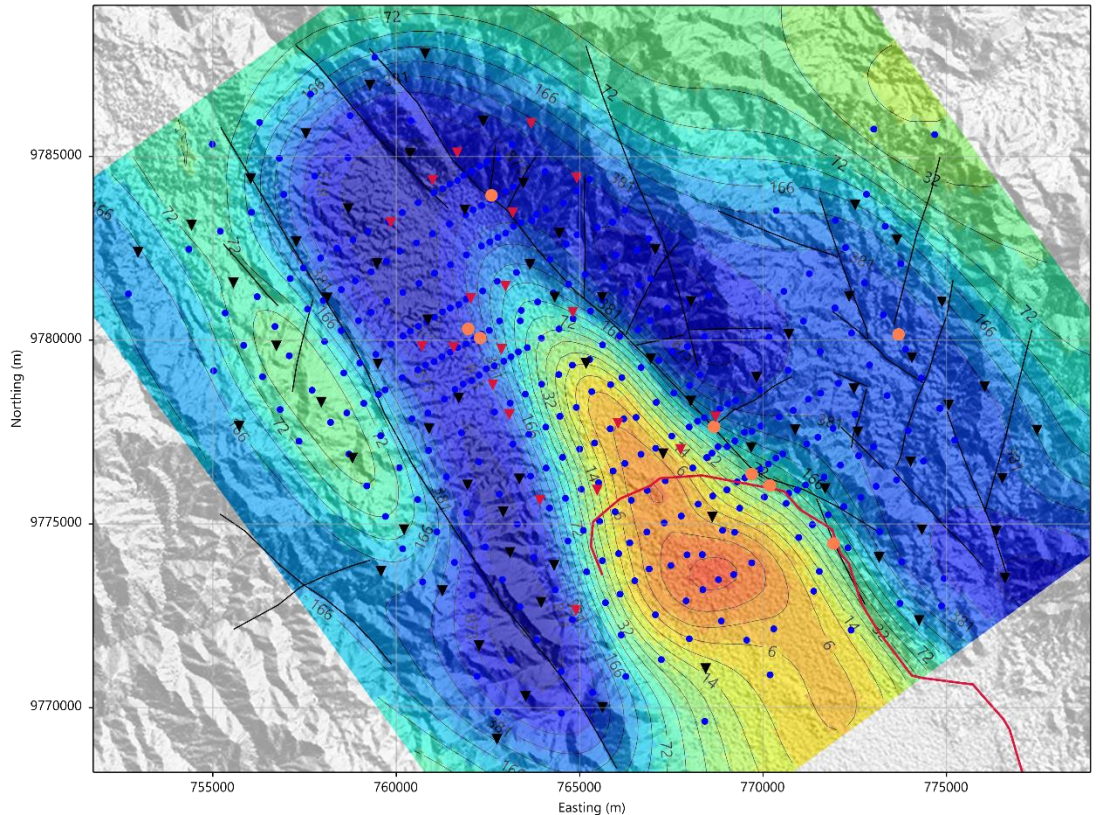


Color: density
Contour: resistivity

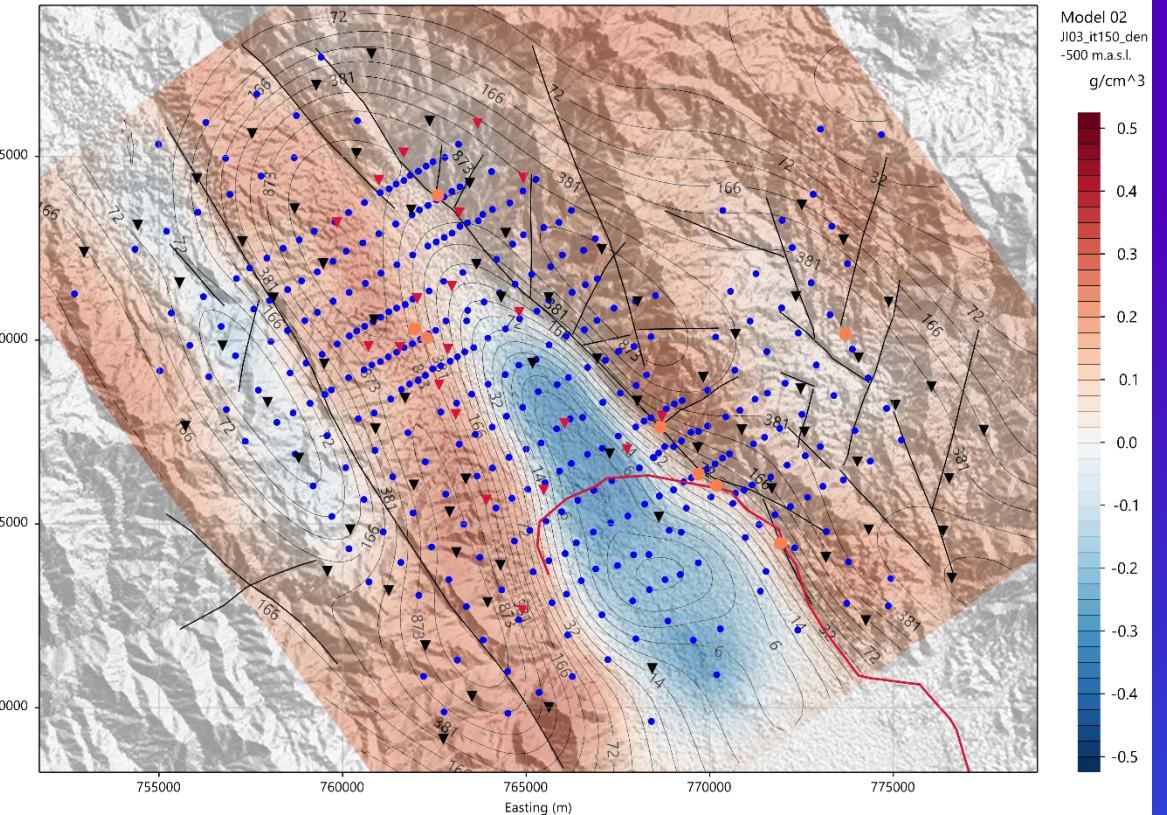
Maps at -500m asl (JI03)



JI03 - Resistivity



JI03 - Density

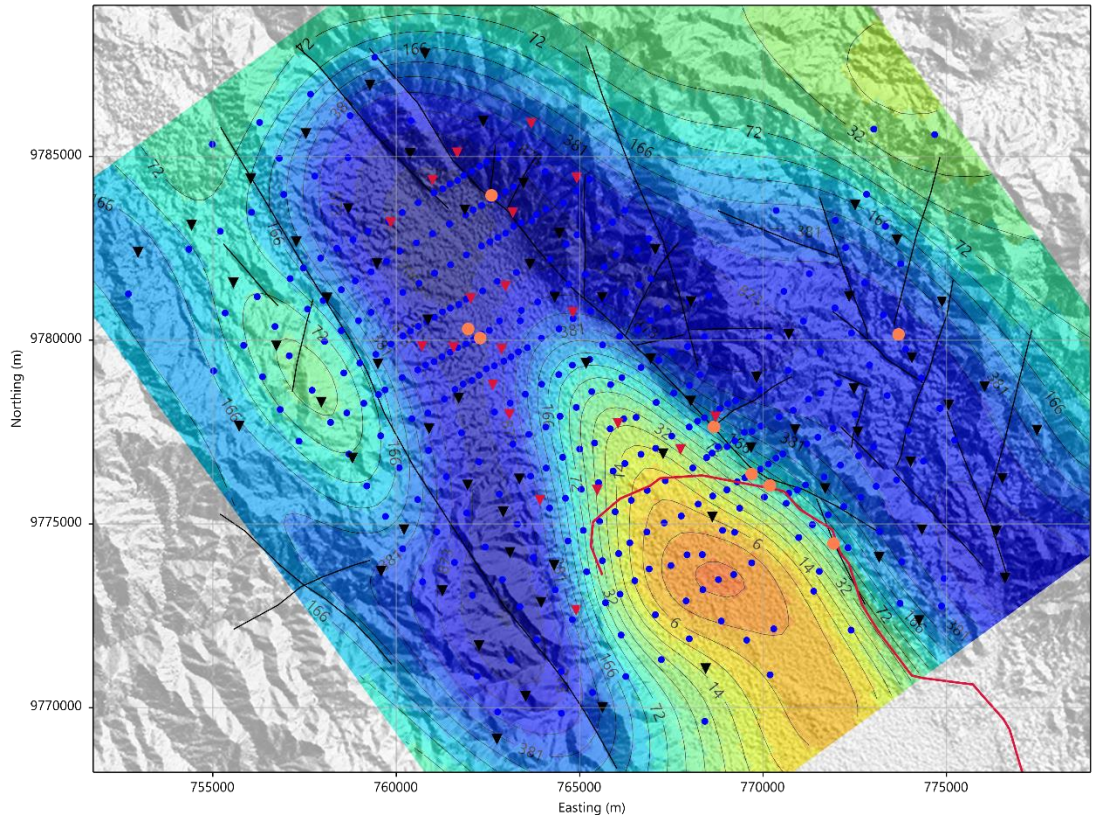


Color: density
Contour: resistivity

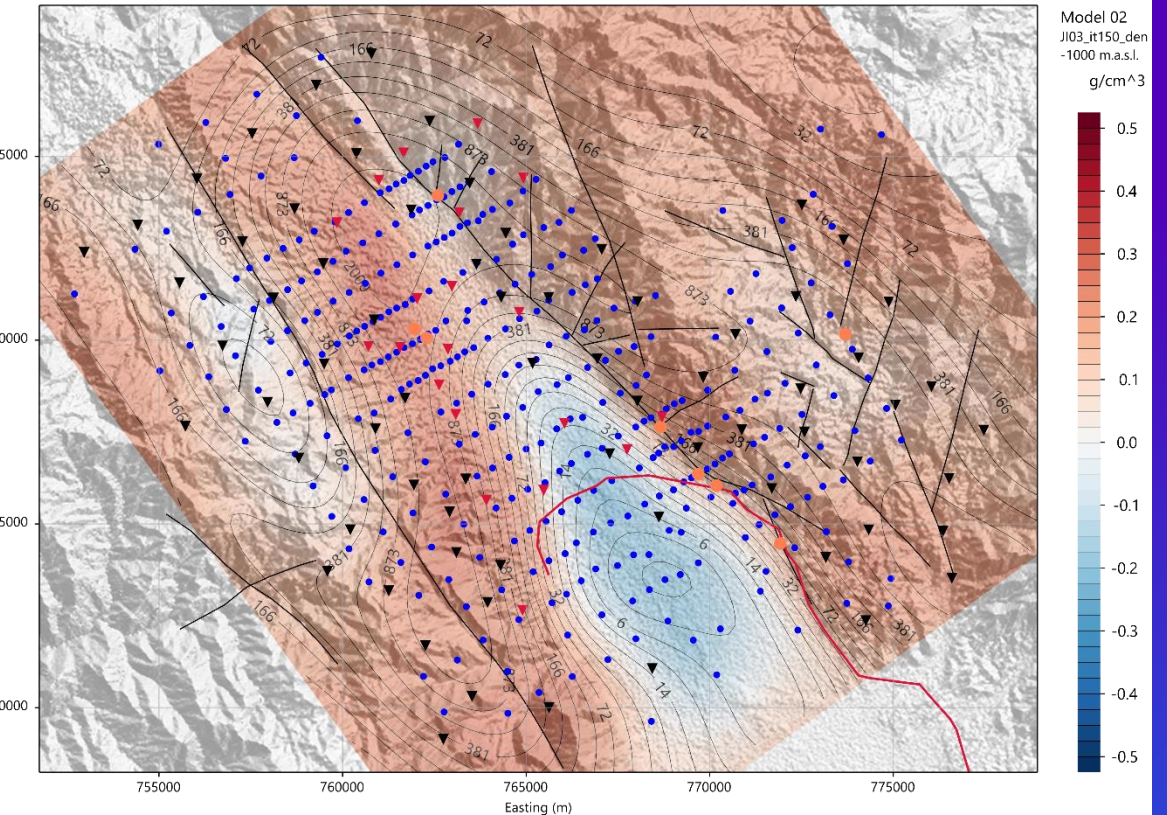
Maps at -1,000m asl (JI03)



JI03 - Resistivity

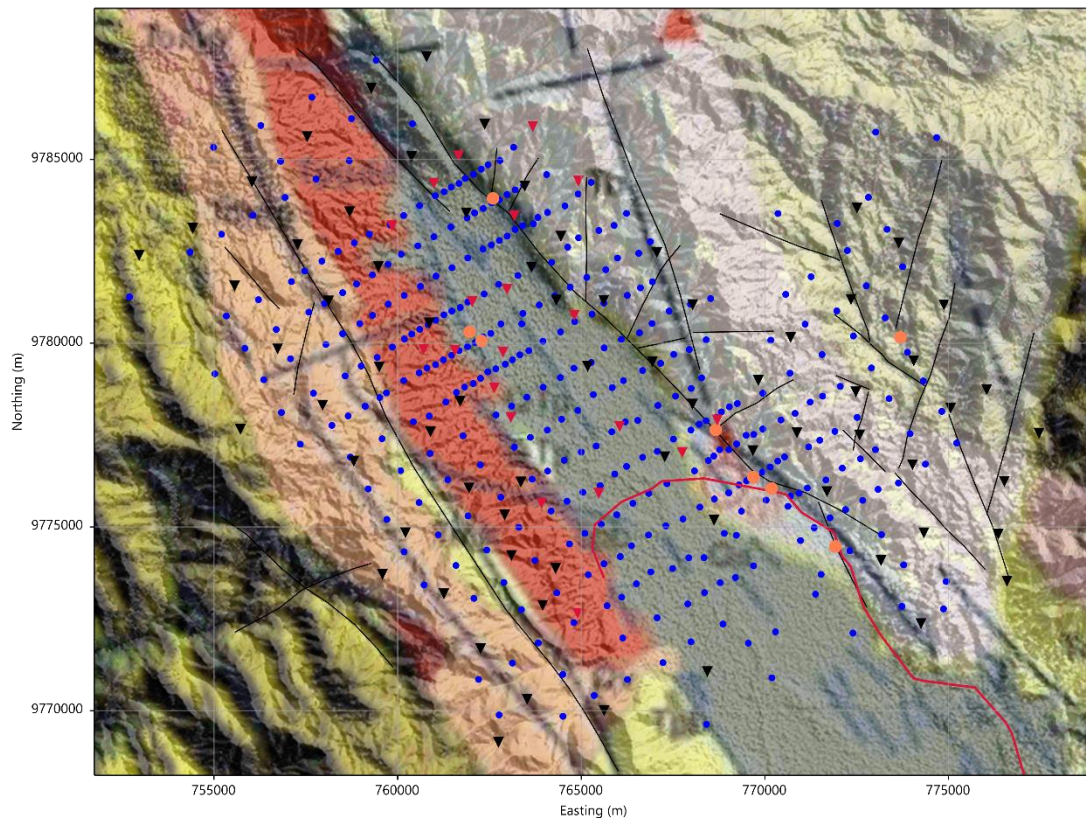
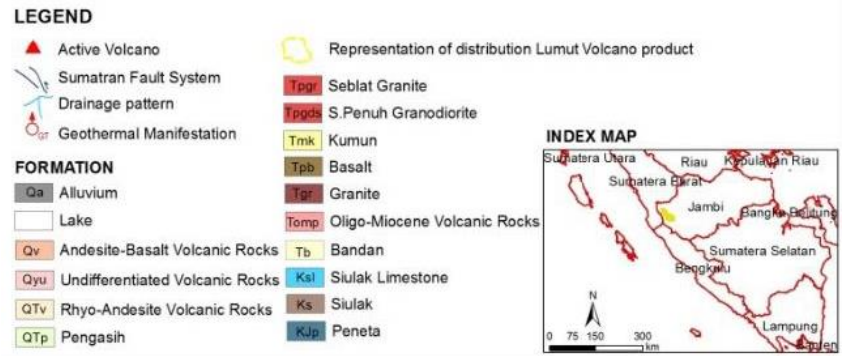


JI03 - Density

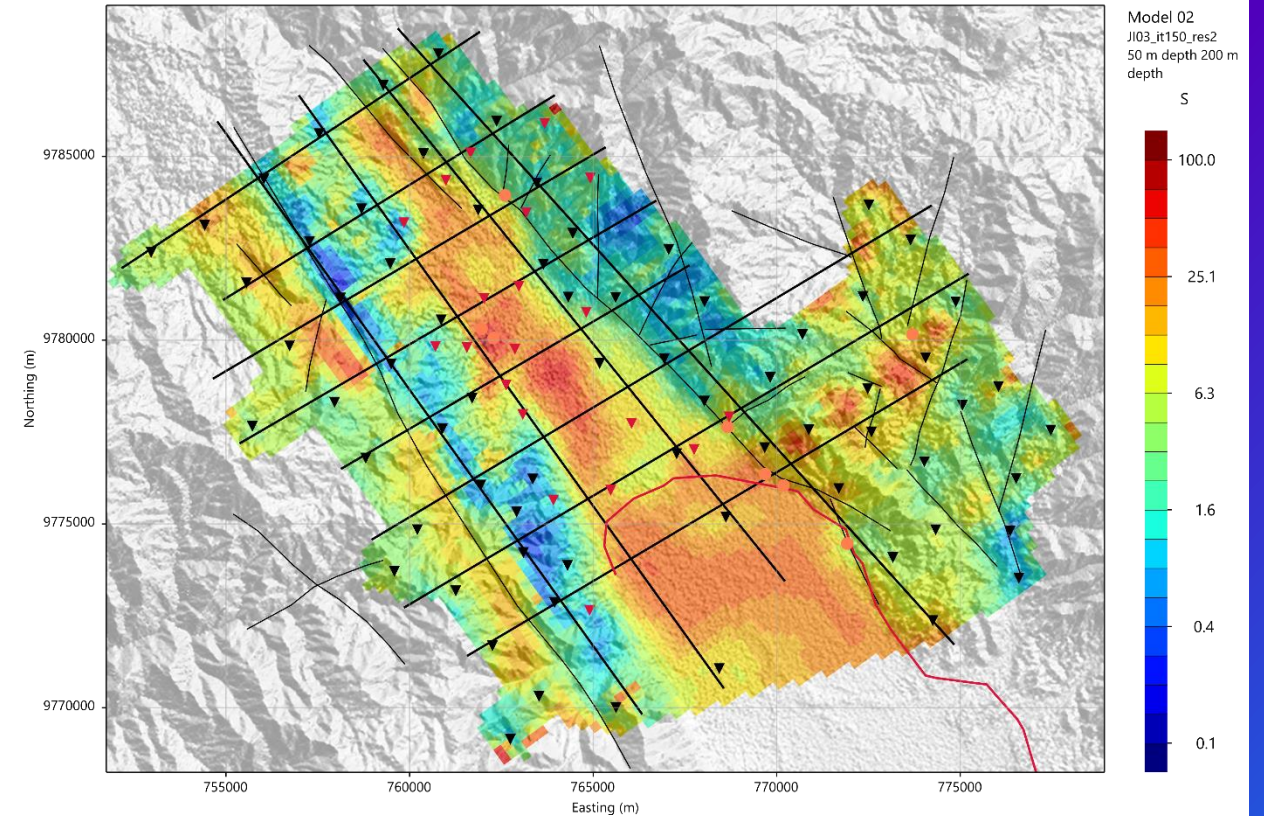


Color: density
Contour: resistivity

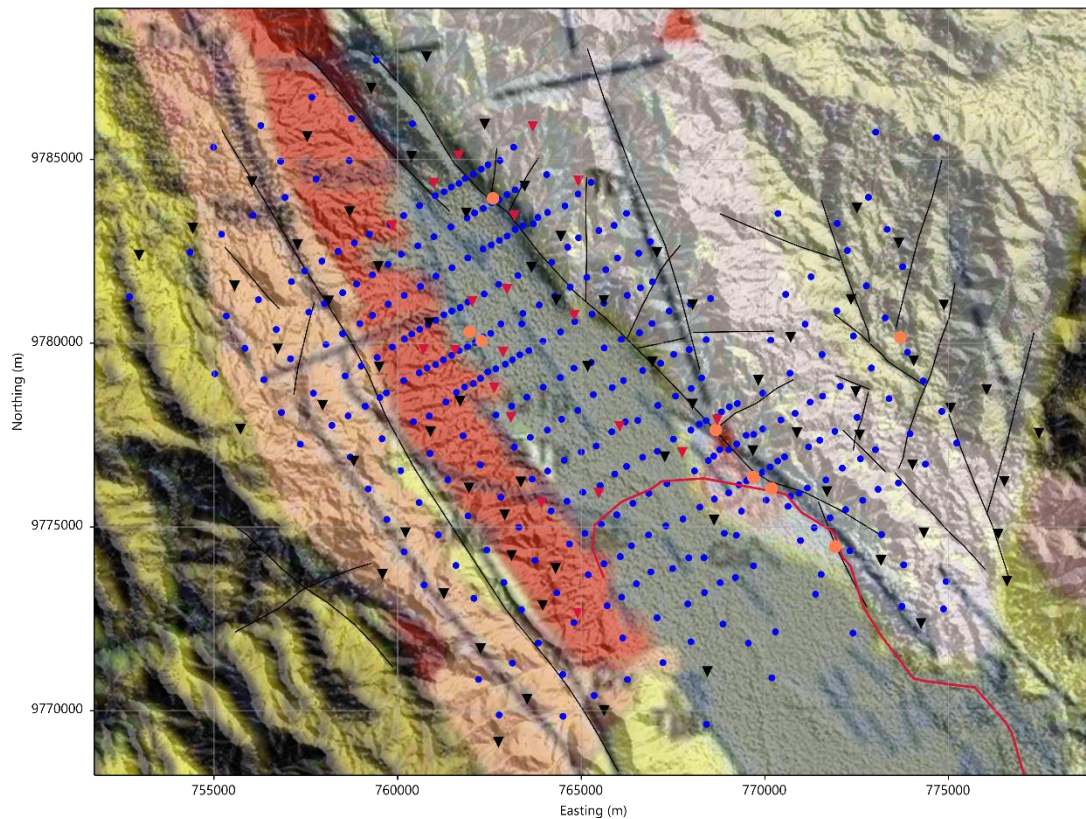
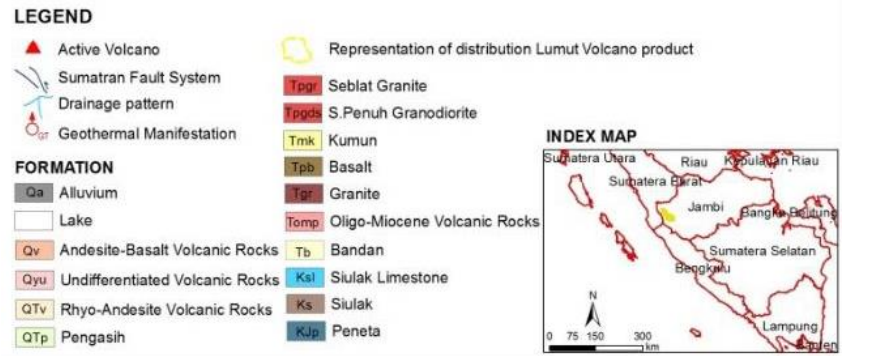
Comparison with geological map - I



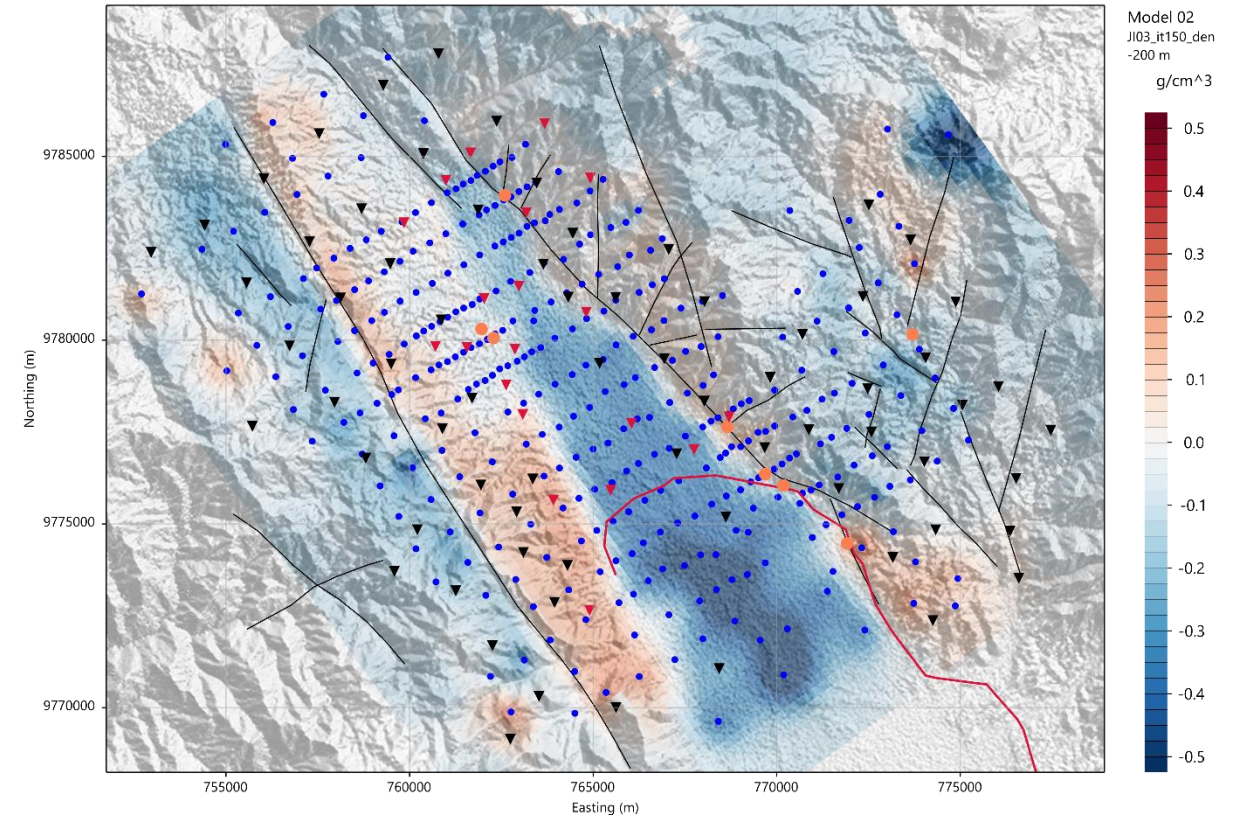
JI03 – Cumulative Conductance between 50 and 200m depth

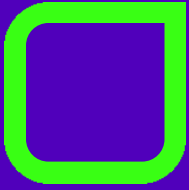


Comparison with geological map - II



JI03 – Density at 200m depth





DISCUSSION

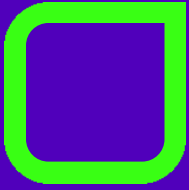


Discussion - I

- 90 MT soundings and 357 gravity measurements were included in the 3D inversion process for the Semurup area, that consisted of both MT and gravity single domain and joint inversions.
- MT data have been collected in 2022 (70 soundings) and in 2024 (20 soundings). Data from all MT stations have been used for 3D modeling. Prior to inversion, data have been rotated to 324 degrees, resulting in impedance tensors rotated accordingly with the main geological strike direction in the area.
- MT input data were full complex tensor impedances, using a 5% error floor for all impedance tensor elements, and magnetic transfer function with an absolute error of 0.02. Data editing was performed on both MT datasets.
- Complete Bouguer anomaly at 2.4g/cc reduction density has been considered as input data for 3D modeling. After data analysis, the gravity dataset consisted of 357 measurements (364 were provided).
- The model covers an area extending over both geophysical datasets. Lateral cell size is 250m x 250m in the core area and vertical cell size is 25m in the range of topography. The total number of cells is about 1.9M. The SRTM1 grid (30m resolution) was used for the definition of the topography in the 3D model, while SRTM15 grid was used to define sea water cells in the NW and SW corners of the 3D model mesh.
- Final data fit between observed and predicted data is good for both the single domain and joint inversions presented here.
- Single domain inversions already show correlation between the modeled resistivity and density structures, with correspondence between high resistivity/high density and low resistivity/low density anomalies, both at shallow and great depths. The correlation between the modeled structures is then increased by the joint inversions, with an impact on both the domains.

Discussion- II

- Cumulative conductance and shallow (200m depth) density extracted from the 3D MT+gravity joint inversions show good correlation with the major structures of the geological map. In the central zone, the ‘aluvium’ area corresponds to high conductance and low density, while the granodiorite formation corresponds to lower conductance and higher density. Significant conductance and density contrasts are modeled along the 2 main NW-SE faults, separating the central graben area from the flanks. The shallow cumulative conductance distribution also reflects structures mapped as ‘minor’ faults.



APPENDIX



Appendix – RLM-3D

The 3D solvers in CGG's proprietary RLM-3D inversion engine handles gravity and gravity gradiometry, magnetics and seismic traveltimes, as well as frequency domain electromagnetic induction. Property regularization follows a minimum-structure Tikhonov approach (Tikhonov and Arsenin, 1977), and the objective function is minimized using a non-linear conjugate gradients (NLCG) scheme as described in Rodi and Mackie (2001).

MT forward modeling is based on the finite integration technique (Weiland 1977) applied on orthogonal Cartesian grids (more details in Mackie and Watts, 2012). The gravity simulation is based on the closed-form solutions for rectangular prisms found in Li and Chouteau (1998). Traveltimes are calculated using a CGG implementation of the FTeik3d code (Noble et al, 2012), solving the Eikonal equation through finite difference approximations.

The standard approach to solving nonlinear geophysical inverse problems is by regularized least-squares, in which the solution is taken to be the minimum of an objective function of the form

$$\Psi(m) = (d - F(m))^T W (d - F(m)) + \lambda (m - m_0)^T K (m - m_0),$$

where d is the observed data vector, F is the forward modeling function, m is the unknown model vector, W is a weighting matrix (usually the inverse variance or covariance), λ is the regularization parameter, K is a discrete form of the stabilizing function, and m_0 is an (optional) a priori model. An additional term may optionally be added that measures the cross-gradient link to a structural reference model.

For joint inversions, this objective function is augmented to minimize the data misfits of more than one data type, the regularizations of all model properties involved, and cross-gradient link between the properties. Labelling the data misfit and model regularization terms of the objective function Φ^{data} and Φ^{reg} , and cross-gradient measures between model properties Φ^{xg} , the joint objective function can be rewritten for the joint inversion as:

$$\Psi(m) = \sum_{j=1,2} \alpha_j \Phi_j^{data} + \sum_{i=a,b} \lambda_i \Phi_i^{reg} + \tau_{a,b} \Phi_{a,b}^{xg} \left[+ \sum_{i=a,b} \tau_{i,ref} \Phi_{i,ref}^{xg} \right],$$

where \bar{m} is an ensemble of model properties (a, b). Indices j refer to different data types. Factors α , λ , and τ effectively weigh the contribution of the respective terms to the objective function. For the data weight, the square root of the ratio between the total numbers of data points of two methods involved is used (Commer and Newman, 2009).



Appendix – RLM-3D MT / AFMAG / Land-CSEM

- Staggered-grid, E-field formulation, based on Finite Integration Technique. Null space of curl curl equations and zero conductivity air is eliminated by gradient-divergence augmentation (\mathbf{J} in Earth, \mathbf{E} in air). Transforms curl curl to Laplacian in homogeneous regions. Resulting solution is robust at high and low frequencies.
- Tested against standard 3D analytic models (Weaver), 3D Finite Element (Wannamaker), and against public domain 3D Commemi model (Mackie and Wannamaker).
- MT: complete impedance tensor (Z_{xy} , Z_{yx} , Z_{xx} , Z_{yy}), vertical magnetic transfer functions (T_{zx} , T_{zy}). Partial tensors / masking supported.
- AFMAG: ZTEM, MobileMT using true setup information. For MobileMT, apparent conductivity data are calculated from the rotational invariant determinant of the horizontal 2x2 complex admittance tensor.
- CSEM: Inversion for either normalized (by current) EM field amplitudes or impedances.
- CSEM: the transmitter – typically an electric dipole – is included in an outer core of wider but sufficient lateral meshing. The transmitter is modeled using its full dimension following topography.
- Handles arbitrary sensor locations correctly, e.g., in T-MT surveys, where magnetic and electric field measurements are not necessarily collocated.
- Number of frequencies for inversion process is not limited. No limitation to far-field in CSEM / CSAMT inversions.
- To accurately model areas with topography (and if relevant, bathymetry) a detailed mesh is used over the MT data area. Near the coast, bathymetry is incorporated to correctly model the 3D effect of the conductive sea/ocean.
- MT: Inversion for galvanic distortion, if relevant; model parameter is extended to a real valued 2×2 distortion matrix for each site, which multiplies to the calculated 3D complex impedances.
- The inversion is normally for isotropic resistivity; this can be substituted by anisotropic inversion, however, if the conditions require.



Appendix – RLM-3D Output Data and Formats

Output files of the 3-D inversions:

- model files, which contain the mesh dimensions and the final property values
- inversion LOG files, containing inversion statistics
- predicted data with computed responses

Model Format

OUT Format (ASCII)

- Coordinate axis:
x = East, y = South, z = down (for orientation $\alpha=0$)
- Origin / anchor:
laterally - cell center of north-westernmost cell (index: 1, 1)
vertically – top of model.
given in [km] at bottom of file (x0/ y0/ z0).
- Orientation: counterclockwise in degrees (α)

UBC Format

- Inversion models are also provided in UBC format (.mesh / .mod),
with padding zones removed.

nx	ny	nz		
dx_1	dx_2	dx_3	...	dx_nx
dy_1	dy_2	dy_3	...	dy_ny
dz_1	dz_2	dz_3	...	dz_nz
1				
$\rho_{1,1,1}$	$\rho_{2,1,1}$	$\rho_{3,1,1}$...	$\rho_{nx,1,1}$
...				
$\rho_{1,ny,1}$	$\rho_{2,ny,1}$	$\rho_{3,ny,1}$...	$\rho_{nx,ny,1}$
...				
nz				
$\rho_{1,1,nz}$	$\rho_{2,1,nz}$	$\rho_{3,1,nz}$...	$\rho_{nx,1,nz}$
...				
$\rho_{1,ny,nz}$	$\rho_{2,ny,nz}$	$\rho_{3,ny,nz}$...	$\rho_{nx,ny,nz}$
Comment				
Name				
1	1			
x0	y0			
α				
z0				



References – I

- CLEMENS, M. AND WEILAND, T., 2001. Discrete electromagnetism with the finite integration technique. *Progress in Electromagnetics Research*, 32, pp. 65-87.
- COLOMBO, D., AND ROVETTA, D., 2018, Coupling strategies in multiparameter geophysical joint inversion, *Geophys. J. Intl.*, v215/2, 1171–1184.
- CONSTABLE, S.C., PARKER, R.L., AND CONSTABLE, C.G., 1987. Occam's inversion: a practical algorithm for generating smooth models from electromagnetic sounding data. *Geophysics*, vol. 52, pp. 289-300.
- GALLARDO, L.A. AND MEJU, M.A., 2003, Characterization of heterogeneous near-surface materials by joint 2D inversion of DC resistivity and seismic data. *Geophys. Res. Lett.*, 30, 1658.
- GALLARDO, L.A. AND MEJU, M.A., 2011, Structure-coupled multiphysics imaging in geophysical sciences, *Review of Geophysics*, 49(1), DOI: 10.1029/2010RG000330.
- KELLER AND FRISCHKNECHT, 1966. Electrical Methods in Geophysical Prospecting, Pergamon Press.
- LI, Y., OLDENBURG, D.W., 1998, 3-D inversion of gravity data. *Geophysics*, 63, 109-119.
- MACKIE, R. L. AND T. R. MADDEN, 1993, Three-dimensional magnetotelluric inversion using conjugate gradients: *Geophys. J. Int.*, 115, 215-229.
- MACKIE, R.L., SCHOLL, M.D., AND WATTS, M.D., 2017, SEAM2: 3D Inversion of Synthetic MT and Airborne EM from a complex Middle East O&G Model, *6th International Symposium on Three-Dimensional Electromagnetics*, Berkeley, California, USA.
- MACKIE, R.L., MEJU, M.A., MIORELLI, F., MILLER, R.V., SCHOLL, C., SHAHIR, A.S., 2020, Seismic image-guided 3D inversion of marine controlled-source electromagnetic and magnetotelluric data. *Interpretation*, 8: SS1-SS13.
- MACKIE, R.L., SOYER, W., HALLINAN, S., AND GODSMARK, B., 2023, Complete Earth 3D Modelling of Land Controlled-Source EM, AEGC, Brisbane.
- MADDEN, T.R., 1972, Transmission systems and network analogies to geophysical forward and inverse problems. ONR Tech. Rep. 72-3.



References – II

- RODI, W. AND MACKIE, R.L., 2001. Nonlinear conjugate gradients algorithm for 2-D magnetotelluric inversion, *Geophysics*, 66, 174--187.
- MORKEL, J., PISTORIUS, P.C., AND VERMAAK, M.K.G., 2007. Cation exchange behavior of kimberlite in solutions containing Cu²⁺ and K⁺, *Minerals Engineering* 20, 1145-1152.
- SCHOLL, C., HALLINAN, S., MIORELLI, F., AND WATTS, M. D., 2017, Geological Consistency from Inversions of Geophysical Data. *79th EAGE Conference and Exhibition*.
- SCHOLL, C. AND MIORELLI, F., 2018, Otze – Airborne EM Inversion on Unstructured Model Grids, *AEM2018, Kolding, Denmark*.
- SOYER, W., MACKIE, R.L., AND MIORELLI, F., 2017, 3D MT inversion modeling considering galvanic distortion matrices: *China Intl. Geo-Electric Workshop, Wuhan, China*.
- SOYER, W., HALLINAN, S., MACKIE, R.L., PAVESI, A., NORDQUIST, G., SUMINAR, A., INTANI, R., AND NELSON, C., 2018, Geologically-consistent multiphysics imaging of the Darajat geothermal steam field, *First Break*, 36 (6), 77-83.
- SOYER, W., MACKIE, R.L. AND MIORELLI, F., 2018, 3D MT inversion modeling considering galvanic distortion matrices: *Extended Abstracts 80th EAGE Conference and Exhibition, Copenhagen*.
- TIKHONOV, A.N., AND ARSENIN, V.Y., 1977. Solution of Ill-posed Problems. *Washington: Winston & Sons*. ISBN 0-470-99124-0.
- TITOV, K., ABRAMOV, V., EMELIANOV, V., AND REVIL, A., 2024. Induced polarization of volcanic rocks. Part 7. Kimberlites, *Geophys. J. Intl.*, v236, 233–248 .
- VOZOFF, K., 1991. The Magnetotelluric Method, in *Electromagnetic Methods in Applied Geophysics*, pub. SEG, vol. 2B, pp. 641-711.
- WATTS, M.D., 2012, Reflections on natural field EM methods. *22nd ASEG Conference and Exhibition, Brisbane, Australia*.
- WEILAND, T., 1977. A discretization method for the solution of Maxwell's equations for six-component fields, *Electronics and Communications AEU*, 31, pp. 116-120.